Offshore Code Comparison Collaboration (OC3) for IEA Task 23 Offshore Wind Technology and Deployment

J. Jonkman and W. Musial

NREL

NATIONAL RENEWABLE ENERGY LABORATORY

Offshore Code Comparison Collaboration (OC3) for IEA Task 23 Offshore Wind Technology and Deployment

J. Jonkman and W. Musial

Prepared under Task No. WE10.1211

NOTICE

Executive Summary of IEA Wind Task 23 Subtask 2

The vast offshore wind resource represents a potential to use wind turbines installed offshore to power much of the world. Design standardization is difficult, however, because offshore sites vary significantly through differences in water depth, soil type, and wind and wave severity. To ensure that offshore wind turbine installations are cost effective, the use of a variety of support structure types is required. These types include fixed-bottom monopiles, gravity bases, and space-frames—such as tripods and lattice frames ("jackets")—and floating structures. In this context, the offshore wind industry faces many new design challenges.

Wind turbines are designed and analyzed using simulation tools (i.e., design codes) capable of predicting the coupled dynamic loads and responses of the system. Land-based wind turbine analysis relies on the use of aero-servo-elastic codes, which incorporate wind-inflow, aerodynamic (aero), control system (servo), and structural-dynamic (elastic) models in the time domain in a coupled simulation environment. In recent years, some of these codes have been expanded to include the additional dynamics pertinent to offshore installations, including the incident waves, sea current, hydrodynamics, and foundation dynamics of the support structure. The sophistication of these aero-hydro-servo-elastic codes, and the limited data available with which to validate them, underscore the need to verify their accuracy and correctness. The Offshore Code Comparison Collaboration (OC3), which operates under Subtask 2 of the International Energy Agency (IEA) Wind Task 23, was established to meet this need.

To test the newly developed codes, the main activities of OC3 were to (1) discuss modeling strategies, (2) develop a suite of benchmark models and simulations, (3) run the simulations and process the simulation results, and (4) compare and discuss the results. These activities fell under broader objectives including:

- Assessing the accuracy and reliability of simulations to establish confidence in their predictive capabilities
- Training new analysts to run and apply the codes correctly
- Identifying and verifying the capabilities and limitations of implemented theories
- Investigating and refining applied analysis methodologies
- Identifying further research and development (R&D) needs.

Such verification work, in the past, led to dramatic improvements in model accuracy as the code-to-code comparisons and lessons learned helped identify model deficiencies and needed improvements. These results are important because the advancement of the offshore wind industry is closely tied to the development and accuracy of system-dynamics models.

The OC3 project was performed through technical exchange among a group of international participants from universities, research institutions, and industry across the United States of America, Germany, Denmark, the United Kingdom, Spain, the Netherlands, Norway, Sweden, and Korea. Moreover, most of the aero-hydro-servo-elastic codes developed for modeling the dynamic response of offshore wind turbines were tested within OC3.

The simulation of offshore wind turbines under combined stochastic aerodynamic and hydrodynamic loading is very complex. The benchmarking task, therefore, required a sophisticated approach that facilitated source identification of modeling discrepancies introduced by differing theories and model implementations in the various codes. This is possible only by (1) meticulously controlling all of the inputs to the codes and (2) carefully applying a stepwise verification procedure in which model complexity is increased one step at a time.

The fundamental set of inputs to the codes controlled within OC3 relates to the specifications of the wind turbine. The OC3 project uses the publicly available specifications of the 5-MW baseline wind turbine developed by NREL, which is a representative utility-scale multi-megawatt turbine. This conventional three-bladed upwind variable-speed, variable-blade-pitch-to-feather controlled turbine is specified with detailed rotor aerodynamic properties; blade, drivetrain, nacelle, and tower structural properties; and generator-torque and blade-pitch control system properties, the latter of which were provided to all OC3 participants in the form of a dynamic link library (DLL). The hydrodynamic and elastic properties of the varying offshore support structures used in the project are also controlled. Furthermore, the turbulent full-field wind inflow and regular and irregular wave kinematics are model inputs controlled within OC3. This approach eliminated any possible differences brought about by dissimilar turbulence models, wave theories, or stochastic realizations.

An important part of the comparison was a stepwise process that allowed the origin of differences between code predictions to be discovered. Various combinations of wave and wind input were introduced with the rotor and tower being rigid or flexible, disentangling the contributions from wind- and wave-applied loads and dynamic response. Finally, the turbine was made operational so that the effect of the control system could be evaluated.

In OC3, emphasis is given to the verification of the offshore support structure dynamics as part of the dynamics of the complete system. This emphasis distinguishes OC3 from previous wind turbine code-to-code verification exercises. To encompass the variety of support structures required for cost effectiveness at varying offshore sites, different support structures (for the same wind turbine) were investigated in separate phases of OC3:

- In Phase I, the NREL offshore 5-MW wind turbine was installed on a monopile with a rigid foundation in 20 m of water.
- In Phase II, the foundation of the monopile from Phase I was made flexible by applying different models to represent the soil-pile interactions.
- In Phase III, the water depth was changed to 45 m and the monopile was replaced with a tripod substructure, which is one of the common space-frame concepts proposed for offshore installations in water of intermediate depth.
- In Phase IV, the wind turbine was installed on a floating spar-buoy in deep water (320 m).

The code-to-code comparisons in Phases I through IV have generally agreed very well. The key reasons for the differences that have remained and the other findings from Phases I through IV are discussed below.

Phase I – Monopile with Rigid Foundation:
- The modal-based codes predict slightly different second and higher coupled eigenmodes than are predicted by the higher fidelity multibody- and FEM-based codes. Differences in the dynamic response and energy content are, therefore, to be expected in the higher frequency range.
- The codes that rely on full-field wind available in polar coordinates predict smoother aerodynamic loads (thus smaller load deviations and smaller DELs) than codes that rely on rectangular coordinates. This results from the method by which the wind datasets were generated. To ensure that all participants used the same wind inflow, the full-field wind datasets were generated in rectangular coordinates and subsequently interpolated to polar coordinates for the codes that needed them. These differences were mitigated as much as possible by using a fine spatial resolution (32×32 points across the rotor disk).
- The differences among the codes relating to the implementation of aerodynamic induction, tower interference, hub and tip loss, and dynamic stall models—and whether or not the aerodynamic

loads were applied in the deflected or undeflected blade state—attribute to variations in the mean values of several key wind turbine loads (e.g., blade-root bending moments, rotor torque, and rotor thrust).

- The blade-pitch controller compensates somewhat for variations that might have been caused between codes with differing aerodynamics and between codes that do and do not have blade-twist degrees of freedom (DOFs).

- Differing model discretizations for the aerodynamic and hydrodynamic loads lead to differences among the code predictions. This is most apparent in the substructure loads that depend highly on the discretization of hydrodynamic loads near the free surface.

- Though every effort was made to standardize model inputs, user error still occurs. It often takes several revisions before the model is developed and run as intended. It is also possible, in some instances, that errors still remain and account for otherwise unexplainable modeling differences.

Phase II – Monopile with Flexible Foundation:

- All of the results of Phase I also apply to the results of Phase II.

- All three of the simplified foundation models—apparent fixity, coupled springs, and distributed springs—can be derived and implemented to ensure that the overall response of the system above the mudline is identical under a given set of loading conditions (at least for the lowest system eigenmodes).

- The discretization problems described for the results of Phase I result in higher excitation in the second eigenmodes of the support structure in Phase II. However, this higher excitation is only visible when the turbine is not operating, because aerodynamic loading tends to limit the amount of additional excitation (i.e., aerodynamic loading tends to damp out the excitation).

- The differing implementations of the aerodynamic models among the codes have more effect on the mean values of the wind turbine loads than on the power spectra.

Phase III – Tripod:

- All of the results of Phase I also apply to the results of Phase III. (The results of Phase II have less bearing on Phase III because Phase III does not use foundation models).

- The most straightforward way to account for buoyancy loads in non-flooded multi-member structures is through direct integration of the hydrostatic pressure that is dependent on the time-varying wave elevation (as opposed to accounting for buoyancy as a displaced volume with corrections for end effects). This is important for non-flooded members that are inclined, tapered, and/or embedded into the seabed (i.e., non-flooded piles). The OC3 code comparisons differed until everyone agreed on this approach.

- The most straightforward way to model a rigid multi-member structure is to increase the Modulus of Elasticity by several orders of magnitude consistently across all members. This permits calculation of how the loads are transmitted through what is a statically indeterminate structure (because of the geometry of the tripod) within the limits of zero deflection. The OC3 code comparisons differed for those load cases that considered a rigid tripod until everyone agreed on this approach.

- Differing discretizations for the hydrodynamic and buoyancy loads along tapered members lead to differences among the code predictions. To eliminate the discrepancy, the hydrodynamic and buoyancy loads along tapered members must be finely discretized. Because the hydrodynamic inertia and buoyancy loads depend on the square of the member diameter, having too long a length between nodes can cause a large error in the total load.

- Because of the large diameter members of the tripod, significant surface areas and volumes are duplicated at the joints, which distort the overall level of loading if the intersection is not accounted for in the mass, stiffness, hydrodynamic loading, and buoyancy loading. This was found to have a large effect on the overall loading and response of the tripod.

- The local shear deflection of the members in a multi-member support structure, which can be modeled with Timoshenko beam elements, was found to have a large effect on the distribution of loads through multi-member structures. This was a surprising finding because all of the beam members of the tripod analyzed in OC3 were thin and slender, such that the Bernoulli-Euler approach, which neglects shear deflection, was thought to be sufficient (and is sufficient in blades, towers, and monopiles). The shear effect was found to be much more important than originally assumed because the beam members are attached rigidly to other members and the relative displacement of each member influences the load distribution. The results of the code comparisons could clearly be grouped between the codes that do and do not account for shear deflection in their beam element formulations.

- The initial transient solution takes time to dissipate due to the small amount of damping in the tripod and the method by which the hydrodynamic loads are initialized at the start of a simulation. The initial transient is longer when the turbine is not operating because aerodynamic loading tends to damp out the initial solution quickly. Each model initializes its solution differently, so, the code comparisons differed during the start-up transient period.

Phase IV – Floating Spar Buoy:
- All of the results of Phase I also apply to the results of Phase IV.

- The natural frequencies of the six (primarily) rigid-body modes of the OC3-Hywind system (with only minor couplings to the turbine flexibilities) are strongly influenced by hydrodynamic added mass. Some codes (such as MSC.ADAMS) can model acceleration-dependent loads within time-domain simulations but neglect acceleration-dependent loads during a linearization solution. To calculate natural frequencies through a linear eigensolution, the models implemented in such codes must have their platform physical mass and inertia augmented with the additional mass and inertia associated with hydrodynamic added mass; otherwise, such codes will predict unreasonably high natural frequencies.

- Gravity has multiple influences on the dynamics of offshore systems (e.g. buoyancy, surface waves, component weight, platform-pitch and -roll natural frequencies). Consequently—while gravity is often neglected in land-based wind turbine codes during model linearization—gravity must be included in the model linearization process by codes that calculate natural frequencies through a linear eigensolution.

- Codes developed to model offshore wind turbines on floating spar buoys incorporate one of two hydrodynamics models: (1) Morison's equation augmented with hydrostatics and wave-excitation heave forces or (2) potential-flow theory augmented with the nonlinear viscous-drag term from Morison's equation. Either hydrodynamic model can be used to predict equivalent hydrodynamic loading of the OC3-Hywind spar in (most) conditions where radiation damping is negligible. For codes that employ Morison's equation, the augmented heave force can be approximated as the change in buoyancy brought about by direct integration of the hydrostatic pressure dependent on the time-varying wave elevation.

- Codes that neglect the additional linear hydrodynamic damping clearly show less overall damping in their responses than codes that include it.

- Codes developed to model offshore floating wind turbines incorporate either quasi-static or dynamic formulations for the mooring system. The quasi-static mooring models can be further divided into (1) a linearized representation of the complete mooring system, (2) a nonlinear load-

displacement relationship of the complete mooring system, (3) a nonlinear load-displacement relationship for each individual mooring line, or (4) direct solution of the implicit nonlinear catenary equations. Due to the nonlinear behavior of the catenary mooring system, the quasi-static model (1) is valid only for small displacements about the linearization point. Quasi-static models (2) through (4) and the dynamic models can be derived and implemented so as to predict equivalent mooring reactions of the OC3-Hywind spar in most conditions. Models (1) and (2), however, cannot be used to calculate the reactions of the individual mooring lines.

- Unlike codes with a quasi-static mooring model, codes (such as SESAM and DeepC) that model the dynamics of the mooring system predict higher energy in the spectra of fairlead tension above the peak wave period. These higher excitations—indicating larger elastic strain and higher dynamic tension—are caused mainly by drag forces normal to the line delaying the static catenary deflection, but are also caused by (nonphysical) problems in the codes' numerical solutions.

- There is considerable statistical uncertainty of the response spectra in the low frequency range of the platform natural frequencies and wave excitation frequencies because of the relatively short duration of the prescribed time series compared to the wave and platform periods. Spectral shape estimates in this frequency range are sensitive to time-series sampling.

- Many offshore floating wind turbine codes cannot model turbine flexibilities such as blade and tower deflection. While neglecting these flexibilities influences the resulting motions and loading of the blades and tower, it does not have a strong influence on the platform motions in the OC3-Hywind system.

- The coupled dynamics of the turbine and platform varied a bit between the codes. The nonzero mean rotor thrust results in nonzero means in the tower-top fore-aft deflection and platform-surge, -pitch, and -heave displacements. The rotor thrust is counteracted by tensions in the mooring lines, with the downstream mooring line less loaded than the upstream lines. The rotor-shaft tilt causes some of the rotor torque to act about the yaw axis that leads to a nonzero mean platform-yaw displacement. Oscillations about these means result from turbulent-wind and regular- or irregular-wave excitation. Oscillations in platform yaw result from a gyroscopic moment produced by platform pitching in combination with spinning rotor inertia.

- While it is desirable to determine the influence of the wave-excitation frequency on the response of a floating wind turbine system, the operation of the turbine makes it impossible to calculate the Response Amplitude Operator (RAO) in a conventional manner, due to (1) nonlinear dynamics, (2) active rotor control, and (3) the rotor rotation introducing additional periodicities. The floating wind turbine system's response to periodic waves will be a superposition of multiple frequencies: (1) the wave excitation frequency, (2) the rotor-rotational frequency, and (3) any system modes natural frequency (such as for platform surge) from which the response is a limit-cycle oscillation due to a controller-induced instability with a reaction limited by nonlinear behavior. To resolve this problem, an "effective RAO" was defined to mean the difference in response amplitudes between nonlinear time-domain simulations run with and without wave excitation. Using this definition, turbine operation at and around rated wind speed—when compared to a parked turbine—was found to have a dramatic effect on the frequency response of the OC3-Hywind system. Moreover, the (potential-flow-based) wave-radiation damping was found to have strong influence on this response. Thus, codes that neglect wave-radiation damping will likely predict vastly different "effective RAOs" for the OC3-Hywind system at and around rated wind speed.

The verification activities performed in OC3 were important because the advancement of the offshore wind industry is closely tied to the development and accuracy of dynamics models. Not only have vital experiences and knowledge been exchanged among the project participants, but the lessons learned have helped identify deficiencies in existing codes and needed improvements, which will be used to improve the accuracy of future predictions.

Contents of Subtask 2

Tables

Figures

IEA Wind Task 23 Subtask 2

1. Chapter 1: Background Information and Objectives

Authors: J. Jonkman and S. Butterfield, NREL, USA; P. Passon, Endowed Chair of Wind Energy (SWE), Universität Stuttgart, Germany

1.1 Overview of IEA Wind Task 23 Subtask 2

Subtask 2 of IEA Wind Task 23 was intended to address technical issues associated with deeper-water implementation of offshore wind energy. In practice, however, the subtask turned into a working group known as the Offshore Code Comparison Collaborative (OC3), which analyzed shallow, transitional, and deep water offshore wind turbine concepts. Under the coordination of the National Renewable Energy Laboratory (NREL), this group worked from 2005 through 2009.

Wind turbines are designed and analyzed using simulation tools (i.e., design codes) capable of predicting the coupled dynamic loads and responses of the system. Land-based wind turbine analysis relies on the use of aero-servo-elastic codes, which incorporate wind-inflow, aerodynamic (aero), control system (servo), and structural-dynamic (elastic) models in the time domain in a coupled simulation environment. In recent years, some of these codes have been expanded to include the additional dynamics pertinent to offshore installations, including the incident waves, sea current, hydrodynamics, and foundation dynamics of the support structure. The sophistication of these aero-hydro-servo-elastic codes, and the limited data available with which to validate them, underscores the need to verify their accuracy and correctness. The OC3 was established to meet this need.

The OC3 project benchmarked system-dynamics models used to estimate offshore wind turbine dynamic loads. Currently, conservative offshore design practices adopted from marine industries are enabling offshore wind development to proceed. But if offshore wind energy is to be economical, reserve margins must be quantified, and uncertainties in the design process must be reduced so that appropriate margins can be applied. Uncertainties associated with load prediction are usually the largest source and hence the largest risk. Model comparisons are the first step in quantifying and reducing load prediction uncertainties. Comparisons with test data would be the next step.

To test the offshore wind turbine system-dynamics models, the main activities of the OC3 project reported here were to (1) discuss modeling strategies, (2) develop a suite of benchmark models and simulations, (3) run the simulations and process the simulation results, and (4) compare and discuss the results. These activities fell under broader objectives including:

- Assessing the accuracy and reliability of simulations to establish confidence in their predictive capabilities
- Training new analysts to run and apply the codes correctly
- Identifying and verifying the capabilities and limitations of implemented theories
- Investigating and refining applied analysis methodologies
- Identifying further research and development (R&D) needs.

Such verification work, in the past has, led to dramatic improvements in model accuracy as the code-to-code comparisons and lessons learned have helped identify model deficiencies and needed improvements. These results are important because the advancement of the offshore wind industry is closely tied to the development and accuracy of system-dynamics models.

The simulation of offshore wind turbines under combined stochastic aerodynamic and hydrodynamic loading is very complex. The benchmarking task, therefore, required a sophisticated approach that facilitated source identification of modeling discrepancies introduced by differing theories and/or model implementations in the various codes. This was possible only by (1) meticulously controlling all of the inputs to the codes and (2) carefully applying a stepwise verification procedure where model complexity was increased one step at a time.

The fundamental set of inputs to the codes controlled within OC3 related to the specifications of the wind turbine. The OC3 project used the publicly available specifications of the 5-MW baseline wind turbine developed by NREL, which is a representative utility-scale multi-megawatt turbine that has also been adopted as the reference model for the integrated European Union (EU) UpWind research program. This wind turbine is a conventional three-bladed, upwind, variable-speed, variable-blade-pitch-to-feather-controlled turbine. The specifications consisted of detailed rotor aerodynamic properties; blade, drivetrain, nacelle, and tower structural properties; and generator-torque and blade-pitch control system properties, the latter of which was provided to all OC3 participants in the form of a dynamic link library (DLL). The specifications of the NREL offshore 5-MW baseline wind turbine are summarized in Table 1 and available in detail [1]. The hydrodynamic and elastic properties of the varying offshore support structures used in the project were also controlled (and are described in the chapters that follow). Furthermore, the turbulent full-field wind inflow and regular and irregular wave kinematics were model inputs controlled in the OC3 project (and are described in the chapters that follow). This approach reduced possible differences brought about by dissimilar turbulence models, wave theories, or stochastic realizations.

Table 1. Summary of properties for the NREL 5-MW baseline wind turbine

Rating	5 MW
Rotor orientation, configuration	Upwind, 3 blades
Control	Variable speed, collective pitch
Drivetrain	High speed, multiple-stage gearbox
Rotor, hub diameter	126 m, 3 m
Hub height	90 m
Cut-in, rated, cut-out wind speed	3 m/s, 11.4 m/s, 25 m/s
Cut-in, rated rotor speed	6.9 rpm, 12.1 rpm
Rated tip speed	80 m/s
Overhang, shaft tilt, precone	5 m, 5º, 2.5º
Rotor mass	110,000 kg
Nacelle mass	240,000 kg
Tower mass	347,500 kg
Coordinate location of overall center of mass (CM)	(-0.2 m, 0.0 m, 64.0 m)

An important part of the comparison was a stepwise process that allowed the origin of differences between code predictions to be discovered. Various combinations of wave and wind input were introduced with the rotor and tower being rigid or flexible, disentangling the contributions from wind- and wave-applied loads and dynamic response. Finally, the turbine was made operational so that the effect of the control system could be evaluated.

In OC3, emphasis was given to the verification of the offshore support structure dynamics as part of the dynamics of the complete system. This emphasis distinguishes the OC3 project from past wind turbine code-to-code verification exercises. Nevertheless, it was important to test the aerodynamic models separately so that modeling differences resulting from the aerodynamics could be identified. This

identification was important because the aerodynamic models are known to be a routine source of differences in wind turbine code-to-code comparisons [2].

The vast offshore wind resource represents a potential to use wind turbines installed offshore to power much of the world. Design standardization is difficult, however, because offshore sites vary significantly through differences in water depth, soil type, and wind and wave severity. To ensure that offshore wind turbine installations are cost effective, the application of a variety of support-structure types is required. These types include fixed-bottom monopiles, gravity bases, and space-frames—such as tripods, quadpods, and lattice frames (e.g., "jackets")—and floating structures. In this context, the offshore wind industry faces many new design challenges.

To encompass the variety of support structures required for cost-effectiveness at varying offshore sites, different types of support structures (for the same wind turbine) were investigated in separate phases of the OC3 project (see Figure 1):

- In Phase I, the NREL offshore 5-MW wind turbine was installed on a monopile with a rigid foundation in 20 m of water.

- In Phase II, the foundation of the monopile from Phase I was made flexible by applying different models to represent the soil-pile interactions.

- In Phase III, the water depth was changed to 45 m and the monopile was replaced with a tripod substructure, which is one of the common space-frame concepts proposed for offshore installations in water of intermediate depth.

- In Phase IV, the wind turbine was installed on a floating spar-buoy in deep water (320 m).

Phase I also included a land-based variation of the 5-MW turbine. The calibration of this model was important because the same rotor-nacelle assembly was used in all subsequent phases of the project.
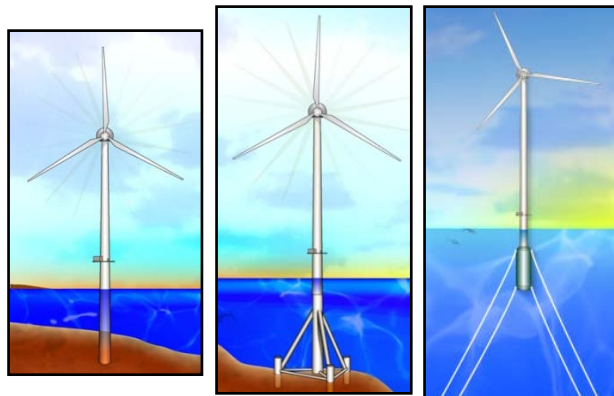
Figure 1. Support structure concepts investigated within the OC3 project

A follow up project to OC3 is being initiated in 2010 through the IEA so that two more phases can be considered, including the analysis of a fixed-bottom jacket and a floating semi-submersible.

During the OC3 project, the reference 5-MW wind turbine, including control system, was developed; the wind and wave data sets were generated; and the simulations and code-to-code comparisons of Phases I through IV were completed. Four conference papers have been published and presented—summarizing the results of each phase—see references [3], [4], [5], and [6] for Phases I, II, III, and IV respectively. This report contains a complete review of all phases, with contributions from each conference paper, including updated results that have been submitted since the papers were first published.

Over the course of the OC3 project, internet meetings were held approximately every one to two months, which were productive and significantly reduced the need for physical meetings and travel. In addition, eleven physical meetings were held at key points in the project: United States: October 2004; Denmark: January 2005; Norway: June 2005; Denmark: October 2005; United States: June 2006; Germany: January, September, and December 2007; Denmark: September 2008 and March 2009; and Sweden: September 2009.

The verification activities performed in OC3 were important because the advancement of the offshore wind industry is closely tied to the development and accuracy of dynamics models. Not only have vital experiences and knowledge been exchanged among the project participants, but the lessons learned have helped identify deficiencies in existing codes and needed improvements, which will be used to improve the accuracy of future predictions.[*]

1.2 References

[1] Jonkman J, Butterfield S, Musial W, and Scott G. *Definition of a 5-MW Reference Wind Turbine for Offshore System Development*. NREL/TP-500-38060, Golden, CO: National Renewable Energy Laboratory, February 2009.

[2] Schepers JG, et al, *Verification of European Wind Turbine Design Codes, VEWTDC; Final Report*, ECN-C-01-055, Petten, The Netherlands: Energy Research Centre of The Netherlands, May 2002.

[3] Passon P, Kühn M, Butterfield S, Jonkman J, Camp T, and Larsen TJ. "OC3—Benchmark Exercise of Aero-Elastic Offshore Wind Turbine Codes," *Journal of Physics: Conference Series, The Second Conference on the Science of Making Torque From Wind, 28–31 August 2007, Copenhagen, Denmark* [online journal], 012071, vol. 75, 2007. www.iop.org/EJ/article/1742-6596/75/1/012071/jpconf7_75_012071.pdf?request-id= 8kI1Ig5u3BGgUobT2wi7Kg. NREL/CP-500-41930. Golden, CO: National Renewable Energy Laboratory.

[4] Jonkman J, Butterfield S, Passon P, Larsen T, Camp T, Nichols J, Azcona J, and Martinez A. "Offshore Code Comparison Collaboration within IEA Wind Annex XXIII: Phase II Results Regarding Monopile Foundation Modeling." *2007 European Offshore Wind Conference & Exhibition, 4–6 December 2007, Berlin, Germany* [online proceedings], BT2.1. www.eow2007proceedings.info/allfiles2/206_Eow2007fullpaper.pdf. NREL/CP-500-42471. Golden, CO: National Renewable Energy Laboratory.

[5] Nichols J, Camp T, Jonkman J, Butterfield S, Larsen T, Hansen A, Azcona J, Martinez A, Munduate X, Vorpahl F, Kleinhansl S, Kohlmeier M, Kossel T, Böker C, and Kaufer D. "Offshore Code Comparison Collaboration within IEA Wind Annex XXIII: Phase III Results Regarding Tripod Support Structure Modeling." *47th AIAA Aerospace Sciences Meeting and Exhibit, 5–8 January 2008, Orlando, Florida, AIAA Meeting Papers on Disc 14(1)*. CD-ROM. AIAA-2009-1038, Reston, VA: American Institute of Aeronautics and Astronautics, January 2009. NREL/CP-500-44810. Golden, CO: National Renewable Energy Laboratory.

[6] Jonkman J, Larsen T, Hansen A, Nygaard T, Maus K, Karimirad M, Gao Z, Moan T, Fylling I, Nichols J, Kohlmeier M, Pascual Vergara J, Merino D, Shi W, and Park H. "Offshore Code Comparison

---

[*] One example of this can already be seen by the application of the OC3 results by the new Fraunhofer Institute for Wind Energy and Energy System Technology (IWES) software system OnWind. The OC3 project established a set of benchmarking scenarios for engineers using aero-elastic simulation software and those who develop these tools. IWES is establishing a new toolset, based on the Modelica language, to facilitate the numerical modeling of systems with the potential to change the level of detail of each individual component of the model during simulation. Even though the OnWind software was not tested within OC3 over the course of the project, the software is now being tested using the OC3 results after the project has ended. It is planned to make these models available to the scientific community in the future.

Collaboration within IEA Wind Task 23: Phase IV Results Regarding Floating Wind Turbine Modeling." *2010 European Wind Energy Conference and Exhibition, 20–23 April 2010, Warsaw, Poland* [in publication]. NREL/CP-500-47534. Golden, CO: National Renewable Energy Laboratory.

2. Chapter 2: Monopile with Rigid Foundation Modeling of Phase I

Authors: J. Jonkman and S. Butterfield, National Renewable Energy Laboratory (NREL), USA; P. Passon, D. Matha, S. Hauptmann, and M. Kühn, Endowed Chair of Wind Energy at the University of Stuttgart (SWE), Germany; T. Camp, Garrad Hassan & Partners Limited (GH), Bristol, UK; T.J. Larsen, Risø National Laboratory, Roskilde, Denmark; J. Azcona and A. Martinez, National Renewable Energies Center (CENER), Spain; Fabian Vorpahl, Fraunhofer Institute for Wind Energy and Energy System Technology (IWES) (formerly, Fraunhofer Center for Wind Energy and Maritime Engineering [CWMT]), Germany; Kristian Bendix Nielsen, Det Norsk Veritas (DNV), Denmark; Niels Kjær Lauritsen, Vestas Wind Systems, Denmark; Rune Rubak, Siemens Windpower, Denmark; and Christian Mørch, Danish Oil and Natural Gas Energy (DONG) (formerly Elsam Engineering), Denmark.

2.1 Phase I Model

In Phase I of OC3, a reference configuration was established for the calibration of codes and model parameters for the turbine and control system. Calibrations in this reference phase were important, especially since the same turbine model was used in all subsequent phases of OC3.

The Phase I system consisted of the NREL 5-MW baseline wind turbine as documented in [1], mounted atop a monopile with a rigid foundation in 20 m water depth. The rotor-nacelle assembly of the NREL 5-MW turbine—including the aerodynamic, structural, and control system properties—remained the same as in [1], but the support structure was changed.

The distributed tower properties of the model are based on the base diameter (6 m) and thickness (0.027 m), top diameter (3.87 m) and thickness (0.019 m), and effective mechanical steel properties of the tower used in the DOWEC study, as given in Table 9 on page 31 of [2]. The radius and thickness of the tower are assumed to be linearly tapered from base to top. The tower is connected to a monopile with a constant diameter of 6 m and a constant thickness of 0.060 m. The tower base begins at an elevation of 10 m above the mean-sea level (MSL). The monopile extends from the tower base down to the mudline, which is at 20 m below MSL. The Young's modulus is taken to be 210×10^9 Pa, the shear modulus is taken to be 80.8×10^9 Pa and the effective density of the steel is taken to be 8,500 kg/m^3. The 8,500 kg/m^3 is meant to be an increase above steel's typical value of 7,850 kg/m^3 in order to account for paint, bolts, welds, and flanges that are not accounted for in the thickness data. The resulting distributed support-structure properties are given in Table 2 below.

Table 2. Distributed support-structure properties for the tower and monopile used in Phase I

Elevation (m)	HtFract (-)	TMassDen (kg/m)	TwFAStif (Nm^2)	TwSSStif (Nm^2)	TwGJStif (Nm^2)	TwEAStif (N)	TwFAIner (kg m)	TwSSIner (kg m)	TwFAcgOf (m)	TwSScgOf (m)
-20.00	0.00000	9517.14	1037.13E+9	1037.13E+9	798.098E+9	235.129E+9	41979.2	41979.2	0.0	0.0
10.00	0.27881	9517.14	1037.13E+9	1037.13E+9	798.098E+9	235.129E+9	41979.2	41979.2	0.0	0.0
10.00	0.27882	4306.51	474.49E+9	474.49E+9	365.133E+9	106.396E+9	19205.6	19205.6	0.0	0.0
17.76	0.35094	4030.44	413.08E+9	413.08E+9	317.878E+9	99.576E+9	16720.0	16720.0	0.0	0.0
25.52	0.42306	3763.45	357.83E+9	357.83E+9	275.356E+9	92.979E+9	14483.4	14483.4	0.0	0.0
33.28	0.49517	3505.52	308.30E+9	308.30E+9	237.242E+9	86.607E+9	12478.7	12478.7	0.0	0.0
41.04	0.56729	3256.60	264.08E+9	264.08E+9	203.220E+9	80.459E+9	10689.2	10689.2	0.0	0.0
48.80	0.63941	3016.86	224.80E+9	224.80E+9	172.987E+9	74.534E+9	9098.9	9098.9	0.0	0.0
56.56	0.71153	2786.13	190.06E+9	190.06E+9	146.252E+9	68.834E+9	7692.7	7692.7	0.0	0.0
64.32	0.78365	2564.46	159.49E+9	159.49E+9	122.735E+9	63.357E+9	6455.7	6455.7	0.0	0.0
72.08	0.85576	2351.87	132.77E+9	132.77E+9	102.167E+9	58.105E+9	5373.9	5373.9	0.0	0.0
79.84	0.92788	2148.34	109.54E+9	109.54E+9	84.291E+9	53.077E+9	4433.6	4433.6	0.0	0.0
87.60	1.00000	1953.87	89.49E+9	89.49E+9	68.863E+9	48.272E+9	3622.1	3622.1	0.0	0.0

The entries in the first column, Elevation, are the vertical locations along the support-structure centerline relative to the MSL. HtFract is the fractional height along the centerline from the mudline (0.0) to the

tower top (1.0). The rest of columns are similar to those described for the distributed blade properties in [1].

The resulting combined (integrated) tower and monopile mass is 522,617 kg and is centered at 37.172m along the centerline above the mudline. This result follows directly from the overall tower height of 87.6m.

The support structure incorporates 1% critical structural damping in all modes of the isolated structure (without the top mass present), which corresponds to the values used in the DOWEC study from page 21 of [2]. Table 3 below summarizes these undistributed support-structure properties.

Table 3. Undistributed support-structure properties for the tower and monopile used in Phase I

Tower-Top Height Above MSL	87.6 m
Tower-Base Height Above MSL	10 m
Water Depth (From MSL)	20 m
Overall (Integrated) Mass	522,617 kg
c.g. Location (w.r.t. Mudline Along Tower Centerline)	37.172 m
Structural Damping Ratio (All Modes)	1 %

2.2 Phase I Simulations

A set of load-case simulations were defined for the Phase I model. The individual subsystems were modeled as flexible or rigid depending on the actual load case. In addition, the environmental conditions in terms of the wind and wave field were varied. This approach reduced the offshore wind turbine model to the following configurations, which allowed for identification of model-dependent differences in the simulation results:

- Load case 1.X: Modal properties in terms of the coupled subsystem eigenfrequencies
- Load case 2.X: Completely rigid structure
- Load case 3.X: Flexible onshore wind turbine (rigid substructure), using the land-based version of the NREL offshore 5-MW baseline turbine, as documented in [1]
- Load case 4.X: Flexible offshore structure with tower top mass (rigid nacelle and rotor); also referred to as an "inverted pendulum"
- Load case 5.X: Fully flexible offshore wind turbine

All relevant aerodynamic and hydrodynamic effects (e.g., turbulence, tower shadow, dynamic stall, wind shear, and Wheeler stretching) were included in the load cases of Phase I and in subsequent phases as well. Table 4 provides an overview of the analyzed load cases in Phase I.

Table 4. Summary specifications for the Phase I load-case simulations

Load Case	Enabled DOFs	Wind Conditions	Wave Conditions	Analysis Type
1.1	Substructure, tower, drivetrain, blades	None: air density = 0	None: water density = 0	Eigenanalysis without gravity or damping
1.2	Substructure, tower, drivetrain, blades	None: air density = 0	None: water density = 0	Eigenanalysis with gravity and structural damping
2.1a	None: constant rotor speed and fixed blade pitch	Steady, uniform, no shear: V_{hub} = 8 m/s	None: water density = 0	Periodic time-series solution
2.1b	None: rotor speed and blade pitch via controller	Steady, uniform, no shear: V_{hub} = 8 m/s	None: water density = 0	Periodic time-series solution
2.2	None: rotor speed and blade pitch via controller	Turbulent: V_{hub} = V_r (11.4 m/s), σ_1 = 1.981 m/s, Mann model	None: water density = 0	Time-series statistics, DELs, power spectra
2.3	None: rotor speed and blade pitch via controller	Turbulent: V_{hub} = 18 m/s, σ_1 = 2.674 m/s, Mann model	None: water density = 0	Time-series statistics, DELs, power spectra
2.4	None	None: air density = 0	Regular Airy: H = 6 m, T = 10 s	Periodic time-series solution
2.5	None	None: air density = 0	Irregular Airy: H_s = 6 m, T_p = 10 s, Pierson-Moskowitz wave spectrum	Time-series statistics, DELs, power spectra
2.6	None	None: air density = 0	Regular stream function (Dean): H = 6 m, T = 10 s	Periodic time-series solution
3.1	Tower, drivetrain, blades	Steady, uniform, no shear: V_{hub} = 8 m/s	None: water density = 0	Periodic time-series solution
3.2	Tower, drivetrain, blades	Turbulent: V_{hub} = V_r (11.4 m/s), σ_1 = 1.981 m/s, Mann model	None: water density = 0	Time-series statistics, DELs, power spectra
3.3	Tower, drivetrain, blades	Turbulent: V_{hub} = 18 m/s, σ_1 = 2.674 m/s, Mann model	None: water density = 0	Time-series statistics, DELs, power spectra
4.1	Substructure, tower	None: air density = 0	Regular Airy: H = 6 m, T = 10 s	Periodic time-series solution
4.2	Substructure, tower	None: air density = 0	Irregular Airy: H_s = 6 m, T_p = 10 s, Pierson-Moskowitz wave spectrum	Time-series statistics, DELs, power spectra
4.3	Substructure, tower	None: air density = 0	Regular stream function (Dean): H = 6 m, T = 10 s	Periodic time-series solution
5.1	Substructure, tower, drivetrain, blades	Steady, uniform, no shear: V_{hub} = 8 m/s	Regular Airy: H = 6 m, T = 10 s	Periodic time-series solution
5.2	Substructure, tower, drivetrain, blades	Turbulent: V_{hub} = V_r (11.4 m/s), σ_1 = 1.981 m/s, Mann model	Irregular Airy: H_s = 6 m, T_p = 10 s, Pierson-Moskowitz wave spectrum	Time-series statistics, DELs, power spectra
5.3	Substructure, tower, drivetrain, blades	Turbulent: V_{hub} = 18 m/s, σ_1 = 2.674 m/s, Mann model	Irregular Airy: H_s = 6 m, T_p = 10 s, Pierson-Moskowitz wave spectrum	Time-series statistics, DELs, power spectra

H – individual wave height	T_p – peak-spectral wave period	V_r – rated wind speed	
H_s – significant wave height	V_{hub} – hub-height wind speed	σ_1 – longitudinal wind speed	
T – individual wave period	averaged over 10 minutes	standard deviation	

Initial transients were present in the first 30 s of most dynamic simulations. These transients have been mostly excluded from the results presented below. Therefore, the first 30 s of the 90-s simulations for the deterministic load cases, as well as the first 30 s of the 630-s simulations involving stochastic conditions, were eliminated.

For each load case, a total of 47 sensors, as indicated in Figure 2, were analyzed. The analyses of the sensors were performed for the deterministic load cases in the time domain and for the stochastic load

cases in the frequency domain (in terms of power spectra), as well as on the basis of statistical parameters and damage-equivalent loads (DELs).

2.3 Phase I Participants and Codes

Phase I results were submitted by participants from the National Renewable Energy Laboratory (NREL) of the U.S.; Garrad Hassan & Partners Limited (GH) of the UK; the National Renewable Energies Center (CENER) of Spain; the Fraunhofer Institute for Wind Energy and Energy System Technology (IWES) and the Endowed Chair of Wind Energy at the University of Stuttgart (SWE) of Germany; and Risø National Laboratory, Det Norsk Veritas (DNV), Vestas Wind Systems, Siemens Windpower, and Danish Oil and Natural Gas Energy (DONG) all of Denmark.
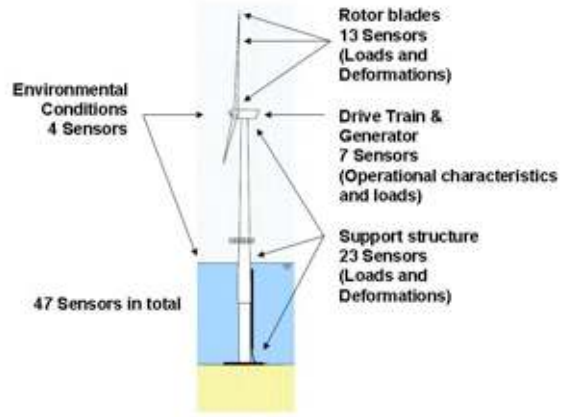
Figure 2. Selected sensors for Phase I simulations

Most of the aero-hydro-servo-elastic codes that have been developed for modeling the dynamic response of offshore wind turbines were tested within OC3. The existing modeling capabilities of the simulation tools used by (and for some, developed by) each participant in Phase I are summarized in Table 5. In the cases where Table 5 shows the same code being used by multiple OC3 participants, the model development, simulation runs, and data processing were done independently.

Table 5. Overview of aero-hydro-servo-elastic modeling capabilities

FAST	FLEX5	Bladed	Bladed Multibody	ADAMS	SIMPACK	HAWC	HAWC2	BHawC	ADCoS-Offshore
Code Developer									
NREL	DTU	GH	GH	MSC + NREL	SIMPACK + SWE + NREL	Risø	Risø	Risø + Siemens	ADC + IWES
OC3 Participant									
NREL + CENER	DONG + SWE + Vestas	CENER + GH	GH	NREL	SWE	DNV + Risø	Risø	Siemens	IWES
Aerodynamics									
(BEM or GDW) + DS	(BEM or GDW) + DS	(BEM or GDW) + DS	(BEM or GDW) + DS	(BEM or GDW) + DS	(BEM or GDW) + DS	(BEM or GDW) + DS	(BEM or GDW) + DS	(BEM or GDW) + DS	(BEM or GDW) + DS
Hydrodynamics									
(Airy$^+$ or UD) + ME	(Airy$^+$ or UD or Stream) + ME	(Airy$^+$ or Stream) + ME	(Airy$^+$ or Stream) + ME	(Airy$^+$ or UD) + ME	None	(Airy$^+$ or UD) + ME	(Airy$^+$ or UD) + ME	(Airy$^+$ or UD) + ME	(Airy$^+$ or UD) + ME
Control System (servo)									
DLL, UD, SM	DLL, UD	DLL	DLL	DLL, UD	DLL, UD	DLL, UD	DLL, UD, SM	DLL, UD	DLL, UD
Structural Dynamics (Elastic)									
FEM^P + (Modal / MBS)	FEM^P + (Modal / MBS)	FEM^P + (Modal / MBS)	MBS	MBS	MBS	FEM	MBS / FEM	MBS / FEM	FEM

ADC – Aero Dynamik Consult Ingenieurgesellschaft mbH **Airy$^+$** – Airy wave theory; (+) with free surface connections **BEM** – blade-element/momentum **DLL** – external dynamic link library	**DS** – dynamic stall **GDW** – generalized dynamic wake **FEM^P** – finite-element method; (P) for mode preprocessing only **MBS** – multibody-dynamics formulation	**ME** – Morison's equation **MSC** – MSC Software Corporation **SM** – interface to Simulink® with MATLAB® **UD** – implementation through user-defined subroutine available

2.4 Phase I Results

2.4.1 Turbulent Wind Field

Turbulent wind conditions were considered for a number of load cases using two sets of turbulent wind fields. These turbulence fields were created with the International Electrotechnical Commission (IEC) Turbulence Simulator from the WAsP Engineering model [3], one at V_{hub} = 11.4 m/s, i.e., rated wind speed and one at V_{hub} = 18 m/s, i.e., in the full load range of the turbine. Both turbulence fields were created with the Mann model [4] in conformity with IEC61400-1 ed.3 using a reference value of I_{ref} = 0.14 for the turbulence intensity. The turbulence datasets were shared with the project partners and used by all for wind load calculations. Both wind field sets were defined in a rectangular grid, as well as in a polar grid, due to requirements within the different codes.

The fields consisted of 8,192 longitudinal planes of cross-sectional grids consisting of 32×32 points for the rectangular format and 16×64+1 point for the polar format. The turbulence fields were established in the rectangular grid first and subsequently interpolated into the polar grid to ensure that the same wind fields were used in the simulations of all codes. However, certain differences between the turbulence fields in the rectangular and polar grid were introduced by the interpolation. Also, the codes requiring the use of a polar grid employed two interpolations (one to create the polar grid and one to interpolate within the grid). These codes exhibited smoother characteristics than the codes using the rectangular grid, which only invoke one interpolation (to interpolate within the grid). This issue was investigated by Thomsen [5] based on simulations with the HAWC2 code applied to a rigid structure with fixed rotor speed and pitch angle and a mean wind speed of 11 m/s at hub height. This approach introduced no differences from the dynamics and controller. Thomsen quantified the differences on the basis of time histories and spectra (i.e., for the relative velocity and angle of attack on a fixed position of one rotor blade, with a radial position of 48 m from the hub center).

Extracted parts from the resulting time histories are given in Figure 3 for the inflow velocity as well as for the angle of attack. The pictures clearly show that the turbulence in the polar grid becomes smoother by the interpolation, affecting the aerodynamic inflow conditions at the rotor blades.
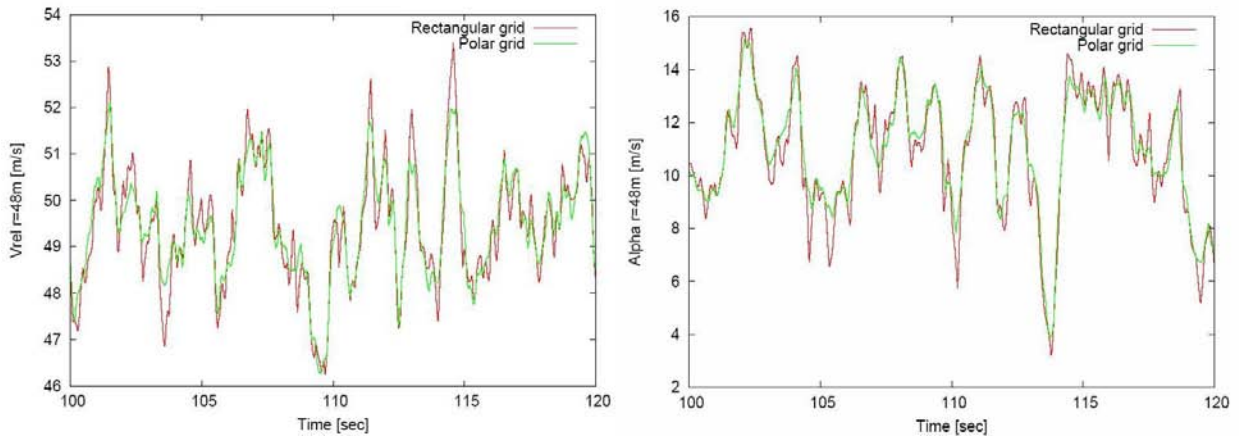
Figure 3. Time history for the inflow velocity (left) and the angle of attack (right) of blade 1 at a radial position of 48 m from the hub center

Table 6 compares the relation of DELs of a rotor blade and the tower obtained for the rectangular and polar grid simulations. The Wöhler material exponent (*m*) used in each DEL calculation is given. While differences of 2–4% occurred for a rotor blade, a difference of more than 10% was introduced for the tower. This must be considered when comparing the results from the codes that use rectangular wind field grids to results from codes that use polar wind field grids. The smoothing effect of the two interpolations is even larger with a more coarse resolution of the grids.

Table 6. Relation of damage-equivalent loads (Rectangular/Polar)

Flapwise blade-root moment (*m*=12)	1.04
Edgewise blade-root moment (*m*=12)	1.02
Tower-bottom fore-aft moment (*m*=4)	1.11

2.4.2 Incident Waves

Wave kinematics for the deterministic and the stochastic wave conditions have been derived using the standard wave generator model from GH Bladed and were used by all partners for wave load calculations. In total, the water particle velocities as well as accelerations were provided with time step sizes of 0.1 seconds (s) for all three spatial directions of 42 nodes along the monopile, with closer nodal spacing in the sea-surface elevation range.

The following waves were included in Phase I simulations of OC3:

- Linear, regular wave based on Airy theory with Wheeler stretching
  $H = 6$ m (wave height), $T = 10$ s (wave period)

- Non-linear, regular wave based on stream function theory according to Chaplin [6]
  $H = 6$ m (wave height), $T = 10$ s (wave period)

- Linear, irregular wave based on composition of Airy waves with Wheeler stretching
  $H_s = 6$ m (significant wave height), $T_p = 10$ s (peak-spectral wave period)

Irregular waves were modeled based on spectra for sea-surface elevations. Such spectra provide information on the energy content dependent on the wave frequencies (i.e., inverse wave periods) of the single wave trains included in the sea state. Commonly, either the Pierson-Moskowitz spectrum for fully developed sea states or the JONSWAP spectrum for developing sea states is used. As shown in Figure 4,

Pierson-Moskowitz spectra show a less pronounced peak at the peak frequency $f_p=1/T_p$, but larger energy contents in the frequency ranges that were approximately 10–15% higher or lower than the peak frequency. Therefore, support structures with natural frequencies outside the peak frequency of a particular sea state experience larger hydrodynamic excitations from fully developed sea states compared to the developing sea-state situation. Certain hydrodynamic excitations of the support structure were desired within the course of OC3 because one of the main objectives is the verification of the coupled aerodynamics, hydrodynamics and structural dynamics of the simulation codes.

The support-structure configuration applied for Phase I has a first eigenfrequency in the range of 0.28 Hertz (Hz), while the support-structure configuration with the flexible foundation of Phase II has an even lower natural frequency of approx. 0.25 Hz. Figure 4 shows the Pierson-Moskowitz spectrum and the JONSWAP spectrum for a peakedness factor of $\gamma = 3.3$ based on the expression by Goda [7] for the irregular wave as well as the first eigenfrequencies of the support-structure configurations applied for Phases I and II.
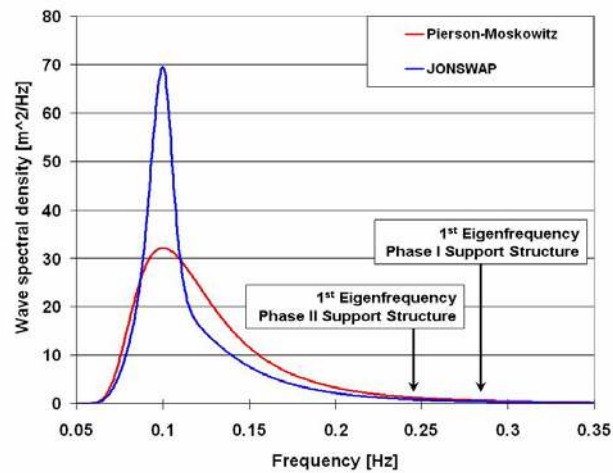
Figure 4. Pierson-Moskowitz and JONSWAP spectra

The main energy content of both spectra were rather low in the range of the first support-structure eigenfrequencies, especially for the Phase I configuration. Relative to the JONSWAP spectrum, the Pierson-Moskowitz spectrum shows approximately 50% larger energy content in the relevant frequency range for wave response dynamic amplification effects and was therefore selected for the Phase I and II investigations of OC3.

2.4.3 Exemplary Results of Comparison

In general, the results from most of the different simulation codes compare very well. However, this was only achieved within a process that included adjustments to codes, modifications to the implementation of the controller interface, and corrections of misinterpreted turbine data specifications and sign conventions. The results provided here are the result of up to five revisions of the simulations and are presented as coupled eigenfrequencies of the main subsystems, time histories for the deterministic load cases, and power spectra for the stochastic load cases. The legend in Figure 5 delineates how the results are presented in the figures that follow. The color shade and line type distinguish the results from separate participants and codes. Some results were not processed by all of the OC3 participants, which is why some of the predictions are left blank or have a zero value. Only a small subset of the results is presented.
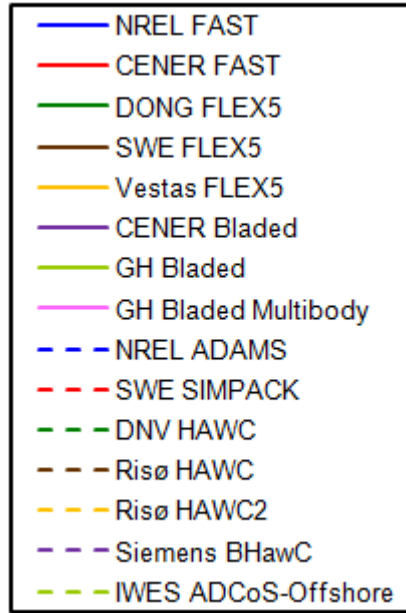
Figure 5. Legend for the Phase I simulation results

2.4.3.1 Full-System Eigenanalysis

Figure 6 gives the lowest 13 natural frequencies calculated for the stationary—but fully flexible—offshore wind turbine atop a monopile with a rigid foundation from load case 1.2. The designation of "pitch" and "yaw" in the asymmetric flapwise and edgewise blade modes identifies coupling of the blade motions with the nacelle-pitching and nacelle-yawing motions respectively.
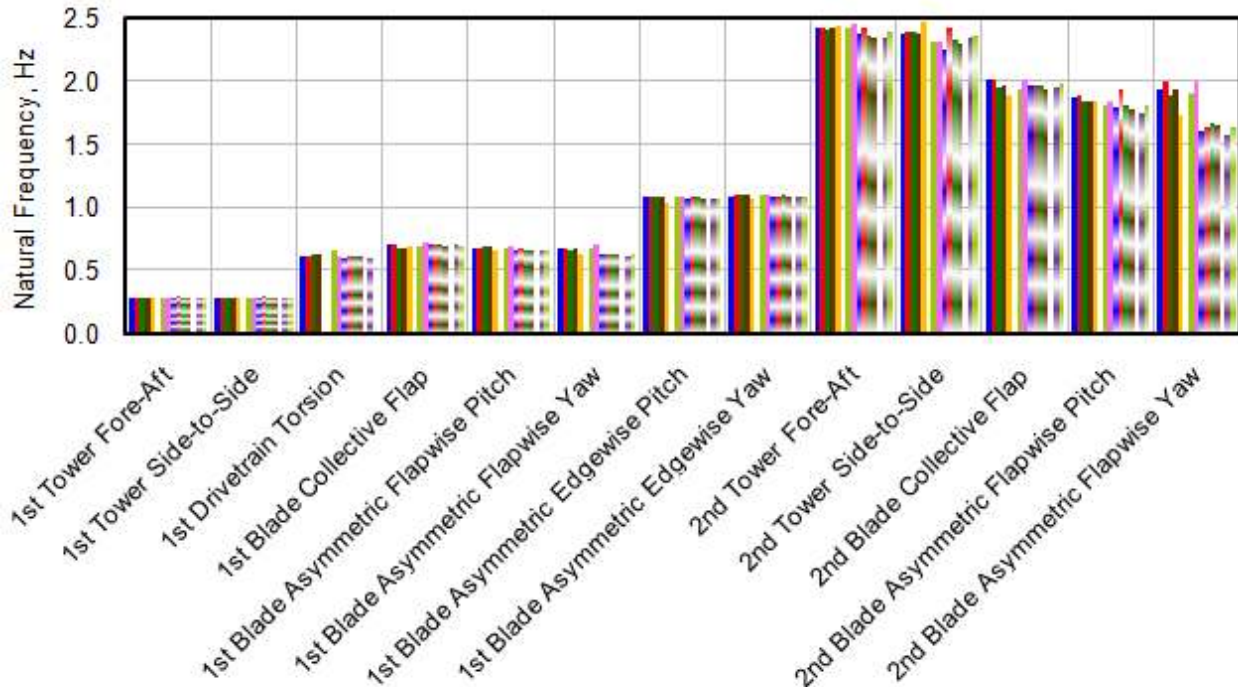
Figure 6. Full-system natural frequencies from load case 1.2

The figure shows that the first eigenfrequencies of the subsystems compare very well for all codes; significant differences occur only for the second tower- and blade-bending eigenfrequencies. For the most part, the modal-based codes predict higher natural frequencies than the multibody- and FEM-based codes for the second tower- and blade-bending eigenfrequencies. Differences can therefore be expected in the higher frequency range in the results of the different codes.

2.4.3.2 Periodic Loads in the Rigid System from Rotor Aerodynamics

Figure 7 and Figure 8 show results for the blade-root loads and the rotor torque from load case 2.1a (i.e., for rigid subsystems and fixed rotor speed and pitch angle). The simulation time of 0 s represents the end of the 30-s start-up transient. This load case was mainly intended to compare the aerodynamic loads as calculated by the individual codes. No hydrodynamic loads were included while a constant wind speed of 8 m/s (i.e. well below rated) and a constant rotor rotation of 9 rotations per minutes (rpm) is applied.
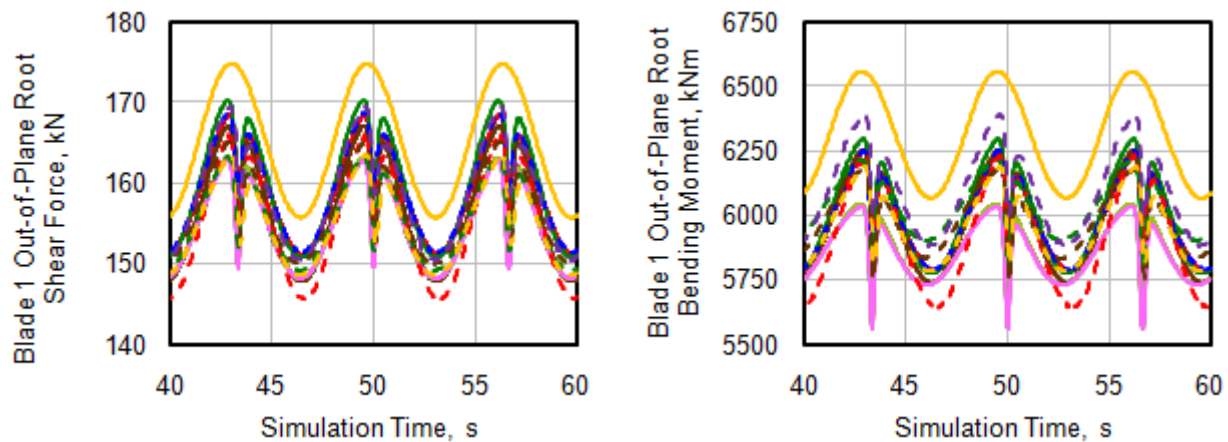
Figure 7. Time series of blade 1 out-of-plane shear force (left) and bending moment (right) at the root for load case 2.1a
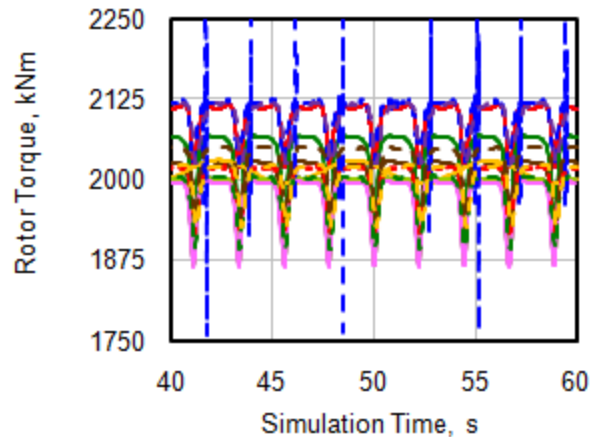
Figure 8. Time series of the rotor torque for load case 2.1a

The figures show very well that differences were apparent in the aerodynamic blade-load calculations. This is due to the variety of aerodynamic models and corrections that were implemented into the individual codes. The differences in the mean magnitude of rotor torque in Figure 8, for example, were

about 5%. The oscillating behaviour is the result of gravity, shaft tilt, and tower shadow influence. The "spikes" in the ADAMS rotor-torque output were the result of numerical problems in the way the code enforces the rigid-system constraints. In practice, these would need to be filtered out.

Similar trends, with a bit larger difference, can be observed in the results from load case 2.1b, which differs from 2.1a in the consideration of the controller, i.e., the variable-speed generator torque is included, so that the rotor speed is a result of the shaft-torque equilibrium instead of the prescribed (fixed) speed. Figure 9 presents comparisons of the results for the rotor torque and the thrust force at yaw bearing level from load case 2.1b.
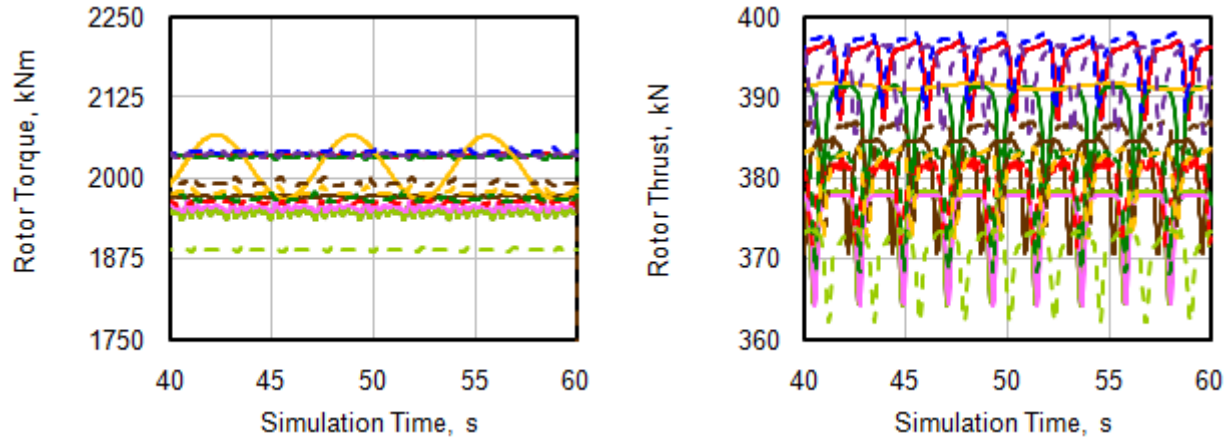
Figure 9. Time series of rotor torque (left) and thrust force (right) on yaw bearing level for load case 2.1b

2.4.3.3 Aero-Servo-Elastic Response of the Land-Based Turbine from Turbulent Winds

Load case set 3.X considered a flexible system under wind excitation only (i.e., a land-based wind turbine). Both deterministic and stochastic wind fields were included. The results from the different codes generally compared very well, especially for the stochastic load case 3.2 (i.e. at rated wind speed) and 3.3 (i.e., well above rated wind speed). Here, differences caused by aerodynamic blade-load calculations were somewhat compensated by the pitch controller. Power spectra are shown for load case 3.2 in Figure 10 and Figure 11 for the out-of-plane and in-plane root bending moments and tip deflections of blade 1. Larger differences occur particularly for the in-plane blade loads and deflections. However, the results still compare very well in the frequency range of high energy contents (i.e., at approximately 0.2 Hz [once-per-revolution]) as well as in the frequency range of approximately 1 Hz (i.e., the first edgewise blade eigenfrequency[†]). The out-of-plane results, on the other hand, compare very well for the individual codes.

[†] The edgewise direction is parallel to in-plane for this load case with a 0° pitch angle.
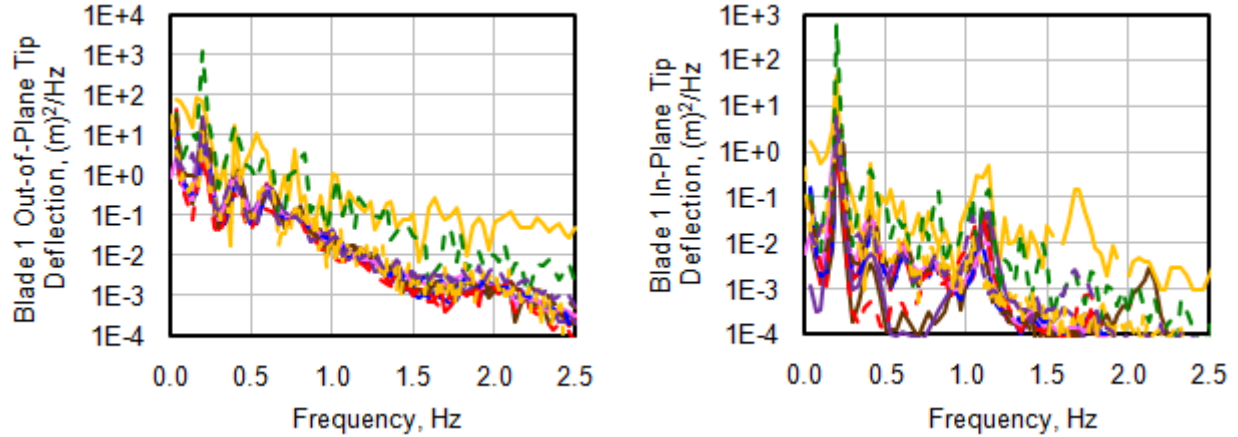
Figure 10. Power spectra of out-of-plane (left) and in-plane (right) tip deflections of blade 1 for load case 3.2
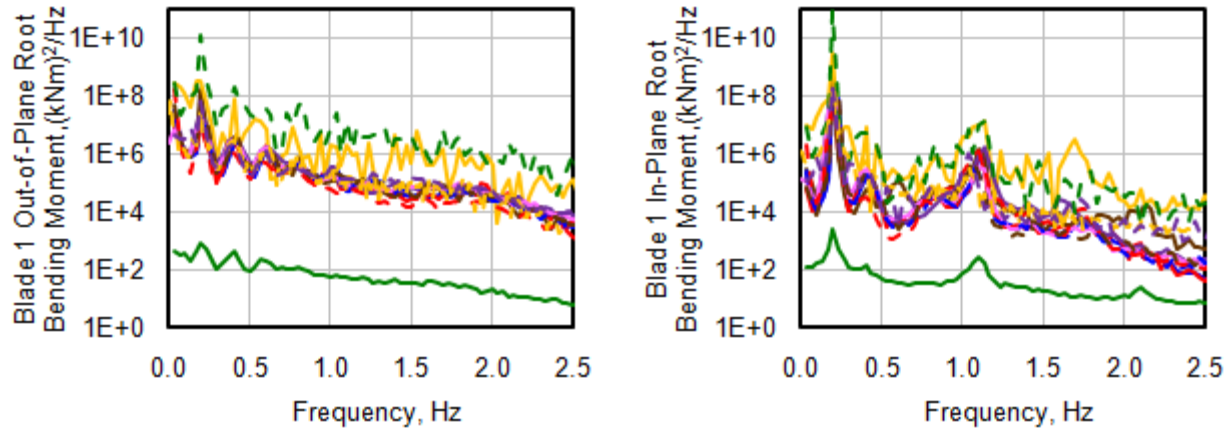
Figure 11. Power spectra of out-of-plane (left) and in-plane (right) root bending moment of blade 1 for load case 3.2

The power spectra output by DNV with HAWC and DONG and Vestas with FLEX5 are similar in form to the power spectra output by the other codes, but differ in orders of magnitude. These differences are likely the result of improper scaling of the power spectra by DNV, DONG, and Vestas; the statistical variations (standard deviations squared)—which should equal the integral of the power spectra across all frequencies—agree better between these and the other codes (but are not shown here).

It should also be noted that some codes include the torsional flexibility of the blades whereas others neglect this flexibility. Tip twists of up to 4 degrees were seen by those codes that include blade torsion in some of the simulations. Here again, differences in the resulting aerodynamic blade loads were somewhat compensated by the pitch controller.

2.4.3.4 Hydro-Elastic Response of Inverted Pendulum with Regular Waves

Results for the 4.X load set (i.e., the flexible offshore structure with no wind data and a rigid rotor-nacelle assembly) also compare very well. Significant differences occur only in the frequency ranges well above the excitation frequency range in which the responses show low energy content. Figure 12 shows the base shear and overturning moment as representative sensors for the deterministic load case 4.3, which uses

the non-linear, regular (periodic) wave. Only very small differences can be observed, except from FLEX5 by Vestas, which (1) is phase-shifted from the other codes as a result of a phase shift in the wave elevation and (2) includes a sign reversal in the base overturning moment. The small differences between the codes were introduced by different structural discretizations, especially in the vicinity of the free sea surface.
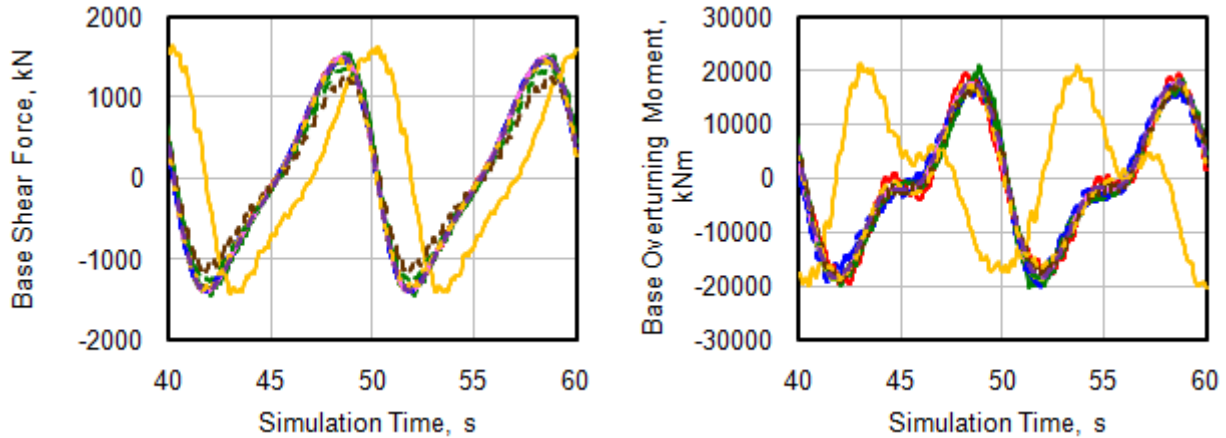
Figure 12. Time history of base shear force (left) and overturning moment (right) for load case 4.3

2.4.3.5 Fully Coupled Aero-Hydro-Servo-Elastic Response

The fully coupled, flexible offshore wind turbine was considered in the load sets 5.X. The following figures show various results from load case 5.3. Here, stochastic wind and wave conditions were applied. Figure 13 shows the generator power as well as the thrust force at yaw bearing level, while Figure 14 addresses the spectral responses of base shear and overturning moment. Figure 15 and Figure 16 show the flapwise and edgewise bending moments of blade 1 at a radial position of 50% of the span and the blade-root pitch moment respectively. The mean wind speed is at 18 m/s (i.e., well above rated). The blade-root pitch moment response agreed well despite a large influence on the overall turbine behaviour introduced by the pitch controller and the differing individual code fidelities in their respective blade models.
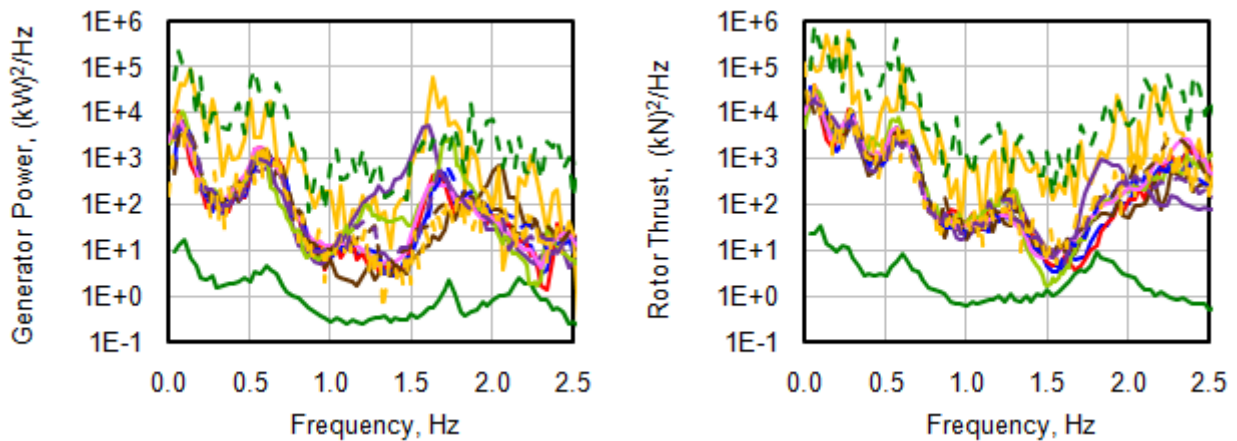
Figure 13. Power spectra of the generator power (left) and thrust force on yaw bearing level (right) for load case 5.3
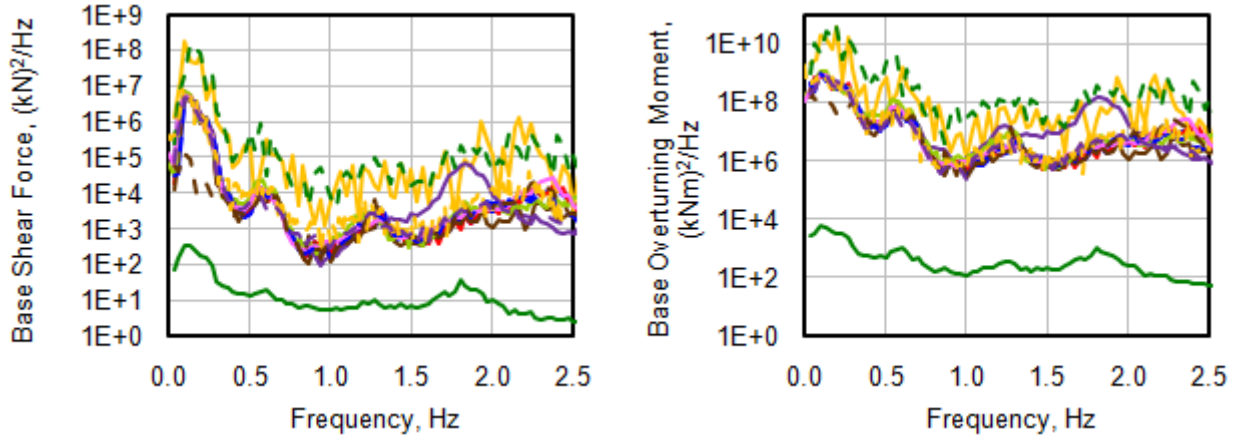
Figure 14. Power spectra of base shear force (left) and overturning moment (right) for load case 5.3
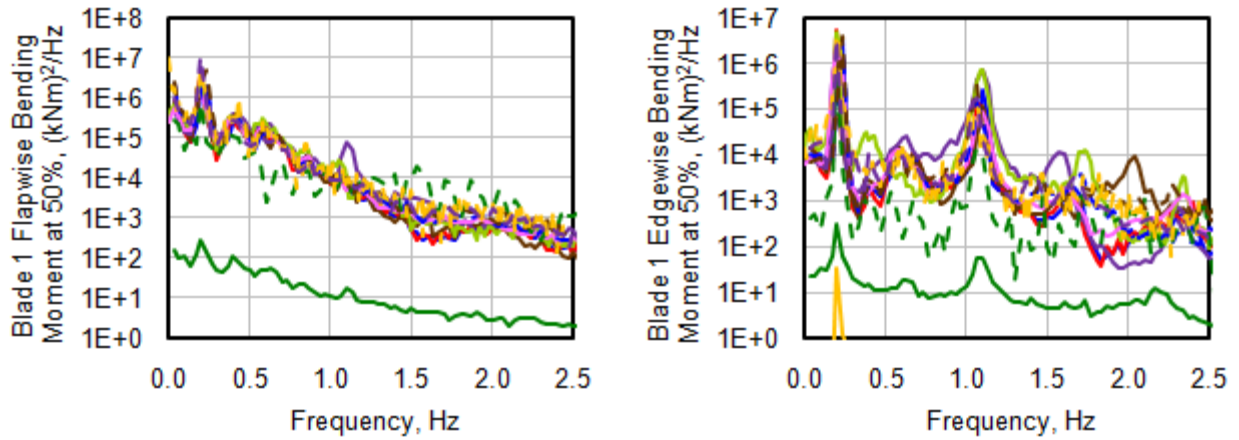
Figure 15. Power spectra of flapwise (left) and edgewise (right) bending moment at 50% span of blade 1 for load case 5.3
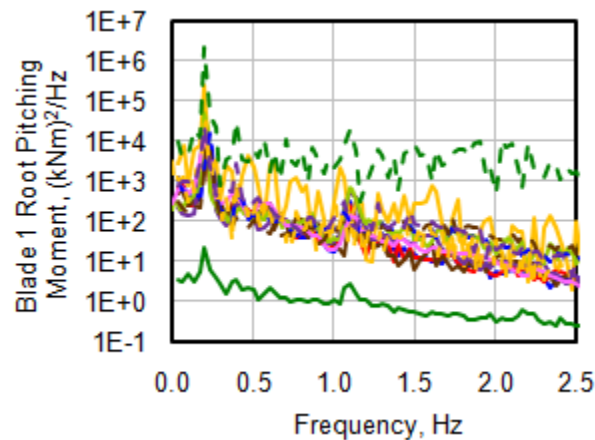
Figure 16. Power spectra of the blade-root pitching moment for load case 5.3

Other than the order of magnitude differences observed in the power spectra output by DNV with HAWC and DONG and Vestas with FLEX5, as reported earlier, in general the results compared very well for the

different codes. This is especially true in the frequency range up to 1.5 Hz. The differences in the higher frequency ranges were influenced by differences in the higher modes of the coupled subsystems as calculated by the individual codes.

However, no significant additional differences are apparent when comparing the results of the fully coupled system load sets 5.X with the results of the simplified system load sets 2.X to 4.X. It can therefore be assumed that the differences in the 5.X load sets were introduced by the same sources as previously identified for the simplified system load-case sets (i.e., different turbulence description, different modal properties of the coupled subsystems, and different rotor aerodynamics between the individual codes).

2.5 Phase I Conclusions

In Phase I of OC3, participants used an assortment of codes to model the coupled dynamic response of the NREL 5-MW wind turbine installed on a monopile with a rigid foundation in 20 m of water. Code predictions were compared from load-case simulations selected to test different model features. The comparisons have resulted in a greater understanding of offshore wind turbine dynamics and modeling techniques and better knowledge of the validity of various approximations. Although the code-to-code comparisons in Phase I agreed very well, in general, the key reasons for the remaining differences were as follows:

- The modal-based codes predict slightly different second and higher coupled eigenmodes than are predicted by the higher fidelity multibody- and FEM-based codes. Differences in the dynamic response and energy content are, therefore, to be expected in the higher frequency range.

- The codes that rely on full-field wind available in polar coordinates predict smoother aerodynamic loads (thus smaller load deviations and smaller DELs) than codes that rely on rectangular coordinates. This results from the method by which the wind datasets were generated. To ensure that all participants used the same wind inflow, the full-field wind datasets were generated in rectangular coordinates and subsequently interpolated to polar coordinates for the codes that needed them. These differences were mitigated as much as possible by using a fine spatial resolution (32×32 points across the rotor disk).

- The differences among the codes relating to the implementation of aerodynamic induction, tower interference, hub and tip loss, and dynamic stall models—and whether or not the aerodynamic loads were applied in the deflected or undeflected blade state—attribute to variations in the mean values of several key wind turbine loads (e.g., blade-root bending moments, rotor torque, and rotor thrust).

- The blade-pitch controller compensates somewhat for variations that might have been caused between codes with differing aerodynamics and between codes that do and do not have blade-twist degrees of freedom (DOFs).

- Differing model discretizations for the aerodynamic and hydrodynamic loads lead to differences among the code predictions. This is most apparent in the substructure loads that depended highly on the discretization of hydrodynamic loads near the free surface.

- Though every effort was made to standardize model inputs, user error still occurs. It often takes several revisions before the model is developed and run as intended. It is also possible, in some instances, that errors still remain and account for otherwise unexplainable modeling differences.

2.6 Phase I References

[1] Jonkman J, Butterfield S, Musial W, and Scott G. *Definition of a 5-MW Reference Wind Turbine for Offshore System Development*. NREL/TP-500-38060. NREL: Golden, CO, 2009.

[2] Kooijman HJT, Lindenburg C, Winkelaar D, and van der Hooft EL. *DOWEC 6 MW Pre-Design: Aero-elastic modeling of the DOWEC 6 MW pre-design in PHATAS*. ECN-CX--01-135, DOWEC 10046_009, Petten, the Netherlands: Energy Research Center of the Netherlands, September 2003.

[3] www.waspengineering.dk

[4] Mann J 1998 *Wind Field Simulation*, Prob. Engng. Mech. Vol. 13 No. 4

[5] Thomsen K, 2005 *Comparison of Rectangular and Polar Turbulence Formats* Risø National Laboratory

[6] Chaplin JR, 1990 *The Computation of Non-Linear Waves on a Current of Arbitrary Non-Uniform Profile* OTH 90 327 HMSO

[7] Goda Y, 1979 *A Review on Statistical Interpretation of Wave Data* Report of the Port and HarbourResearch Institute vol. 18 No.2

3. Chapter 3: Monopile with Flexible Foundation Modeling of Phase II

Authors: J. Jonkman and S. Butterfield, National Renewable Energy Laboratory (NREL), USA; P. Passon, Endowed Chair of Wind Energy at the University of Stuttgart (SWE), Germany; T. Larsen, Risø National Laboratory, Denmark; T. Camp and J. Nichols, Garrad Hassan & Partners Limited (GH), UK; J. Azcona and A. Martinez, National Renewable Energies Center (CENER), Spain

3.1 Phase II Model

Phase II of OC3 considered the same NREL 5-MW wind turbine [2], tower, and monopile used in Phase I, but with a flexible foundation. The monopile foundation was designed by SWE and its specifications were supplied to the OC3 participants. The intent of the design was to apply realistic soil properties and typical design procedures, and yet obtain a design that has a noticeable impact on the system's dynamic response to facilitate verification of the foundation models within the codes. Auxiliary effects such as axial displacement, torsion displacement, and scouring are neglected. The resulting design, consequently, may not be an optimal—and may not even be a representative—design solution that is cost effective.

Pile foundations use lateral loading of the soil to withstand the loads induced in the supported structure. Under static lateral loading, typical soils, such as sand or clay, generally behave as a plastic material, which makes it necessary to nonlinearly relate soil resistance, p, to pile / soil deflection, y. The OC3 design used the nonlinear p-y model for sand under cyclic loading conditions as defined by the American Petroleum Institute (API) [3]. This p-y model is dependent on the effective weight, γ, and angle of internal friction, $\varnothing'$, of the sand—as well as on the pile diameter, D, and local soil depth, z. A layered soil profile was chosen with soil density (and $\varnothing'$) increasing with depth. By this approach, a large participation of the soil-pile interactions in the dynamic response could be expected from the upper (less dense, less stiff) layer while the lower (denser, stiffer) layer ensured a sufficient bearing capacity of the soil. Figure 17 illustrates the soil profile and the properties of each soil layer.

The subsoil portion of the monopile was designed to have the same properties (i.e., the same diameter, thickness, and material) as the portion above the soil for the monopile designed and used in Phase I. The pile penetration depth of 36 m was selected to minimize pile head deflections under ultimate loading conditions.

Most of the codes that have been developed for offshore wind turbines do not permit one to model the soil-pile interaction through detailed nonlinear and depth-dependent p-y models. Nor is it appropriate to assume that the API p-y model—which is normally intended for static analysis—is valid for transient dynamic analysis. Instead, most codes use one or more of a number of simplified linear foundation models suitable for dynamic analysis. SWE derived three such models for use in Phase II of the OC3 project. These models are illustrated in Figure 18 and are described below:

Figure 17. Soil profile

- The apparent (or effective) fixity length (AF) model idealizes the monopile with flexible foundation as a cantilever beam whose properties are different above and below the mudline.
- The beam above the mudline has the real properties (i.e., diameter, thickness, and material) of the monopile. The beam below the mudline has effective properties and a fictive length (i.e., the distance from the mudline to the cantilevered base) that are tuned to ensure that the overall response of the monopile above the mudline is the same as the response of the higher fidelity p-y
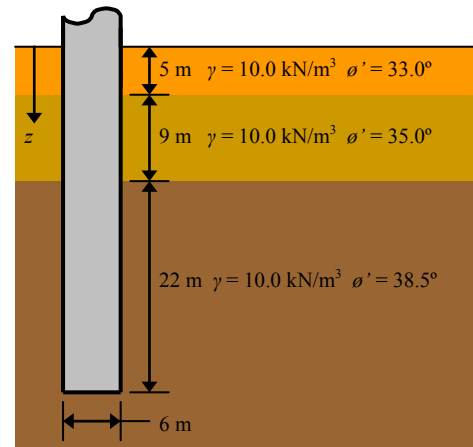
model. The response can only be identical under a particular set of conditions, however, because the AF model is of lower fidelity. In the OC3 project, specifically, the properties of the fictive beam were tuned such that the mudline displacement and rotation for both models would be the same when loaded by a mudline shear force and bending moment that are representative of the loading that exists when the offshore wind turbine is operating under normal conditions.

- The coupled springs (CS) model idealizes the foundation compliance as a set of translational and rotational DOFs with coupled springs (i.e., a stiffness matrix) positioned at the mudline. Above the mudline, the monopile is modeled as a beam with the real properties of the monopile. The mudline spring stiffness constants were derived to give the same response as the AF model under the same loading conditions.

- The distributed springs (DS) model idealizes the monopile with flexible foundation as a free-free beam with lateral (Winkler-type) springs distributed along the subsoil portion of the monopile. The beam uses the real properties of the monopile both above and below the mudline—including the real penetration depth. The subsoil spring stiffness constants are depth-dependent and were calculated based on linearization of the *p-y* model under the same loading conditions chosen for the AF model.
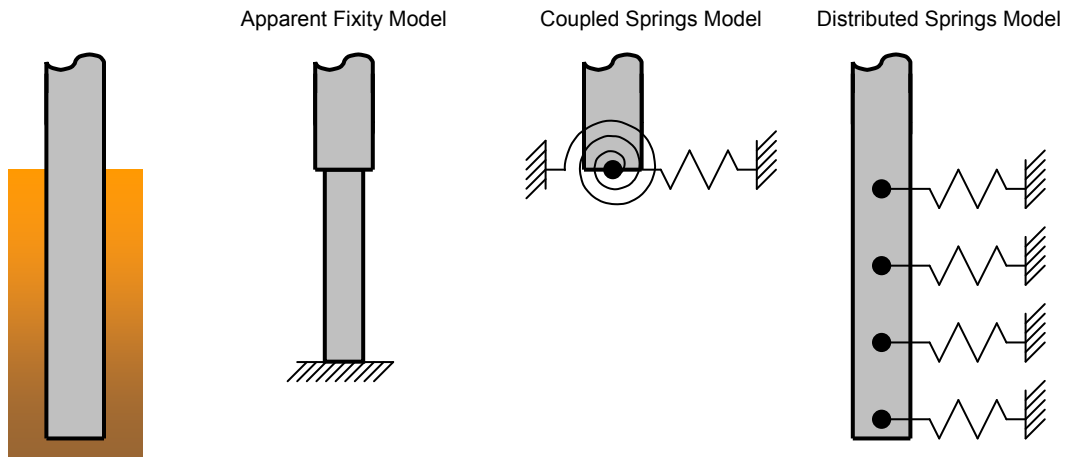
Figure 18. Simplified models of a monopile with flexible foundation

Greater detail on the development and specifications of these foundation models are given in [1].

3.2 Phase II Simulations

A set of load-case simulations were defined for the Phase II model and are summarized in Table 7. The load-case identifiers in Table 7 correspond to the identifiers used by the equivalent simulations from Phase I. In Phase II, though, it was not necessary to independently test the aerodynamic, hydrodynamic, and aero-servo-elastic models—as was done in Phase I—because these models were identical between Phases I and II. Fewer combinations of wind and wave conditions were also needed to test the foundation models in Phase II. Consequently, the set of simulations from Phase II was much smaller than the set used in Phase I and the load-case identifiers are not sequential as a result.

Table 7. Summary specifications for the Phase II load-case simulations

Load Case	Enabled DOFs	Wind Conditions	Wave Conditions	Analysis Type
1.2	Foundation, substructure, tower, drivetrain, blades	None: air density = 0	None: water density = 0	Eigenanalysis
4.1	Foundation, substructure, tower	None: air density = 0	Regular Airy: H = 6 m, T = 10 s	Periodic time-series solution
4.2	Foundation, substructure, tower	None: air density = 0	Irregular Airy: H_s = 6 m, T_p = 10 s	Time-series statistics, DELs, power spectra
5.2	Foundation, substructure, tower, drivetrain, blades	Turbulent: V_{hub} = V_r (11.4 m/s), σ_1 = 1.981 m/s, Mann model	Irregular Airy: H_s = 6 m, T_p = 10 s, Pierson-Moskowitz wave spectrum	Time-series statistics, DELs, power spectra

H	– individual wave height	T_p	– peak-spectral wave period	V_r	– rated wind speed
H_s	– significant wave height	V_{hub}	– hub-height wind speed averaged over 10 minutes	σ_1	– longitudinal wind speed standard deviation
T	– individual wave period				

For each load-case simulation, a total of 57 model outputs were analyzed. In addition to the 47 outputs analyzed in Phase I for the rotor, drivetrain, nacelle, tower, monopile, and environment, 10 outputs were used in Phase II to analyze the loads and deformations within the now-flexible foundation.

3.2.1 Additional Phase II Analyses

In Phase II, a separate set of load-case simulations was also run to verify the conclusion from Phase I that many of the code-to-code differences were the result of differing implementations of the aerodynamics models. To verify this conclusion, load cases 5.1, 5.2, and 5.3 from Phase I were run by all OC3 participants in Phase II with no aerodynamic induction, no tower interference, no hub and tip losses, and no dynamic stall (i.e., the aerodynamic loads that were computed within the simulations depended only on the geometric angle of attack, the dynamic pressure of the undisturbed inflow, and the given local force coefficients and chord length). The results (not presented here) showed that the responses were not influenced by model discretization fidelity and confirmed the Phase I conclusion.

3.3 Phase II Participants and Codes

Phase II results were submitted by OC3 participants from the National Renewable Energy Laboratory (NREL) of the U.S., the Endowed Chair of Wind Energy (SWE) at the University of Stuttgart in Germany, Risø National Laboratory of Denmark (Risø), Garrad Hassan & Partners Limited (GH) of the UK, and the National Renewable Energies Center (CENER) of Spain. As in Phase I, NREL applied the FAST and ADAMS codes, GH applied Bladed, SWE applied FLEX5, Risø applied HAWC2, and CENER applied FAST and Bladed. Each of the codes can employ all three of the simplified foundation models.

3.4 Phase II Results

The eigenanalysis and load-case simulations of Phase II were each run by every OC3 participant. The legend in Figure 19 delineates how the results are presented in all of figures included in the subsections that follow. The results from the AF, CS, and DS foundation models are given

NREL FAST AF	NREL FAST CS	NREL FAST DS
CENER FAST AF	CENER FAST CS	CENER FAST DS
CENER Bladed AF		
GH Bladed AF	GH Bladed CS	GH Bladed DS
SWE FLEX5 AF	SWE FLEX5 CS	SWE FLEX5 DS
NREL ADAMS AF	NREL ADAMS CS	NREL ADAMS DS
Risø HAWC2 AF	Risø HAWC2 CS	Risø HAWC DS
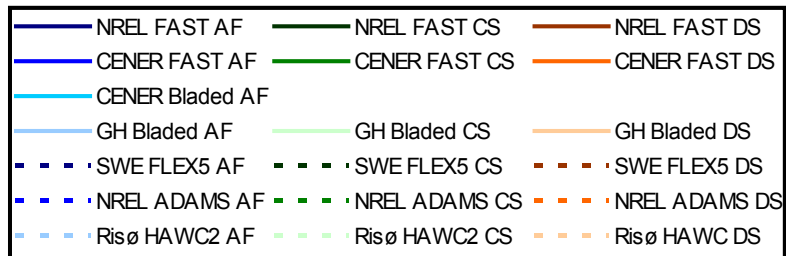
Figure 19. Legend for the Phase II simulation results

in varying shades of blue, green, and orange, respectively. The color shade and line type distinguish the results from separate participants and codes. Only a small subset of the results is presented.

3.4.1 Full-System Eigenanalysis

Figure 20 gives the lowest 13 natural frequencies calculated for the stationary—but fully flexible—offshore wind turbine atop a monopile with flexible foundation from load case 1.2. The designation of "pitch" and "yaw" in the asymmetric flapwise and edgewise blade modes identifies coupling of the blade motions with the nacelle-pitching and nacelle-yawing motions, respectively.

Mode	Description
1	1st Support Structure Fore-Aft
2	1st Support Structure Side-to-Side
3	1st Drivetrain Torsion
4	1st Blade Collective Flap
5	1st Blade Asymmetric Flapwise Pitch
6	1st Blade Asymmetric Flapwise Yaw
7	1st Blade Asymmetric Edgewise Pitch
8	1st Blade Asymmetric Edgewise Yaw
9	2nd Support Structure Fore-Aft
10	2nd Support Structure Side-to-Side
11	2nd Blade Collective Flap
12	2nd Blade Asymmetric Flapwise Pitch
13	2nd Blade Asymmetric Flapwise Yaw
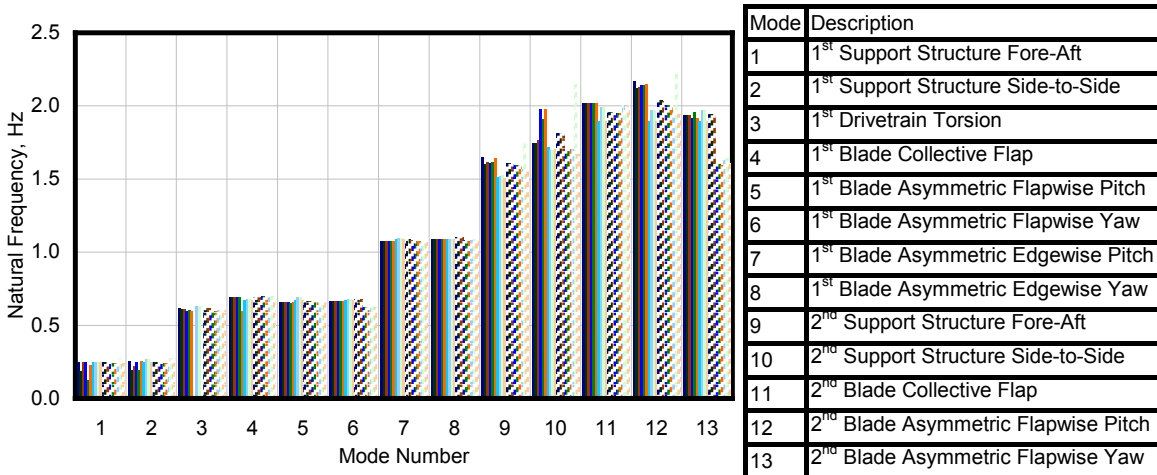
Figure 20. Full-system natural frequencies from load case 1.2

The natural frequencies of the first fore-aft and side-to-side modes of the support structure (Modes 1 and 2) with the CS foundation model are predicted lower by NREL and CENER with the FAST code. Additionally, the natural frequencies of the first and second support structure fore-aft and side-to-side modes (Modes 1, 2, 9, and 10) and the second blade asymmetric flapwise pitch mode (Mode 12) with the CS foundation model are predicted higher by Risø with the HAWC2 code. These lower and higher predictions are both a result of numerical problems in the linearization and eigensolution for the CS foundation model systems. The numerical problems, in turn, are the result of ill conditioning of the linearized system matrices originating from too large of linearization perturbations in FAST and numerical round-off error in HAWC2. The nonlinear time-domain solutions in the FAST and HAWC2 codes, however, are not affected by these numerical problems; the time-domain solutions have response frequencies that are consistent with the other foundation models.

The natural frequencies of the second support-structure side-to-side mode (Mode 10) with all foundation models are predicted higher by CENER with the FAST code. NREL's predictions from FAST of these frequencies, however, are similar to what were predicted by the other codes. These frequencies depend on the mode shapes of the support structure, which are inputs to FAST. CENER found these mode shapes by performing an eigenanalysis on a model of the support structure assembled within NASTRAN, while NREL found them independently using the results of their eigenanalysis from ADAMS. CENER still needs to investigate why NASTRAN predicts different mode shapes as compared to ADAMS.

The addition of the flexible foundation in Phase II reduced the natural frequencies of the support structure by about 10% for the first mode and 25% for the second mode when compared with the responses obtained in Phase I, which employed a rigid foundation. The flexible foundation, however, had little effect on the natural frequencies of the drivetrain and blades, except for the first and second blade

asymmetric flapwise yaw modes (Modes 6 and 13) in the codes (ADAMS and HAWC2) that account for torsion within the support structure. In this mode, the vertically positioned blade remains stationary, while the two other blades flap out of phase with each other. These blade motions couple with torsion of the support structure in ADAMS and HAWC2, which drops the natural frequency when compared to the codes that do not account for support structure torsion (FAST, Bladed, and FLEX5). This coupling is more noticeable in Phase II than in Phase I because the support structure is longer in Phase II, making its effective stiffness lower.

3.4.2 Hydro-Elastic Response of Inverted Pendulum with Regular Waves

Figure 21 shows time histories of the bending moment within the monopile—both at the mudline ($z = 0$ m) and 7 m below the mudline ($z = 7$ m)—from load case 4.1, which models the offshore system as an inverted pendulum (i.e., the system has flexible foundation, substructure, and tower, but rigid rotor-nacelle assembly) excited by regular (i.e., periodic) waves. The responses are shown for one passage (i.e., period) of the wave after all start-up transients have died out. The instantaneous wave elevation at the tower centerline is highest at 50 s and lowest at 55 s. The hydrodynamic loading is dominated by inertia (not viscous drag) because the monopile bending moments are about 90º out-of-phase with the wave elevation.
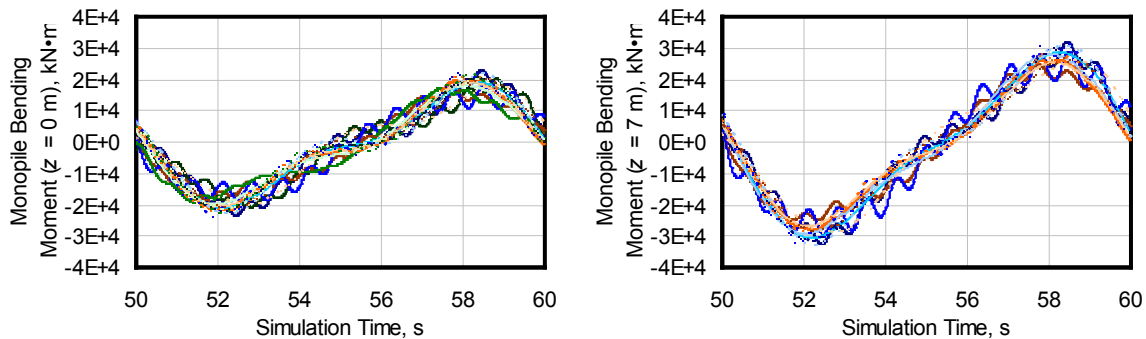
Figure 21. Time histories from load case 4.1

The mean values of the monopile bending moments are predicted very similarly between the codes. The second mode of the support structure (indicated by the higher frequency oscillations), however, gets excited in some codes (FAST, ADAMS) but not the others (Bladed, FLEX5, HAWC2). This difference is more visible in the monopile loads than in the monopile deflections (not shown). The difference is the result of a numerical problem within FAST and ADAMS that exists when they read in externally generated wave data, as is done within the OC3 project. The problem is likely related to how the wave kinematics data are interpolated at the elements passing through the free surface, which might be causing a stepwise loading of these elements that tends to excite high frequencies within the model. The impact of the numerical problem can be mitigated by using a finer discretization of the hydrodynamic loads. Further study will be required, however, to isolate the exact problem and to identify a suitable correction.

The monopile bending moment 7 m below the mudline is slightly higher than the bending moment at the mudline. The location 7 m below the mudline is roughly the location within the foundation where the magnitude of the monopile bending moment reaches its maximum. Surprisingly, the bending moments at this location are predicted very similarly between the AF and DS models by all codes. (There is no output at this location for the CS model.) This similarity between the AF and DS models happens in this case because the soil is least dense (least stiff) in the upper layer and should not be expected between the

models in general. (The AF model is of lower fidelity and should be less accurate than the DS model and should not be used, in general, to predict subsoil pile loads.)

3.4.3 Hydro-Elastic Response of Inverted Pendulum with Irregular Waves

Figure 22 shows response statistics and DELs from load case 4.2, which tests the same model used in load case 4.1, but this time with excitation from irregular (stochastic) waves. The DELs were computed using two different values of the Wöhler material fatigue-strength exponent (*m*) as indicated. Responses of the monopile translational and rotational displacement, shear force, and bending moment at the mudline are presented. These responses were not processed by all of the OC3 participants, which is why some of the predictions are zero-valued.
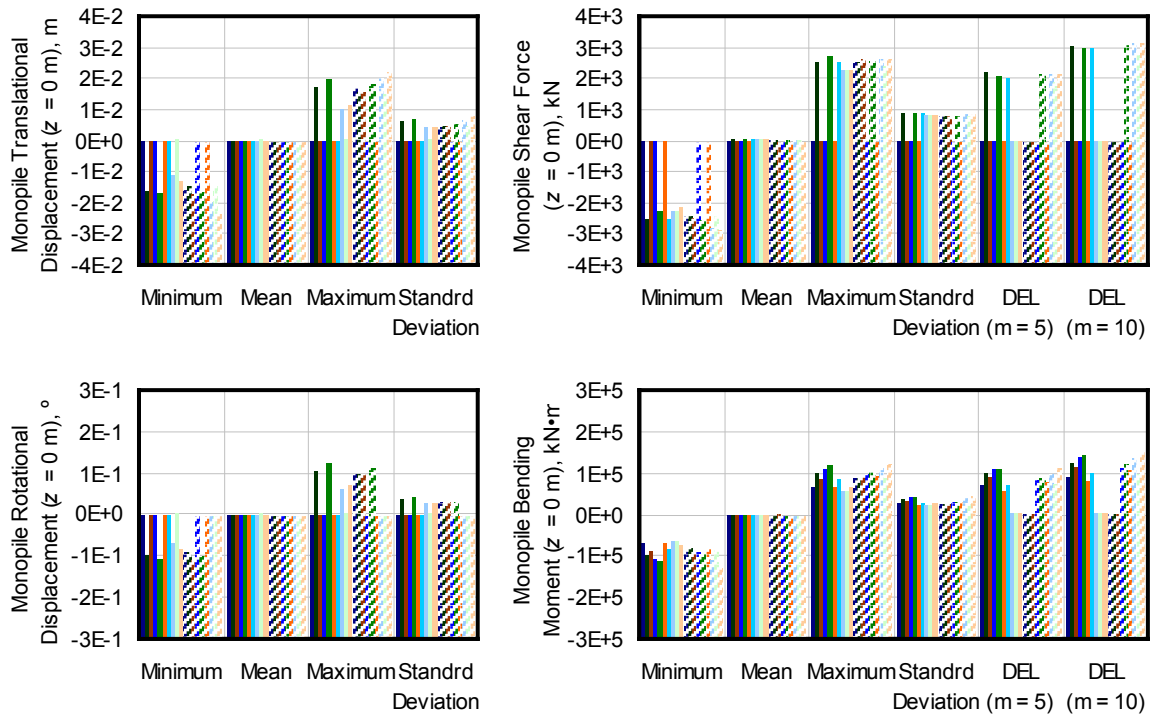
Figure 22. Statistics and DELs from load case 4.2

As in the results from load case 4.1, the near-zero mean values of all outputs are predicted very similarly between the codes in load case 4.2. There is some deviation, however, between the code predictions of the minimums, maximums, standard deviations, and DELs. The deviations between the code predictions are greater for the monopile bending moment at the mudline than for the shear force, which implies that the deviations are perhaps the result of the differing discretizations of the hydrodynamic loads near the free surface. (The discretization of hydrodynamic loads near the free surface has more of an effect on the bending moments than the shear forces because the hydrodynamic loads are weighted by the moment arm—which is largest for the loads at the free surface—in the bending-moment calculation.)

The power spectra of the time series were also calculated for load case 4.2. The power spectra of the monopile shear force and bending moment at the mudline are shown in Figure 23. The predictions are very similar among all the codes at and below the first natural frequency of the support structure (about 0.25 Hz). HAWC2, however, predicts more excitation than FAST, Bladed, FLEX5, and ADAMS across
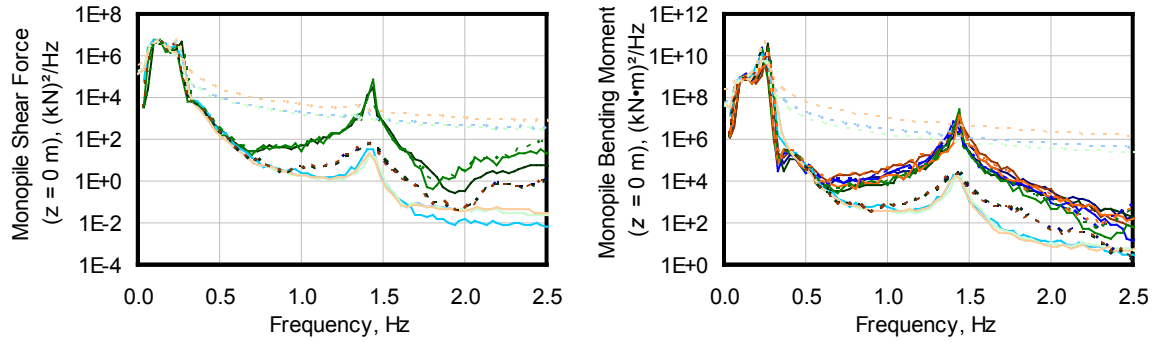
Figure 23. Power spectra from load case 4.2

all higher frequencies (except at 1.45 Hz). Risø still needs to investigate why these power spectra predictions are so different. Additionally, FAST and ADAMS predict more excitation than do Bladed and FLEX5 at the second natural frequency of the support structure (about 1.45 Hz). (The value of 1.45 Hz is lower than what is shown in Figure 20 because the rotor-nacelle assembly is rigid in load case 4.2, which removes any coupling with the blade motions and decreases the natural frequency.) This difference is consistent with the higher frequency oscillations predicted from FAST and ADAMS in load case 4.1 and is believed to be caused by the same numerical problem.

3.4.4 Fully Coupled Aero-Hydro-Servo-Elastic Response

Figure 24 shows the power spectra of the monopile shear force and bending moment at the mudline from load case 5.2, which models the full aero-hydro-servo-elastic response of the offshore wind turbine atop a monopile with flexible foundation subject to stochastic wind and wave loading.
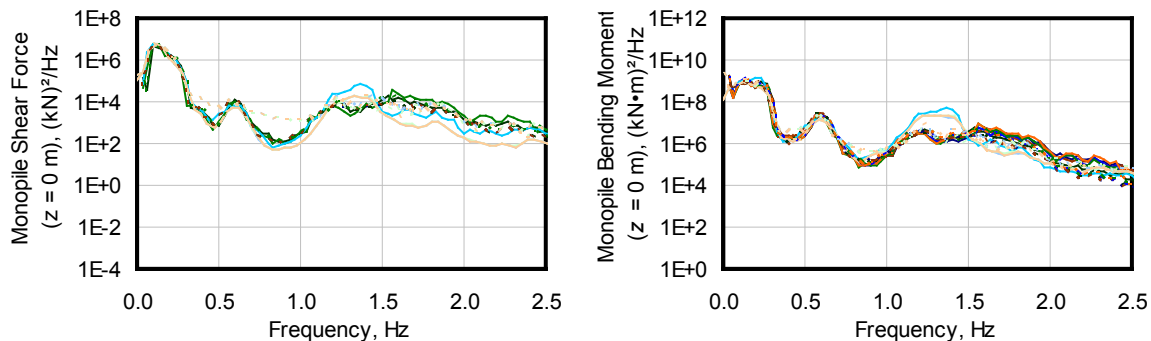
Figure 24. Power spectra from load case 5.2

The results compare very well among the codes, in general, especially in the frequency range encompassing the first natural frequencies of the support structure, drivetrain, and blades (up to about 1.1 Hz). The differences in the higher frequency range are influenced by differences among the codes in their predictions of the higher modes of the coupled system, as well as the other differences already described. What is perhaps surprising, however, is that the codes' predictions of the power spectra in the higher frequency range compare better in load case 5.2 than in load case 4.2. In particular, FAST and ADAMS in load case 5.2 no longer predict higher excitation than the other codes at the second natural frequency of the support structure (they did in load case 4.2—see Figure 23). This improvement among the code predictions implies that the monopile loads at this frequency are heavily influenced (and perhaps being damped out) by the aerodynamic loading, which was absent in load case 4.2. The differing

36

implementations of the aerodynamic models among the codes have more effect on the mean values of the wind turbine loads than on the power spectra.

3.5 Phase II Conclusions

In Phase II of the OC3 project, a variety of project participants using an assortment of codes have modeled the coupled dynamic response of the NREL 5-MW wind turbine installed on a monopile with flexible foundation in 20 m of water. Foundation models included the simple AF model, a CS model, and the more complicated DS model, all of which were tuned to ensure that the overall response of the monopile above the mudline would be the same under a given set of loading conditions. The code predictions from a set of load-case simulations—each selected to test different features of the models—were compared. The comparisons, in general, agreed quite well. Differences that existed among the predictions were traced back to differences in the model fidelity, aerodynamic implementation, hydrodynamic load discretizations, and numerical difficulties within the codes. The key results of Phase II are as follows:

- All of the results of Phase I also apply to the results of Phase II.
- All three of the simplified foundation models—AF, CS, and DS—can be derived and implemented to ensure that the overall response of the system above the mudline is identical under a given set of loading conditions (at least for the lowest system eigenmodes).
- The discretization problems described for the results of Phase I result in higher excitation in the second eigenmodes of the support structure in Phase II. However, this higher excitation is only visible when the turbine is not operating, because aerodynamic loading tends to limit the amount of additional excitation (i.e., aerodynamic loading tends to damp out the excitation).
- The differing implementations of the aerodynamic models among the codes have more effect on the mean values of the wind turbine loads than on the power spectra.

3.6 Phase II References

[1] Passon P. OC3 memo from SWE, *Memorandum: Derivation and Description of the Soil-Pile-Interaction Models*, OC3-Derivation and Description of the Soil-Pile-Interaction Models.pdf, July 7, 2006.

[2] Jonkman J, Butterfield S, Musial W, and Scott G. *Definition of a 5-MW Reference Wind Turbine for Offshore System Development*. NREL/TP-500-38060. NREL: Golden, CO, 2009.

[3] American Petroleum Institute (API), *Recommended Practice for Planning, Designing, and Constructing Fixed Offshore Platforms—Working Stress Design* (API RP 2A-WSD), 21st ed., December 2000.

4. Chapter 4: Tripod Support-Structure Modeling of Phase III

Authors: J. Nichols and T. Camp, Garrad Hassan & Partners Limited (GH) UK; J. Jonkman and S. Butterfield, National Renewable Energy Laboratory (NREL), USA; T. Larsen and A. Hansen, Risø National Laboratory for Sustainable Energy, Technical University of Denmark (Risoe); J. Azcona, A. Martinez, and X. Munduate, National Renewable Energies Center (CENER), Spain; F. Vorpahl and S. Kleinhansl, Fraunhofer Institute for Wind Energy and Energy System Technology (IWES), Germany; M. Kohlmeier, T. Kossel, and C. Böker, Leibniz University of Hannover (LUH), Germany; and D. Kaufer, Endowed Chair of Wind Energy at the University of Stuttgart (SWE), Germany.

4.1 Phase III Model

In Phase III of OC3, the water depth was increased to 45 m and the monopile used in Phases I and II was replaced with a tripod substructure, which is one of the space-frame concepts proposed for offshore installations in water of intermediate depth. The rotor-nacelle assembly of the NREL 5-MW turbine—including the aerodynamic, structural, and control system properties—remained the same as in [2], but the support structure (tower and substructure) was changed. The tripod support structure is shown in Figure 25; the concept is documented in much greater detail in [1].

The tripod structure presents new challenges in wind turbine modeling. For instance, it is not a tree-like structure and has to support dynamic loads through axial forces rather than bending moments. The tripod is also a good test for the offshore structure modeling capabilities of codes because it incorporates a number of features not present in conventional monopile support structures:

- No overall axial symmetry; there is asymmetry between forward and backward and between fore-aft motion and side-side motion
- Different numbers of members connect at various nodes
- The central member is significantly tapered
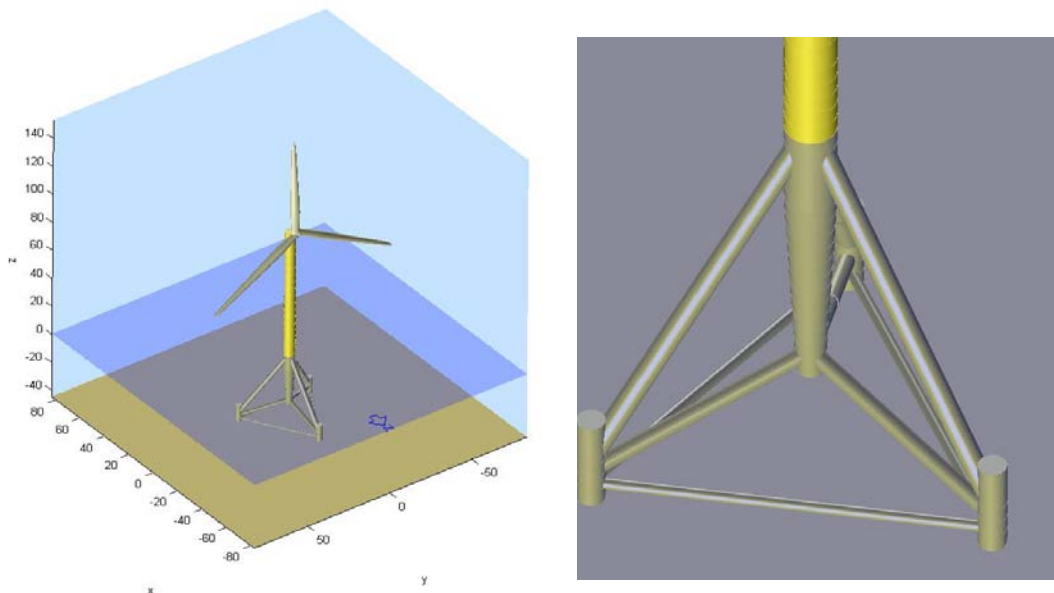- Members are at varying angles to the vertical.

Figure 25. NREL 5-MW wind turbine on tripod support structure

4.2 Phase III Simulations

In Phase III, a set of six load-case simulations were defined. The specifications of each load-case simulation are summarized in Table 8.

The load-case identifiers in Table 8 correspond to the identifiers used by the equivalent simulations from Phase I. In Phase III, though, it was not necessary to independently test the aerodynamic, hydrodynamic, and aero-servo-elastic models—as was done in Phase I—because these models were identical between Phases I and III. In addition, fewer combinations of wind and wave conditions were needed to test the tripod substructure models in Phase III. Consequently, the set of simulations from Phase III is much smaller than the set used in Phase I; and, as a result, the load case identifiers are not sequential.

The only load cases new to Phase III were cases 2.7 and 2.8. Because a tripod structure has to support dynamic loads through axial forces rather than bending moments, it was decided in case 2.7 to compare the loads on the structure caused solely by gravity—without complications caused by buoyancy and wave loads—to iron out differences in the structural modeling. Case 2.8 was similar to 2.7 except that the buoyancy loads in still water were added.

Table 8. Summary specifications for the Phase III load-case simulations

Load Case	Enabled DOFs	Wind Conditions	Wave Conditions	Analysis Type
1.2	Substructure, tower, drivetrain, blades	None: air density = 0	None: water density = 0	Eigenanalysis
2.6	None	None: air density = 0	Regular stream function (Dean): H = 8 m, T = 10 s	Periodic time-series solution
2.7	None	None: air density = 0	None: water density = 0	Static solution
2.8	None	None: air density = 0	Still water	Static solution
4.3	Substructure, tower	None: air density = 0	Regular stream function (Dean): H = 8 m, T = 10 s	Periodic time-series solution
5.1	Substructure, tower, drivetrain, blades	Steady, uniform, no shear: V_{hub} = 8 m/s	Regular stream function (Dean): H = 8 m, T = 10 s	Periodic time-series solution
H – individual wave height T – individual wave period		V_{hub} – hub-height wind speed averaged over 10 minutes		

For each load-case simulation, a total of 114 model outputs were analyzed. In addition to the 33 outputs analyzed in Phase I for the rotor, drivetrain, nacelle, tower, and environment, 81 more outputs were analyzed in Phase III. These included loads throughout the various members of the tripod, as well as water particle velocities and accelerations, to better understand the differences between the results of the different codes.

4.3 Phase III Participants and Codes

Phase III results were submitted by participants from the Risø National Laboratory of the Technical University of Denmark (Risoe), Garrad Hassan & Partners Limited (GH), the Leibniz University of Hannover (LUH), the National Renewable Energies Center (CENER), the Endowed Chair of Wind Energy at the University of Stuttgart (SWE), and the Fraunhofer Institute for Wind Energy and Energy System Technology (IWES).

Phase III stretched the abilities of the codes that were mainly developed to model simple monopile towers. HAWC2 modeled the turbine with a combined multibody plus linear finite-element

representation. ADCoS-Offshore modeled the turbine as a nonlinear finite-element system. FAST, Bladed, and FLEX5 modeled the turbine using a combined modal plus multibody representation with modal elements derived from a finite-element-based preprocessor.

Phase III considers the tripod support structure. GH has recently released a multimember support-structure module in Bladed that allows the modes of complicated structures to be analyzed. In addition to applying Bladed, CENER has used the NASTRAN code to model the wave interaction with a tripod model and has used a Guyan reduction technique [3] to interface these dynamics with FAST. SWE coupled FLEX5 to a finite-element-based tool called Poseidon to model the tripod. Risoe modeled the tripod structure with the finite-element components inherent to HAWC2. Likewise, IWES used the finite-element capabilities of ADCoS-Offshore to model the tripod, with hydrodynamic forces applied as nodal forces derived from ASAS. LUH has modeled the tripod structure in ANSYS and used WaveLoads to apply the hydrodynamic forces.

4.4 Phase III Results

4.4.1 Full-System Eigenanalysis

Figure 26 depicts the lowest 13 natural frequencies calculated for the stationary—but fully flexible—system consisting of the turbine atop a tripod support structure in the absence of water from load case 1.2. The designation of "pitch" and "yaw" in the asymmetric flapwise and edgewise blade modes identifies coupling of the blade motions with the nacelle-pitching and nacelle-yawing motions respectively.
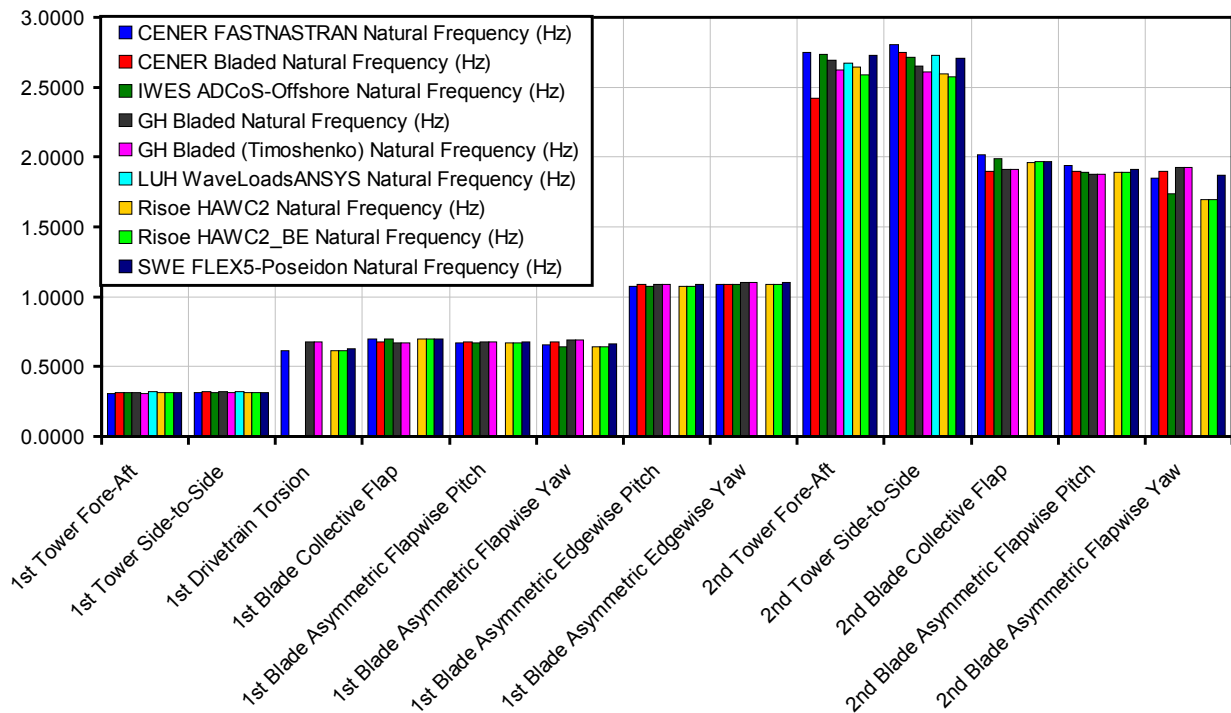
Figure 26. Full-system natural frequencies from load case 1.2

The tripod support structure is stiffer than the monopile used in Phases I and II, increasing the tower natural frequencies by 15%–20%. The increased stiffness of the tower has little effect on the natural

frequencies of the blades; however, the drivetrain frequency is increased slightly. The discrepancy in second tower fore-aft modes is partially due to the coupling between rotor and tower modes. In particular, the Bladed version used by CENER is an older version in which there was no coupling term between the tower nodding motion and the rotor out-of-plane motion. The lower values of the second blade asymmetric flapwise yaw mode found by Risoe with HAWC2 and IWES with ADCoS-Offshore are due to the inclusion of the tower torsional mode. For this mode, the vertical blade remains stationary, whereas the other two blades move out of phase with each other. When the support-structure model permits twist, the effective stiffness of this mode is reduced and therefore the frequency decreases.

4.4.2 Specific Problems Resolved

One difference that could not be overcome between the multibody codes and modal codes was the issue of modal damping. For HAWC2, Rayleigh damping was used; the damping for a mode was calculated from a sum over the members. It was not possible to reduce the Rayleigh damping coefficient sufficiently to produce the same modal damping that was used in Bladed and FAST without causing numerical problems.

4.4.2.1 Wave Loads Near the Sea Surface

One of the first problems observed in Phase III was the appearance of stepwise jumps in the member loads near the free surface of the sea predicted by some codes. These were reduced to negligible levels by discretizing the hydrodynamic loads more finely near the sea surface. Figure 27 shows the axial force in the upwind leg of the tripod with both a coarse and a fine discretization.
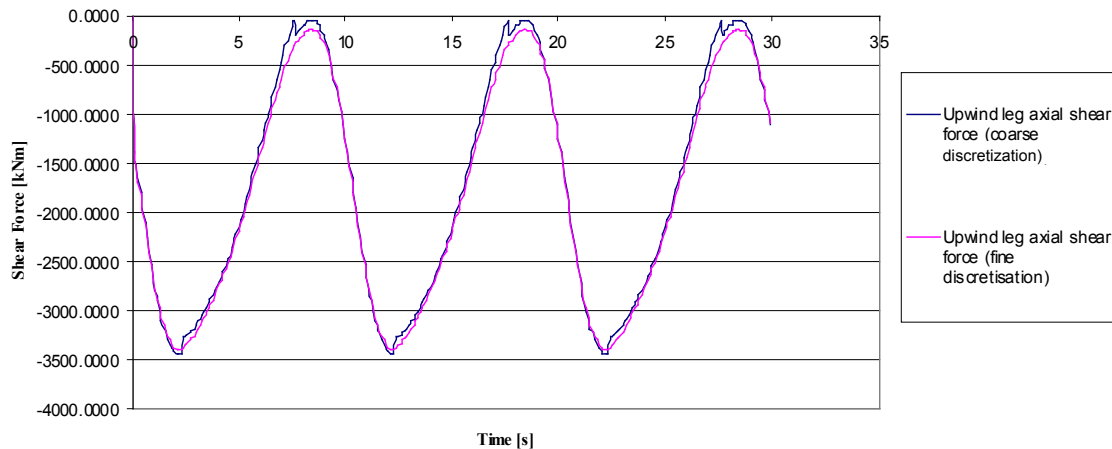
Figure 27. Effect of increasing resolution of hydrodynamic loads near the free surface

4.4.2.2 Tapered Members

The discretization of the tapered, central element of the tripod had a large effect on the loads. Buoyancy and inertial Morison's forces per unit length both depend on the square of the diameter of the member, so having too long a length between members can cause a large error in the total force. Figure 28 shows the fore-aft shear force in the central member when the tapered member is divided into 6 sections and the difference when the member is divided into 17 sections.
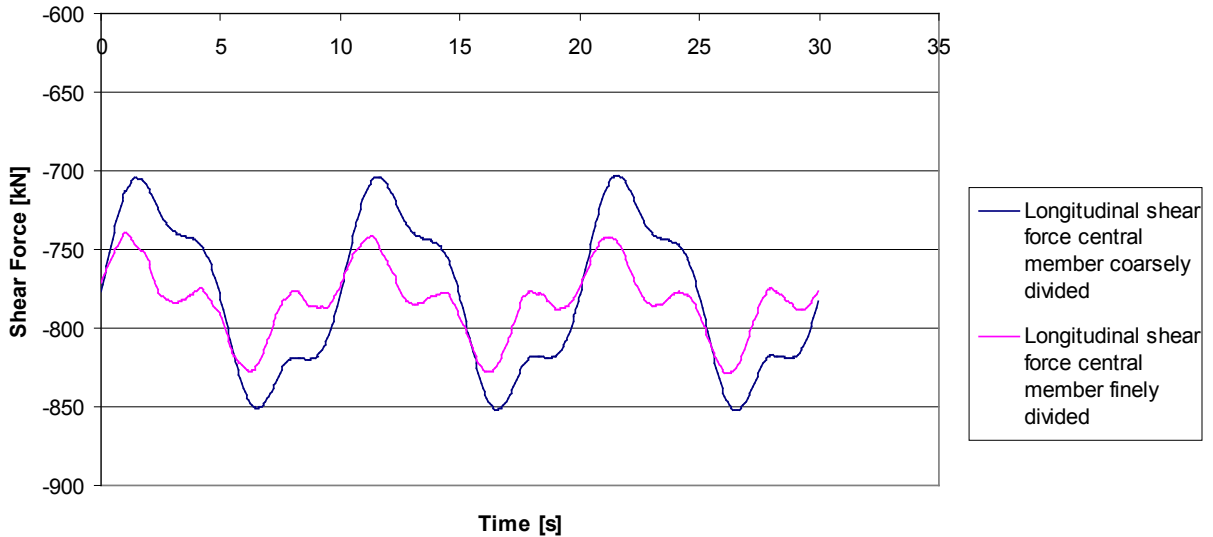
Figure 28. Effect of increasing number of members making up the central, tapered member

4.4.2.3 Overlap of Tripod Members

Another large effect is caused by the overlapping of members at joints. Figure 29 shows an example of the overlapping region close to the mean sea level in the tripod. For the large diameter members of the tripod configuration, significant surface areas and volumes are duplicated, distorting the overall level of wave and buoyancy loading. The intersecting members also have an influence on the mass of the tripod. This latter influence does not show up in the code-to-code comparison because all of the participants assumed that the overlapping sections of mass are negligible.
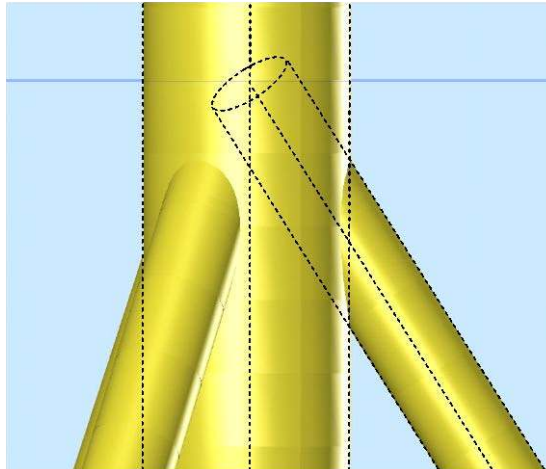
Figure 29. Schematic of overlapping region between two members

In all, 18 sections overlap, neglecting the sections in which the overlap occurs between three members in total. The difference between assuming the members intersect at the defined nodes and removing these

overlapping sections is 159 m³, or 8% of the total volume below sea level. Therefore, overlapping members have a significant effect on the buoyancy calculation as well as the applied Morison's equation forces. More discussion of this issue is provided in [4].

4.4.2.4 Shear Deflection in Tripod Members

For a long time, it was not possible to match the results between the codes. To find the reason, a simplified study of the turbine mounted on the tripod was performed. The simplest case of this was a static analysis with gravity as the only external load (case 2.7). Even for this simple case, there were major discrepancies. Actually, the HAWC2 results deviated from the rest of the results. The reason found for the discrepancies was the difference in beam model, which was demonstrated by IWES using different kinds of beam elements in ANSYS. The importance can be seen in Figure 30, where only the static loads from gravity are shown. In HAWC2, a Timoshenko beam is used as the default, where all other codes used Bernoulli-Euler beams. Because all beams are thin and slender, the Bernoulli-Euler approach was thought to be sufficient, but because the beams are attached rigidly in all ends of the tripod structure, the shear effect is much more important than was originally assumed. To verify these findings, HAWC2 results were delivered using both Timoshenko beams and the same beams neglecting the shear effects by increasing the form factor by 10^4. Also, the Bladed results were delivered using both Timoshenko beams and Bernoulli-Euler beams, with the same results. In Figure 30, the axial compression force in the vertical center member of the tripod is shown. The forces are different by a factor of 1.9. However, this is the part of the structure where the difference is largest. This difference in solution will also be present for external loads transmitted from the turbine to the tripod as occurs, for example, with aerodynamic loads.
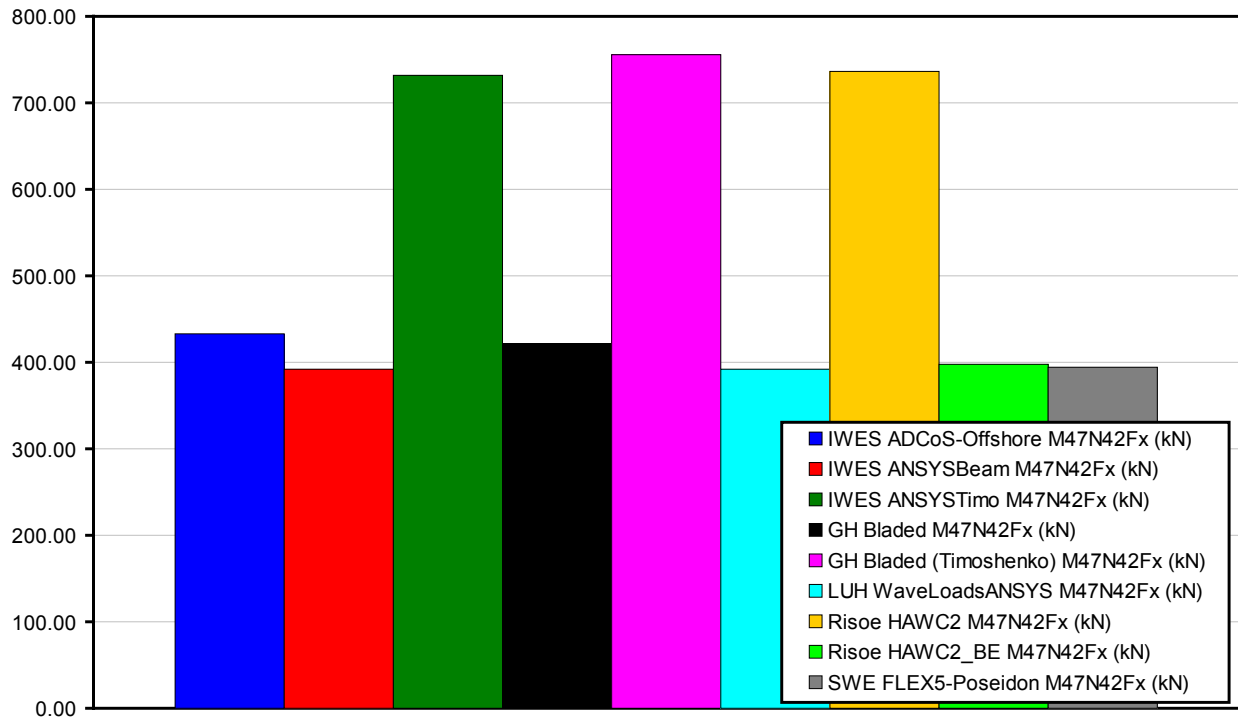
Figure 30. Axial force in the vertical center beam of the tripod

In Figure 30, a clear difference can be seen between codes using Bernoulli-Euler or Timoshenko beams. The HAWC2, Bladed, and ANSYS results are submitted in two versions with either Timoshenko beams or Bernoulli-Euler beams.

4.4.3 Loading Simulations

To aid in the code-to-code comparisons presented here, six locations were chosen for output to best capture the influence of the waves on the structure and are shown in Figure 31. The first station, 2 m above the mean sea level, illustrates the effects of wave kinematics near the top of the wave; the second station is at the intersection of three slanted legs and one central member; the third is a tapered member; the fourth and fifth are in the center of the two upwind slanted members; and the final is the load at the start of the foundation.
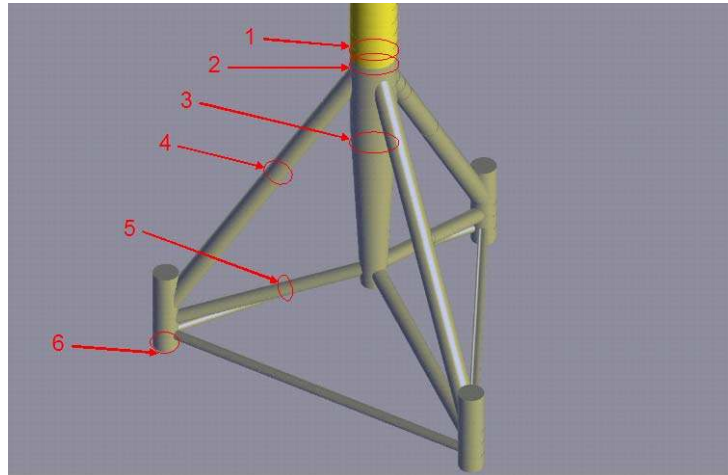
Figure 31. Locations for load output

Six participants contributed time-domain simulations with six different code combinations being used. The legend that will be used for the results of these simulations is shown in Figure 32.
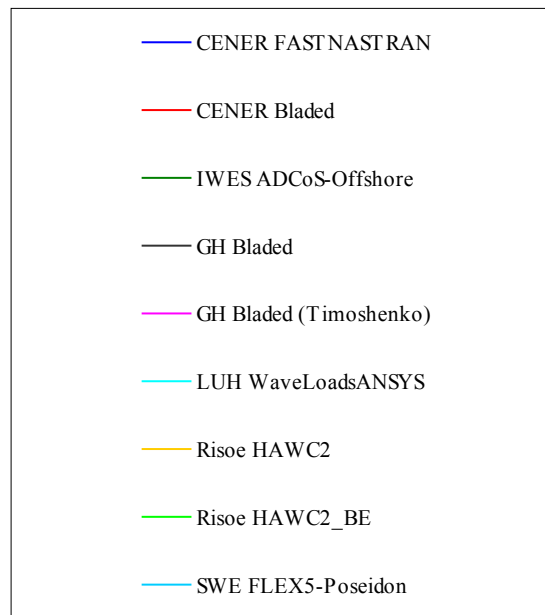
Figure 32. Phase III results legend

4.4.3.1 Static Loads in the Rigid Structure out of the Water

Static loads on the rigid structure in the absence of water from load case 2.7 are shown in Table 9, Table 10, and Table 11. Because of the differences between the two beam definitions (Section 4.3.2.4), the results are presented in two groups; one for the Euler-Bernoulli formulation and one for the Timoshenko formulation. Bladed, FLEX5-Poseidon, ADCoS-Offshore, WaveLoads-ANSYS, HAWC2_BE and ANSYS Beam all used the Euler-Bernoulli element. HAWC2, ANSYS Pipe, and Bladed (Timoshenko) used the Timoshenko element. The overall spread is also shown to illustrate which loads are most affected by the beam formulation. As shown in Table 9 and Table 10, the shear force and bending moment at the mudline split significantly into two groups, as does the axial force in the central member and at the lower brace (see Table 11).

Table 9. Static bending moment at locations 1–6 from load case 2.7

Location	Bending moment									Spread Euler-Bernoulli	Spread Timoshenko	Overall Spread
	IWES	IWES	IWES	GH	GH	LUH	Risoe	Risoe	SWE			
	ADCoS-Offshore	ANSYS Beam	ANSYS Timo	Bladed	Bladed (Timoshenko)	WaveLoads ANSYS	HAWC2	HAWC2_BE	FLEX5 Poseidon			
1	-1382.00	-1386.60	-1386.60	-1382.00	-1382.00	-1386.65	-1383.07	-1383.07	-1435.49	3.84%	0.33%	3.85%
2	-1382.00	-1386.60	-1386.60	-1382.00	-1382.00	-1386.65	-1383.07	-1383.07	-1435.48	3.84%	0.33%	3.85%
3	-746.29	-814.74	-810.80	-811.86	-811.86	-814.74	-808.41	-812.39	-826.61	9.98%	0.42%	9.96%
4	855.37			870.37	893.03	871.29	894.53	871.67	875.40	2.31%	0.17%	4.47%
5	207.15			232.16	239.50	213.32	226.09	213.39	213.36	11.59%	5.76%	14.66%
6	-9469.80	-8972.90	-7318.20	-8975.00	-7320.00	-8972.86	-7330.73	-8983.10	-8930.95	5.95%	0.17%	25.39%

Table 10. Static shear force at locations 1–6 from load case 2.7

| Location	Shear Force									Spread Euler-Bernoulli	Spread Timoshenko	Overall Spread
	IWES	IWES	IWES	GH	GH	LUH	Risoe	Risoe	SWE			
	ADCoS-Offshore	ANSYS Beam	ANSYS Timo	Bladed	Bladed (Timoshenko)	WaveLoads ANSYS	HAWC2	HAWC2_BE	FLEX5 Poseidon			
1												
2												
3	43.33	38.24	37.83	38.03	37.76	38.24	37.72	38.13	38.96	13.53%	0.28%	14.49%
4	37.66			35.97	37.00	35.73	36.93	35.77	35.88	5.34%	0.17%	5.31%
5	58.05			59.28	60.02	54.97	56.98	55.04	54.68	8.15%	5.19%	9.36%
6	-2824.30	-2879.60	-2228.90	-2865.00	-2219.00	-2879.58	-2232.41	-2882.17	-2872.23	2.02%	0.60%	24.99%

Table 11. Static axial force at locations 1–6 from load case 2.7

Location	Axial Force									Spread Euler-Bernoulli	Spread Timoshenko	Overall Spread
	IWES	IWES	IWES	GH	GH	LUH	Risoe	Risoe	SWE			
	ADCoS-Offshore	ANSYS Beam	ANSYS Timo	Bladed	Bladed (Timoshenko)	WaveLoads ANSYS	HAWC2	HAWC2_BE	FLEX5 Poseidon			
1	-7087.10	-7100.70	-7100.70	-7101.00	-7101.00	-7100.69	-7101.87	-7101.87	-7054.62	0.67%	0.02%	0.67%
2	-7223.80	-7237.40	-7237.40	-7237.00	-7237.00	-7237.38	-7238.64	-7238.64	-7191.31	0.65%	0.02%	0.65%
3	432.70	392.00	731.35	422.05	755.80	391.97	736.25	397.38	391.54	10.17%	3.30%	70.49%
4	-3902.70			-3889.00	-4020.00	-3877.73	-4013.30	-3880.68	-3861.51	1.06%	0.17%	4.04%
5	-1107.80			-1127.00	-792.40	-1149.59	-813.63	-1150.95	-1149.84	3.79%	2.64%	34.42%
6	-5028.80	-5027.70	-5027.80	-5028.00	-5028.00	-5027.73	-5031.63	-5031.53	-5013.91	0.35%	0.08%	0.35%

Overall, there is agreement once the beam element formulation is taken into account. Results are typically within a few percentage points of each other, though the percentage increases when the load is small compared to the loads in surrounding members; for example, the axial force at location 3, the central, tapered member.

4.4.3.2 Periodic Loads in the Rigid Structure from Regular Waves

Figure 33, Figure 34, and Figure 35 show time series of the periodic loads from regular waves acting on the rigid support structure from load case 2.6.

Overall, the results for bending moment (Figure 33) agree well. Above the waterline (locations 1 and 2) there are offsets, but the amplitude of the change caused by the passing of the wave is similar. There is good agreement in the tapered member (location 3) and in the upwind leg (location 4). By the lower brace and pile (locations 5 and 6), there are variations between the codes caused by different methods of accounting for the overlap and for implementing the beam model.
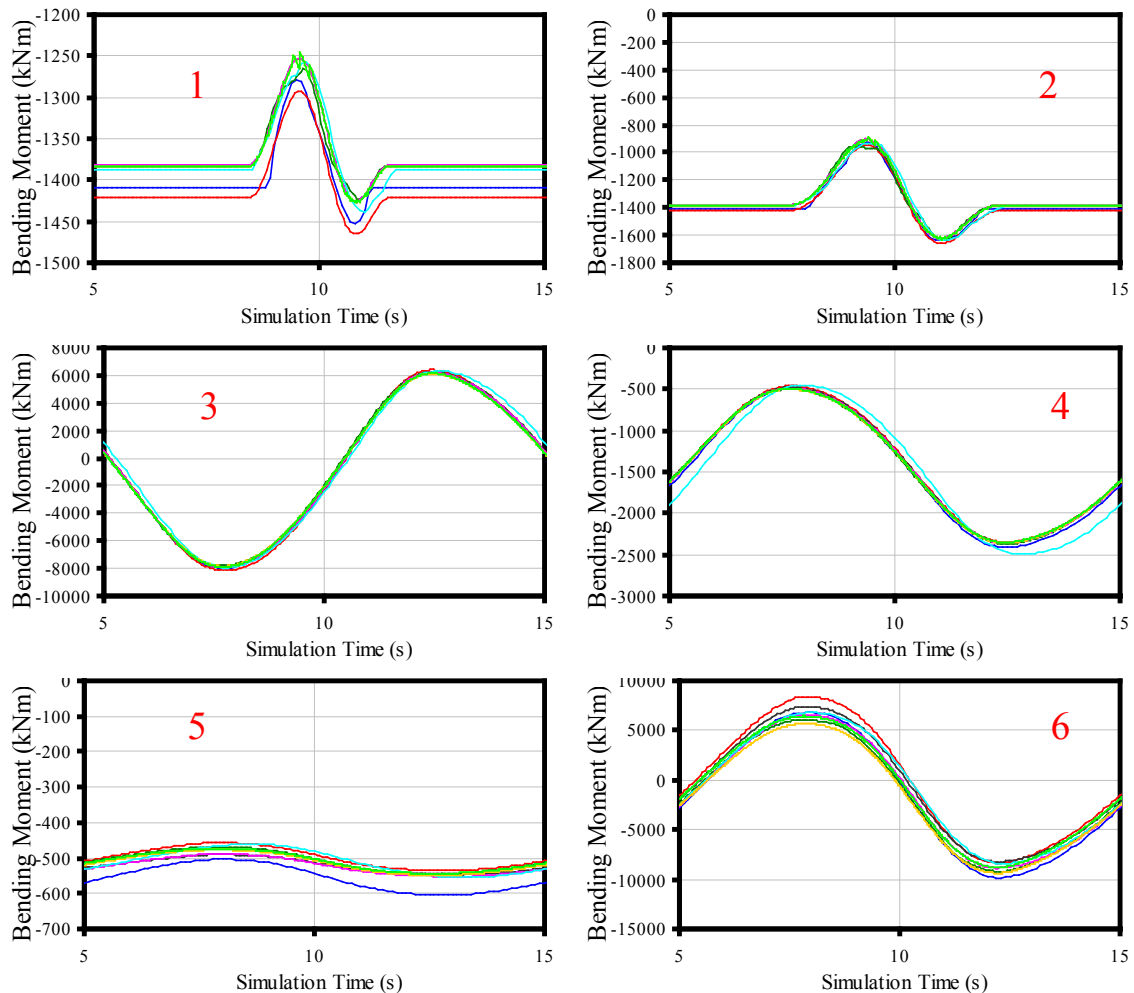
Figure 33. Fore-aft bending moment at locations 1–6 from load case 2.6

The shear forces agree less well than the bending moments (Figure 34). There are some differences because of the implementation of the wave kinematics. Although a standard set was created, some codes were unable to use this as input. Therefore, there are some differences caused by the wave models used.

The widest variation is seen in the central member (location 3). There are several complications for the calculations of this force: the member is tapered; it is not inside a tree-like structure, so there are many

paths that the loads can be distributed along; and it is at the height at which the wave loads are strongest. Better agreement is seen in the two braces and at the mudline.
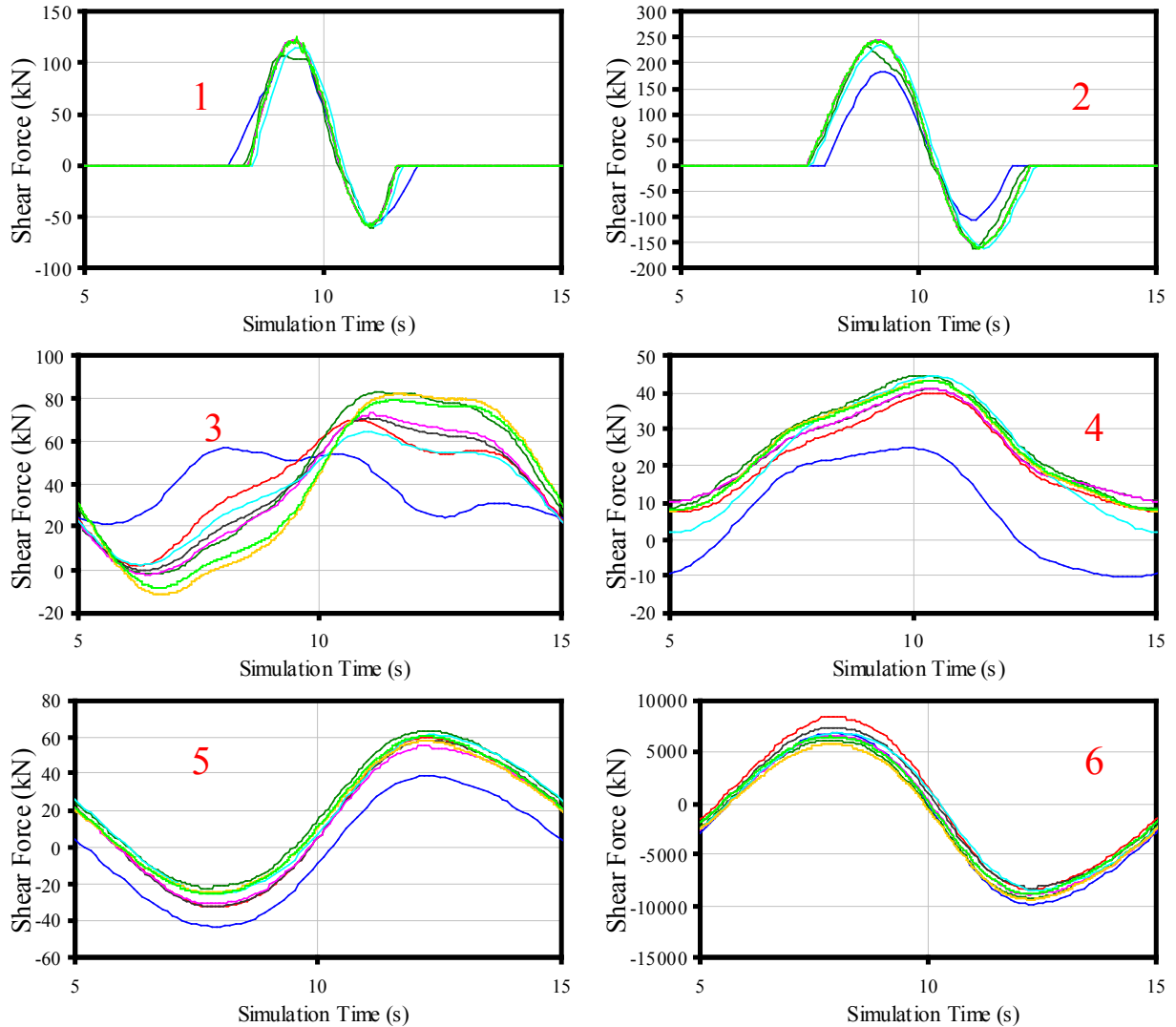
Figure 34. Fore-aft shear force at locations 1–6 from load case 2.6

Overall, the agreement is good for the axial forces (Figure 35). One difference that can be seen is between the three Bladed simulations. One (in red) has the model strictly defined as in the specification; the others have some parts of the members made invisible to waves and buoyancy to estimate the effect that the members do not overlap. During the course of the project, it was found that the area of overlap is a relatively large effect for tripod-like structures and should not be ignored.
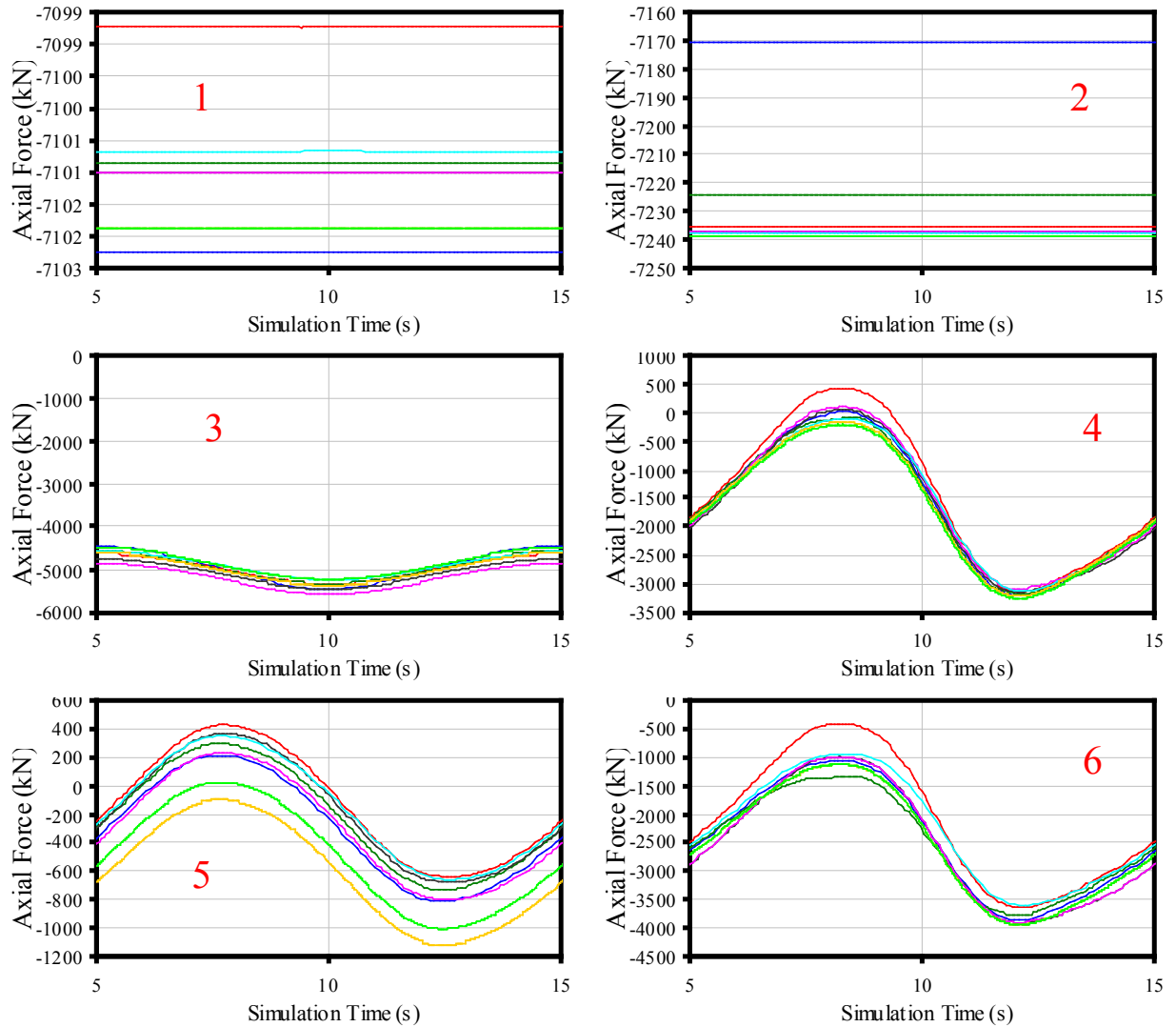
Figure 35. Axial force at locations 1–6 from load case 2.6

In general, the design of the tripod will be determined by the maximum stresses for extreme loads and the cycles of loads for fatigue loads. A comparison of the absolute maximum and range of load for the different codes is shown in Table 12 and Table 13. Results are not presented for all codes because some of the codes did not have the ability to produce full results for each simulation.

Table 12. Maximum bending moment at locations 1–6 from load case 2.6

	Maximum Absolute Bending Moment [kNm]						
	CENER	CENER	IWES	GH	LUH	Risoe	
Location	FAST NASTRAN	Bladed	ADCoS-Offshore	Bladed	WaveLoads ANSYS	HAWC2	Spread
1	1452.57	1465.27	1423.00	1426.00	1437.86	1427.03	2.94%
2	1638.13	1659.97	1639.00	1621.00	1638.33	1628.39	2.38%
3	7975.49	8143.26	7805.70	7913.00	7942.55	6153.88	4.25%
4	2413.70	2349.06	2367.00	2354.00	2490.04	2355.77	5.90%
5	604.25	534.93	545.86	545.96	553.61	547.86	12.47%
6	9829.42	8393.65	9210.20	8201.00	8414.37	9359.72	18.47%

Table 13. Bending moment range at locations 1–6 from load case 2.6

	Bending Moment Range [kNm]						
	CENER	CENER	IWES	GH	LUH	Risoe	
Location	FAST NASTRAN	Bladed	ADCoS-Offshore	Bladed	WaveLoads ANSYS	HAWC2	Spread
1	174.18	171.90	158.30	173.00	180.98	116.67	13.32%
2	710.74	712.26	684.35	716.04	706.22	472.75	7.54%
3	14252.62	14549.55	14081.80	14149.00	14277.51	9791.10	3.28%
4	1925.56	1889.33	1872.07	1877.89	2042.09	1310.24	8.89%
5	100.44	78.15	76.88	55.86	93.28	50.55	57.23%
6	16647.57	16746.48	15297.70	15583.00	15229.90	10788.55	9.59%

4.4.3.3 Hydro-Elastic Response with Regular Waves

Figure 36, Figure 37, and Figure 38 show the periodic response from load case 4.3 when the support structure is made flexible and is excited by regular waves. The rotor-nacelle assembly is modeled rigidly in this case and the aerodynamics are disabled.

Figure 36 shows that the tower-top displacement is relatively similar in character between the codes but there is a fairly wide variation in the phase of the motion. This could be due to the initial conditions that are used for the simulation that have not had the opportunity to die out. More discussion of this issue is provided in [4].

The support-structure displacement at mean sea level (see Figure 37) shows much better agreement. In this case, most of the motion is dominated by the action of the waves.
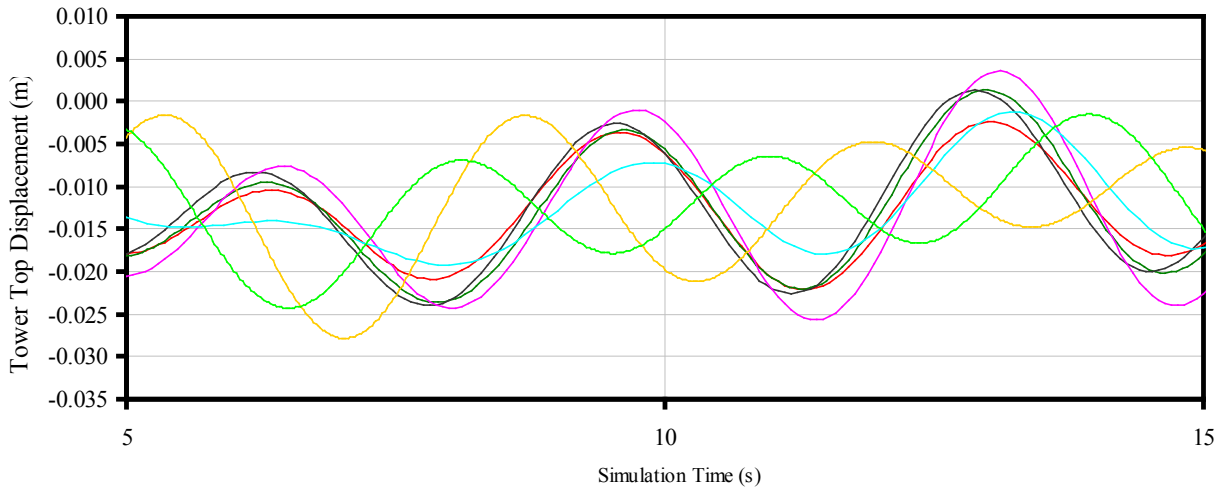
Figure 36. Tower-top fore-aft displacement from load case 4.3
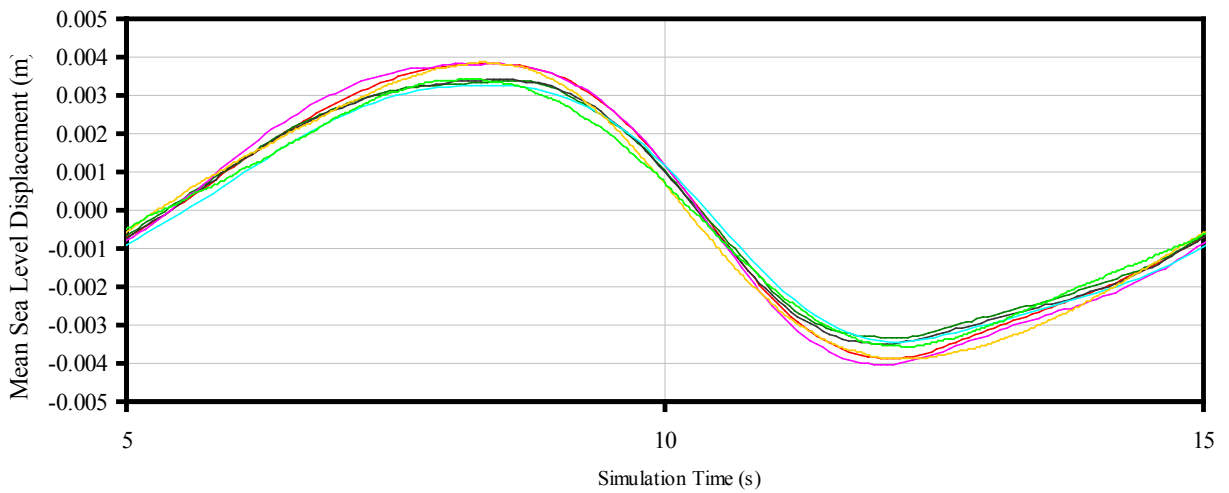
Figure 37. Mean sea level fore-aft support-structure displacement from load case 4.3
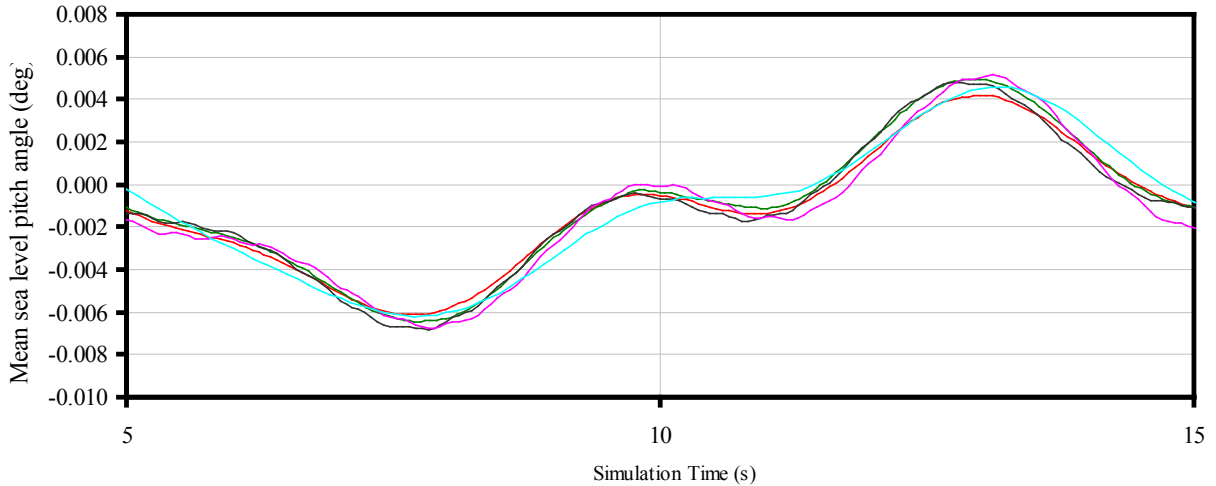
Figure 38. Mean sea level fore-aft support-structure pitch angle from load case 4.3

To show how important the consideration of dynamics is to the loading on the tower, the differences in maximum bending moment and bending moment range between load cases 2.6 and 4.3 are presented in Table 14 and Table 15.

Table 14. Increase in maximum bending moment taking dynamics into account between load cases 2.6 and 4.3

	Maximum bending moment increase [%]						
	CENER	CENER	IWES	GH	LUH	Risoe	Risoe
Location	FAST NASTRAN	Bladed	ADCoS-Offshore	Bladed	WaveLoads ANSYS	HAWC2	HAWC2_BE
1	115.12%	87.01%	114.50%	118.02%	106.53%	149.46%	123.18%
2	93.36%	78.46%	102.18%	105.86%	88.87%	129.51%	98.00%
3	-31.36%	9.17%	12.31%	12.55%	11.83%	15.97%	-4.33%
4	-1.07%	0.63%	0.96%	0.93%	0.85%	1.29%	0.44%
5	0.79%	-0.02%	0.05%	0.32%	-0.26%	0.28%	0.74%
6	0.61%	-0.24%	0.23%	0.09%	0.19%	-1.44%	-0.90%

Table 15. Increase in bending moment range taking dynamics into account between load cases 2.6 and 4.3

Location	Bending moment range increase [%]						
	CENER	CENER	IWES	GH	LUH	Risoe	Risoe
	FAST NASTRAN	Bladed	ADCoS-Offshore	Bladed	WaveLoads ANSYS	HAWC2	HAWC2_BE
1	1658.89%	1499.32%	2100.49%	1968.61%	1709.17%	3310.23%	1701.81%
2	343.06%	370.64%	498.80%	488.67%	435.99%	788.80%	349.34%
3	-50.27%	9.39%	13.63%	13.61%	12.28%	5.40%	0.45%
4	-41.46%	1.75%	2.48%	2.45%	2.17%	1.18%	0.02%
5	-30.18%	-1.70%	-2.29%	9.55%	2.73%	10.96%	17.41%
6	-40.14%	-0.17%	-0.26%	-0.24%	-0.10%	-1.10%	-0.04%

4.5 Phase III Conclusions

In Phase III of OC3, participants used an assortment of codes to model the coupled dynamic response of the NREL 5-MW wind turbine installed on a fixed-bottom tripod with rigid foundation in 45 m of water. Code predictions were compared from load-case simulations selected to test different model features. The comparisons have resulted in a greater understanding of multimember support-structure modeling techniques and better knowledge of the validity of various approximations.

Overall, the Phase III results have been encouraging. Modal-based, multibody, and finite-element codes have produced similar results. There have been many stages of comparison, as modeling complex offshore support structures is a relatively new development in wind turbine design. With each comparison, the results have converged.

The results of Phase III can be summarized as follows:
- All of the results of Phase I also apply to the results of Phase III. (The results of Phase II have less bearing on Phase III because Phase III does not use foundation models).
- The most straightforward way to account for buoyancy loads in non-flooded multi-member structures is through direct integration of the hydrostatic pressure that is dependent on the time-varying wave elevation (as opposed to accounting for buoyancy as a displaced volume with corrections for end effects). This is important for non-flooded members that are inclined, tapered, and/or embedded into the seabed (i.e., non-flooded piles). The OC3 code comparisons differed until everyone agreed on this approach.
- The most straightforward way to model a rigid multi-member structure is to increase the Modulus of Elasticity by several orders of magnitude consistently across all members. This permits calculation of how the loads are transmitted through what is a statically indeterminate structure (because of the geometry of the tripod) within the limits of zero deflection. The OC3 code comparisons differed for those load cases that considered a rigid tripod until everyone agreed on this approach.
- Differing discretizations for the hydrodynamic and buoyancy loads along tapered members lead to differences among the code predictions. To eliminate the discrepancy, the hydrodynamic and buoyancy loads along tapered members must be finely discretized. Because the hydrodynamic

inertia and buoyancy loads depend on the square of the member diameter, having too long a length between nodes can cause a large error in the total load.

- Because of the large diameter members of the tripod, significant surface areas and volumes are duplicated at the joints, which distort the overall level of loading if the intersection is not accounted for in the mass, stiffness, hydrodynamic loading, and buoyancy loading. This was found to have a large effect on the overall loading and response of the tripod.

- The local shear deflection of the members in a multi-member support structure, which can be modeled with Timoshenko beam elements, was found to have a large effect on the distribution of loads through multi-member structures. This was a surprising finding because all of the beam members of the tripod analyzed in OC3 were thin and slender, such that the Bernoulli-Euler approach, which neglects shear deflection, was thought to be sufficient (and is sufficient in blades, towers, and monopiles). The shear effect was found to be much more important than originally assumed because the beam members are attached rigidly to other members and the relative displacement of each member influences the load distribution. The results of the code comparisons could clearly be grouped between the codes that do and do not account for shear deflection in their beam element formulations.

- The initial transient solution takes time to dissipate due to the small amount of damping in the tripod and the method by which the hydrodynamic loads are initialized at the start of a simulation. The initial transient is longer when the turbine is not operating because aerodynamic loading tends to damp out the initial solution quickly. Each model initializes its solution differently, so, the code comparisons differed during the start-up transient period.

4.6 Phase III References

[1] Camp T. OC3 internal communication from GH, *tower definition_NEW.xls*, March 11, 2008.

[2] Jonkman J, Butterfield S, Musial W, and Scott G. *Definition of a 5-MW Reference Wind Turbine for Offshore System Development*. NREL/TP-500-38060. NREL: Golden, CO, 2009.

[3] Guyan RJ. Reduction of Stiffness and Mass Matrices, AIAA Journal, Vol. 3, No. 2, 1965.

[4] Vorpahl FR, Van Wingerde A, Blunk M, Busmann HG, Kleinhansl S, Kossel T, Kohlmeier M, Boker C, Kaufer D, Azcona J, Martinez A, and Munduate X. "Validation of a Finite Element Based Simulation Approach for Offshore Wind Turbines within IEA Wind Annex XXIII – Simulation Challenges and Results for a 5-MW Turbine on a Tripod Substructure." *Proceedings of the Nineteenth International Offshore and Polar Engineering Conference*, 2009

5. Chapter 5: Floating Spar-Buoy Modeling of Phase IV

Authors: J. Jonkman, National Renewable Energy Laboratory (NREL), USA; T. Larsen and A. Hansen, Risø National Laboratory, Technical University of Denmark (Risø-DTU), Denmark; T. Nygaard, Institute for Energy Technology (IFE), Norway; K. Maus, Norwegian University of Life Sciences (UMB), Norway; M. Karimirad, Z. Gao and T. Moan, Norwegian University of Science and Technology (NTNU), Norway; I. Fylling, Marintek, Norway; J. Nichols, Garrad Hassan & Partners Limited (GH), United Kingdom; M. Kohlmeier, ForWind, Leibniz University of Hannover (LUH), Germany; J. Pascual Vergara and D. Merino, Acciona Energia, Spain; W. Shi and H. Park, Pohang University of Science and Technology (POSTECH), Korea

5.1 Phase IV Model

Phase IV of OC3 considered an offshore floating wind turbine. Numerous floating platform concepts are possible for offshore wind turbines, including spar-buoys, tension leg platforms (TLPs), barges, and hybrid concepts. In OC3 Phase IV, the spar-buoy concept called "Hywind," developed by Statoil of Norway, was imitated. This concept was chosen for its simplicity in design, suitability to modeling, and the existence of a full-scale prototype. Statoil graciously supplied detailed platform and mooring system data for the conceptual version of the Hywind platform that was developed to support a 5-MW wind turbine, as analyzed in [2], [3], and [4]. Per the request of Statoil, the original data was condensed and sanitized to make it suitable for public dissemination. Aspects of the original data were also adapted slightly so that the platform design appropriately supports the NREL 5-MW baseline turbine, which has slightly different properties than the turbine Statoil used to develop their system. The rotor-nacelle assembly of the NREL 5-MW turbine—including the aerodynamic and structural properties—remained the same as in [1], but the support structure (tower and substructure) and control system properties were changed. The new system is referred to as the "OC3-Hywind" system, to distinguish it from Statoil's original Hywind concept. The OC3-Hywind system features a deeply drafted, slender spar buoy with catenary mooring lines as illustrated in Figure 39. Some of the system data is listed in Table 16; the concept is documented in much greater detail in [5].

Figure 39. Illustration of the NREL 5-MW wind turbine on the OC3-Hywind spar

Table 16. Summary of OC3-Hywind spar properties

Depth to Platform Base Below SWL (Total Draft)	120 m
Elevation to Platform Top (Tower Base) Above SWL	10 m
Depth to Top of Taper Below SWL	4 m
Depth to Bottom of Taper Below SWL	12 m
Platform Diameter Above Taper	6.5 m
Platform Diameter Below Taper	9.4 m
Platform Mass, Including Ballast	7,466,330 kg
CM Location Below SWL Along Platform Centerline	89.9155 m
Platform Roll Inertia about CM	4,229,230,000 kg·m2
Platform Pitch Inertia about CM	4,229,230,000 kg·m2
Platform Yaw Inertia about Platform Centerline	164,230,000 kg·m2
Number of Mooring Lines	3
Angle Between Adjacent Lines	120º
Depth to Anchors Below SWL (Water Depth)	320 m
Depth to Fairleads Below SWL	70.0 m
Radius to Anchors from Platform Centerline	853.87 m
Radius to Fairleads from Platform Centerline	5.2 m
Unstretched Mooring Line Length	902.2 m
Mooring Line Diameter	0.09 m
Equivalent Mooring Line Mass Density	77.7066 kg/m
Equivalent Mooring Line Weight in Water	698.094 N/m
Equivalent Mooring Line Extensional Stiffness	384,243,000 N
Additional Yaw Spring Stiffness	98,340,000 Nm/rad

The lessons learned during the development of the Phase IV model are summarized below:

- Several hydrodynamic characteristics of the of the OC3-Hywind spar were determined: (1) diffraction effects are negligible in moderate to severe sea states, (2) radiation damping in most modes of motion is small, and (3) flow separation will occur in severe sea states along the upper regions of the spar.

- According to Statoil, the hydrodynamic damping for the motions of the real Hywind platform is not captured by summing the linear radiation damping (from potential-flow theory) and the nonlinear viscous drag (from the relative form of Morison's formulation). Therefore, these hydrodynamic loads must be augmented with additional damping. The additional linear damping required for the OC3-Hywind system was found by matching modeled still-water free-decay responses with data provided by Statoil.

- The load-displacement relationships of the OC3-Hywind mooring system include some interesting asymmetries, which result from the nonlinear behavior of the three-point moorings. Whereas the loads are either symmetric or anti-symmetric about zero for the sway and roll displacements, the loads are asymmetric about zero for the surge and pitch displacements. The mooring system stiffens up for the surge and pitch displacements, and the surge forces, heave forces, and pitching moments increase nonlinearly. This asymmetry induces surge forces and pitching moments due to sway and roll displacements. Also, the heave forces change with all displacements because these displacements cause more line to lift off of—or allow more line to settle on—the seabed. Moreover, unless large loads are applied to the platform to react with the rapidly increasing mooring loads, the platform will tend to pitch as it translates in surge and will tend to roll as it translates in sway.

- Conventional wind turbine control systems must be modified to eliminate the potential for negative damping of the platform-pitch mode and to improve the floating turbine system's response. The original control system for the NREL 5-MW turbine needed two modifications to make it suitable when the turbine is mounted on the OC3-Hywind spar-buoy. First, the blade-pitch-controller-response natural frequency was reduced below the platform-pitch natural frequency and wave-excitation frequency of most sea states; this reduction leads to a drop in the proportional (P) and integral (I) gains of the PI-based blade-pitch controller, ensuring that the platform-pitch motions remain positively damped. Second, the above-rated torque-control law was changed from a constant generator-power to a constant generator-torque control region; this change reduces the rotor-speed excursions that are exaggerated by the reduction in gains in the blade-pitch controller at the expense of some overloading of the generator, as power increases with rotor-speed excursions above rated.

Floating offshore wind turbines are a good test for aero-hydro-servo-elastic codes because they incorporate a number of features not present in conventional fixed-bottom offshore support structures:

- The introduction of very low frequency modes that can impact the aerodynamic damping and stability of the system

- The possibility of significant translational and rotational motions of the support structure, which can couple with the motions of the rotor-nacelle assembly

- The mooring system and anchoring is a new component that must be considered in the overall analysis

- The support structure need not be slender and cylindrical (although this is nearly the case in the OC3-Hywind system), such that hydrodynamic radiation, diffraction and other wave effects can become important

5.2 Phase IV Simulations

In Phase IV, a set of load-case simulations has been specified for the OC3-Hywind system, as summarized in Table 17. Most of the load cases in Table 17 correspond to those of equivalent simulations from earlier phases. In Phase IV, though, it was not necessary to run all of the earlier simulations, and as a result, the load-case identifiers are not sequential. The load cases new to Phase IV are cases 1.3, 1.4, and 5.4.

Case 1.3 is used to compare the static equilibrium condition of the full system void of wind or wave excitation. This case is useful for checking that the combined weight of the rotor-nacelle assembly, tower, and platform balances with the static buoyancy (i.e., weight of the displaced fluid) and mooring reactions identically between the models.

Case 1.4 is used to test the OC3-Hywind system's hydrodynamic damping through free-decay tests. This case considers only the six rigid-body DOFs of the platform in still water; each DOF is perturbed separately, and the time-series responses are compared.

Case 5.4 is used to test the OC3-Hywind's frequency response. This case considers steady uniform winds without shear at 8 m/s, regular Airy 2-m high waves with different frequencies in each simulation, the turbine control system and all DOFs enabled, and simulates until a periodic steady-state condition is reached. The outputs of case 5.4 are the time-series-generated Response Amplitude Operators ("effective RAOs"). An "effective RAO" is defined here to mean the difference in response amplitudes between nonlinear time-domain simulations run with and without wave excitation. That is, the outputs are the effective amplitudes of the platform motions, turbine displacements, loads, etc. normalized by the wave

amplitude (1 m) versus wave frequency. The word "effective" is used to distinguish these values from RAOs that are typically found using linear frequency-domain techniques.

For each load-case simulation, a total of 57 model outputs were analyzed. In addition to the 33 outputs analyzed in Phases I through III for the rotor, drivetrain, nacelle, tower, and environment, 24 outputs were used in Phase IV to analyze the loads and deflections of the floating platform and mooring system.

Table 17. Summary specifications for the Phase IV load-case simulations

Load Case	Enabled DOFs	Wind Conditions	Wave Conditions	Analysis Type
1.2	Platform, tower, drivetrain, blades	None: air density = 0	Still water	Eigenanalysis
1.3	Platform, tower, drivetrain, blades	None: air density = 0	Still water	Static equilibrium solution
1.4	Platform	None: air density = 0	Still Water	Free-decay test time series
4.1	Platform, tower	None: air density = 0	Regular Airy: H = 6 m, T = 10 s	Periodic time-series solution
4.2	Platform, tower	None: air density = 0	Irregular Airy: H_s = 6 m, T_p = 10 s, JONSWAP wave spectrum	Time-series statistics, DELs, power spectra
5.1	Platform, tower, drivetrain, blades	Steady, uniform, no shear: V_{hub} = 8 m/s	Regular Airy: H = 6 m, T = 10 s	Periodic time-series solution
5.2	Platform, tower, drivetrain, blades	Turbulent: V_{hub} = V_r (11.4 m/s), σ_1 = 1.981 m/s, Mann model	Irregular Airy: H_s = 6 m, T_p = 10 s, JONSWAP wave spectrum	Time-series statistics, DELs, power spectra
5.3	Platform, tower, drivetrain, blades	Turbulent: V_{hub} = 18 m/s, σ_1 = 2.674 m/s, Mann model	Irregular Airy: H_s = 6 m, T_p = 10 s, JONSWAP wave spectrum	Time-series statistics, DELs, power spectra
5.4	Platform, tower, drivetrain, blades	Steady, uniform, no shear: V_{hub} = 8 m/s	Regular Airy: H = 2 m, ω = 0.1, 0.2,…, 3.5 rad/s	Time-series-generated "effective RAOs"

H	– individual wave height	V_{hub}	– hub-height wind speed averaged over 10 minutes	σ_1	– longitudinal wind speed standard deviation
H_s	– significant wave height				
T	– individual wave period	V_r	– rated wind speed	ω	– individual wave frequency
T_p	– peak-spectral wave period				

5.3 Phase IV Participants and Codes

Phase IV results were submitted by participants from the National Renewable Energy Laboratory (NREL), Risø National Laboratory of the Technical University of Denmark (Risø-DTU), MARINTEK, the Norwegian University of Science and Technology (NTNU), the Institute for Energy Technology (IFE), the Norwegian University of Life Sciences (UMB), Garrad Hassan & Partners Limited (GH), the Leibniz University of Hannover (LUH), Acciona Energia, and the Pohang University of Science and Technology (POSTECH).

Most of the aero-hydro-servo-elastic codes that have been developed for modeling the dynamic response of offshore wind turbines were tested within OC3. The existing modeling capabilities of the simulation tools used by (and for some, developed by) each participant are summarized in Table 18. In the cases where Table 18 shows the same code being used by multiple OC3 participants, the model development, simulation runs, and data processing were done independently.

Table 18. Overview of aero-hydro-servo-elastic modeling capabilities

FAST	Bladed	ADAMS	HAWC2	3Dfloat	Simo	SESAM/DeepC
Code Developer						
NREL	GH	MSC + NREL + LUH	Risø-DTU	IFE-UMB	MARINTEK	DNV
OC3 Participant						
NREL + POSTECH	GH	NREL + LUH	Risø-DTU	IFE-UMB	MARINTEK	Acciona + NTNU
Aerodynamics						
(BEM or GDW) + DS	(BEM or GDW) + DS	(BEM or GDW) + DS	(BEM or GDW) + DS	(BEM or GDW)	BEM	None
Hydrodynamics						
Airy+ + ME, Airy + PF + ME	(Airy+ or Stream) + ME	Airy+ + ME, Airy + PF + ME	Airy + ME	Airy + ME	Airy + PF + ME	Airy+ + ME, Airy + PF + ME
Control System (Servo)						
DLL, UD, SM	DLL	DLL, UD	DLL, UD, SM	UD	DLL	None
Structural Dynamics (Elastic)						
Turbine: FEMP + (Modal / MBS), Moorings: QSCE	Turbine: FEMP + (Modal / MBS), Moorings: UDFD	Turbine: MBS, Moorings: QSCE, UDFD	Turbine: MBS / FEM, Moorings: UDFD	Turbine: FEM, Moorings: FEM, UDFD	Turbine: MBS, Moorings: QSCE, MBS	Turbine: MBS, Moorings: QSCE, FEM

Airy$^+$ – Airy wave theory; (+) with free surface connections **BEM** – blade-element/momentum **DLL** – external dynamic link library **DNV** – Det Norsk Veritas **DS** – dynamic stall	**GDW** – generalized dynamic wake **FEM^P** – finite-element method; (P) for mode preprocessing only **MBS** – mulibody-dynamics formulation **ME** – Morison's Software Corporation	**PF** – linear potential flow with radiation and diffraction **QSCE** – quasi-static catenary equations **SM** – interface to Simulink® with MATLAB® **UD** – implementation through user-defined subroutine available **UDFD** – implementation through user-defined force-displacement relationships

5.4 Phase IV Results

Each load-case simulation of Phase IV was run by the OC3 participants. The legend in Figure 40 delineates how the results are presented in the figures that follow. The color shade and line type distinguish the results from separate participants and codes. Some results were not processed by all of the OC3 participants, which is why some of the predictions are left blank or have a zero value. Only a small subset of the results is presented.

5.4.1 Full-System Eigenanalysis

Figure 41 gives the lowest 19 natural frequencies calculated for the stationary OC3-Hywind system in still water from load case 1.2. Results were obtained from all codes except FAST by POSTECH and Bladed. While case 1.2 calls for enabling all system DOFs, the rotor-nacelle assembly is modeled rigidly in ADAMS by LUH and 3Dfloat, and the rotor-nacelle assembly and tower are modeled rigidly in Simo, SESAM, and DeepC. The designation of "pitch" and "yaw" in the asymmetric flapwise and edgewise blade modes identifies coupling of the blade motions with the nacelle-pitching and nacelle-yawing motions, respectively.
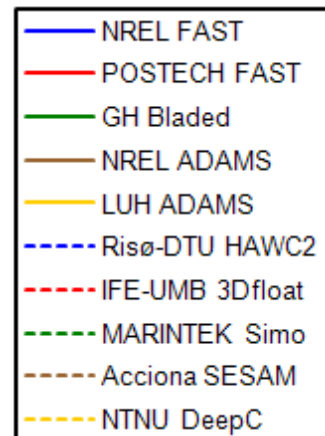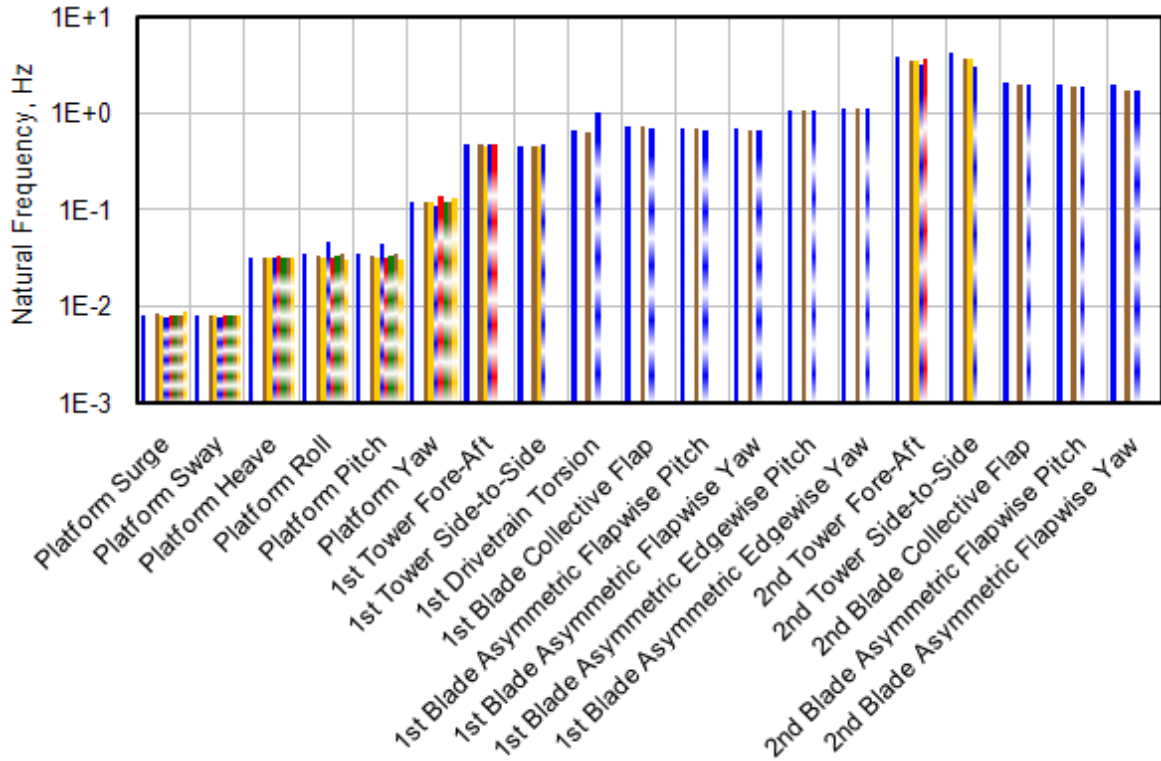

Figure 40. Results Legend

Figure 41. Full-system hydro-elastic natural frequencies from load case 1.2

Most of the codes agree on their predictions of the lowest six natural frequencies, which correspond to the six (primarily) rigid-body modes of the floating support platform (with only minor couplings to the turbine flexibilities). The platform roll and pitch natural frequencies are predicted higher by Risø-DTU with the HAWC2 code. While these differences are still being investigated, one thought is that they are caused by the treatment of gravity in the model linearization process, as gravity has a strong influence on the roll and pitch restoring of a deep-drafted spar.

Not all of the codes predict the natural frequencies of the flexible body modes. The codes that model the tower and blade bending and drivetrain torsion modes predict similar natural frequencies, with only slight discrepancies. The discrepancy in the second blade asymmetric flapwise yaw frequency has been seen in earlier phases of OC3, particularly Phase II. In this mode, the vertically positioned blade remains stationary, while the two other blades flap out of phase with each other. These blade motions couple with the torsion of the tower and—in Phase IV—the yaw of the platform (both being rotations about the tower centerline). The codes which do not account for tower torsion (FAST) predict higher natural frequencies—corresponding to the stiffer compliance about the tower centerline—than the codes that do (ADAMS, HAWC2).

5.4.2 Free Decay

Figure 42, Figure 43, and Figure 44 give the platform surge, heave, and pitch time series from perturbations in platform surge, heave, and pitch, respectively, from the free-decay tests of load case 1.4. Results were obtained from all codes except Bladed and DeepC.
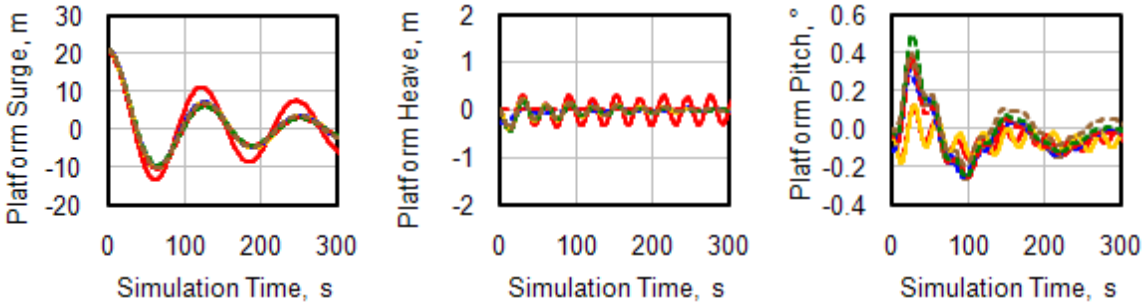
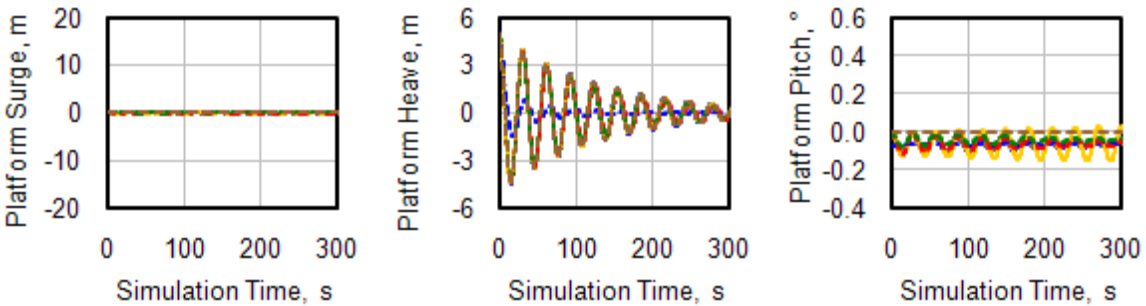**Figure 42.** Free decay in platform surge from load case 1.4

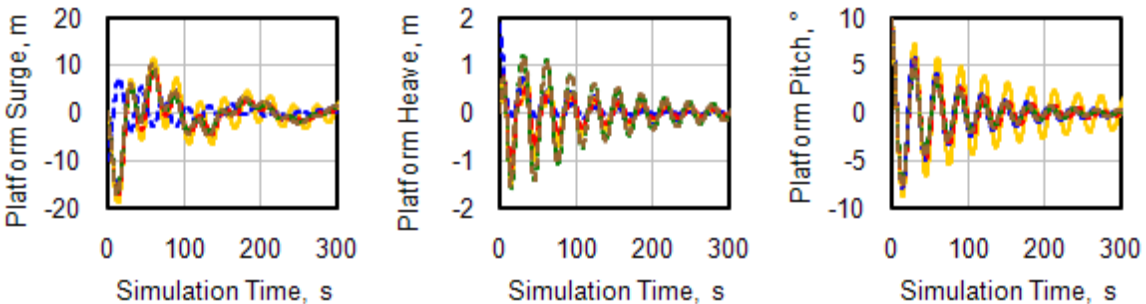**Figure 43.** Free decay in platform heave from load case 1.4

Figure 44. Free decay in platform pitch from load case 1.4

For the surge free-decay test of Figure 42, all codes except FAST by POSTECH agree on the surge displacement. Both NREL and POSTECH used FAST and their results compare well, except that there is less hydrodynamic damping in POSTECH's results. This is caused by POSTECH's FAST model missing one hydrodynamic damping term (the so-called "additional linear damping" specified for the OC3-Hywind spar). When comparing the heave-surge coupling between the codes, 3Dfloat predicts less coupling, HAWC2 predicts more damping, and FAST by POSTECH predict less damping. The pitch-surge coupling can be placed into two groups—FAST by POSTECH and ADAMS by LUH in one, and FAST and ADAMS by NREL, HAWC2, 3Dfloat, and SESAM in another. The pitch offset results from the overhanging mass of the rotor-nacelle assembly from the centerline of the tower and platform.

For the heave and pitch-heave coupling responses in the heave free-decay test of Figure 43, all codes agree well except SESAM, which predicts no coupling to pitch, and HAWC2, which has too much heave and pitch damping.

All codes agree on the platform-pitch response in the pitch free-decay test of Figure 44, except ADAMS by LUH, which predicts too little damping. HAWC2 predicts different surge-pitch and heave-pitch couplings than the other codes.
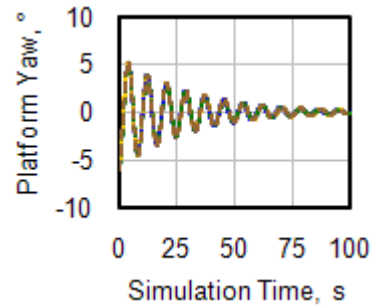

Figure 45. Free decay in platform yaw from load case 1.4

Figure 45 gives the platform-yaw response from the yaw free-decay test of load case 1.4. All codes agree very well.

5.4.3 Hydro-Elastic Response with Regular Waves

Figure 46 shows time histories of platform surge, heave, and pitch displacements; tower-top fore-aft deflection and shear force; and downstream fairlead tension (from mooring line #1) from load case 4.1. This case considers the response of the platform and flexible tower (with rigid rotor-nacelle-assembly) excited by regular (i.e., periodic) waves. Results were obtained from NREL with FAST and ADAMS, Risø-DTU with HAWC2, UMB with 3Dfloat, MARINTEK with Simo, and Acciona with SESAM. The responses for two wave passages (i.e., periods) are shown. All codes removed start-up transients from their results. The instantaneous wave elevation at the platform centerline is highest at 0 and 10 s and lowest at 5 and 15 s, except in 3Dfloat and Simo, which are phase-shifted relative to the other codes.

In these results, all codes agree on the platform-surge amplitude except HAWC2, which may simply have output the wrong parameter. For pitch and heave, all codes agree. For tower fore-aft deflection—deflection induced by platform motion—most codes agree quite well. Simo and SESAM predict no
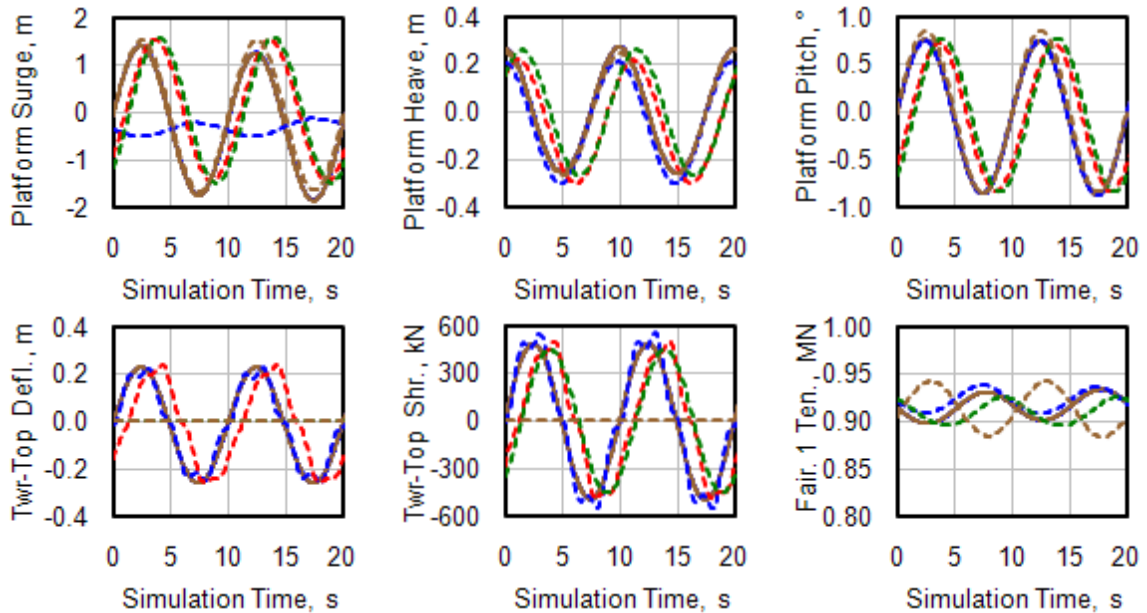

Figure 46. Hydro-elastic time series with regular waves from load case 4.1

deflection because the tower was modeled rigidly in those codes. The tower-top fore-aft shear force (induced by the oscillating mass of the rotor-nacelle assembly) and downstream fairlead tension agree well in all codes except SESAM.

5.4.4 Hydro-Elastic Response with Irregular Waves

Figure 47 shows power spectra computed in load case 4.2 for the same parameters shown in Figure 46. Case 4.2 tests the same model used in case 4.1, but with excitation from irregular (stochastic) waves. Results were obtained from all codes except FAST by POSTECH, ADAMS by LUH, and 3Dfloat. Because several codes contain start-up transients, the statistical results from this case are difficult to compare and are not presented.

The wave spectrum has the highest amount of energy at 0.1 Hz, corresponding to the peak-spectral period of 10 s. All codes agree on the energy content of the system responses at this frequency, except SESAM in platform pitch. The platform natural frequencies (about 0.008 Hz in surge, 0.032 Hz in heave, and 0.034 Hz in pitch) are easily visible in the platform-displacement power spectra of all codes; however, the codes differ on their predictions of energy content at and around these frequencies (with the farthest outliers being Bladed in surge, Simo in heave, and SESAM in pitch). Spectral shape estimates in this frequency range are sensitive to time-series sampling. There is considerable statistical uncertainty of response spectra because of the relatively short duration of the prescribed time series compared to the wave and platform periods.

In the tower-top fore-aft deflection and shear force power spectra, the platform-pitch and first tower bending (about 0.46 Hz) natural frequencies are clearly visible. Bladed, however, shows more energy just below the first tower bending natural frequency and less energy at the platform-pitch natural frequency.
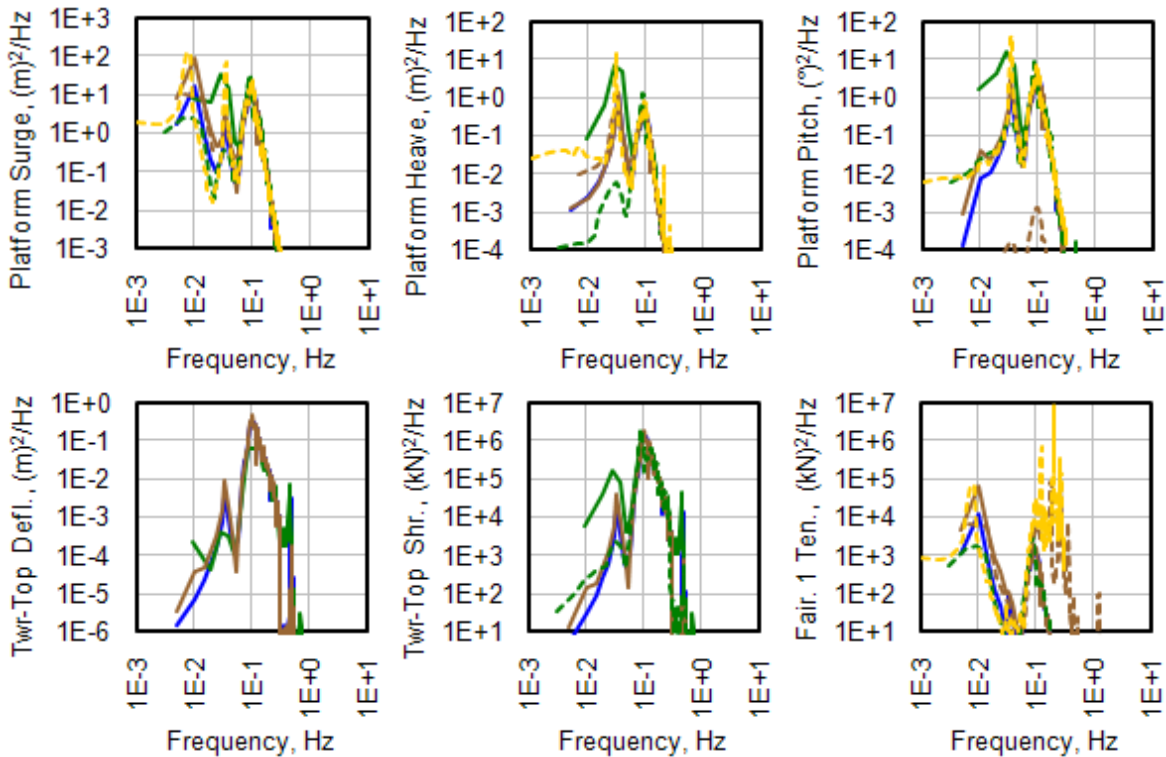

Figure 47. Hydro-elastic power spectra with irregular waves from load case 4.2

SESAM and DeepC predict higher energy than the other codes in fairlead tension above 0.1 Hz, likely the result of undamped high-frequency motions in their FEM-based mooring line solution.

5.4.5 Aero-Hydro-Servo-Elastic Response with Regular Waves

Figure 48 gives time histories of out-of-plane blade-tip deflection; generator power; rotor speed; platform surge, heave, pitch, and yaw displacements; tower-top fore-aft deflection, shear force, and rotor torque; and downstream and upstream fairlead tensions (from mooring line #1 and #2) from load case 5.1. This case is like 4.1 except that the rotor and drivetrain are flexible, the controller is enabled, and the turbine is operating in uniform wind below rated wind speed. In addition to the wind excitation, which leads to nonzero mean loads and displacements, the system is again excited by regular waves that induce oscillations about the means. The responses are shown for two wave passages (i.e., periods)—which equates to about three rotor revolutions—after all start-up transients have died out. Results were obtained from all codes but Bladed, ADAMS by LUH, and DeepC. The instantaneous wave elevation at the
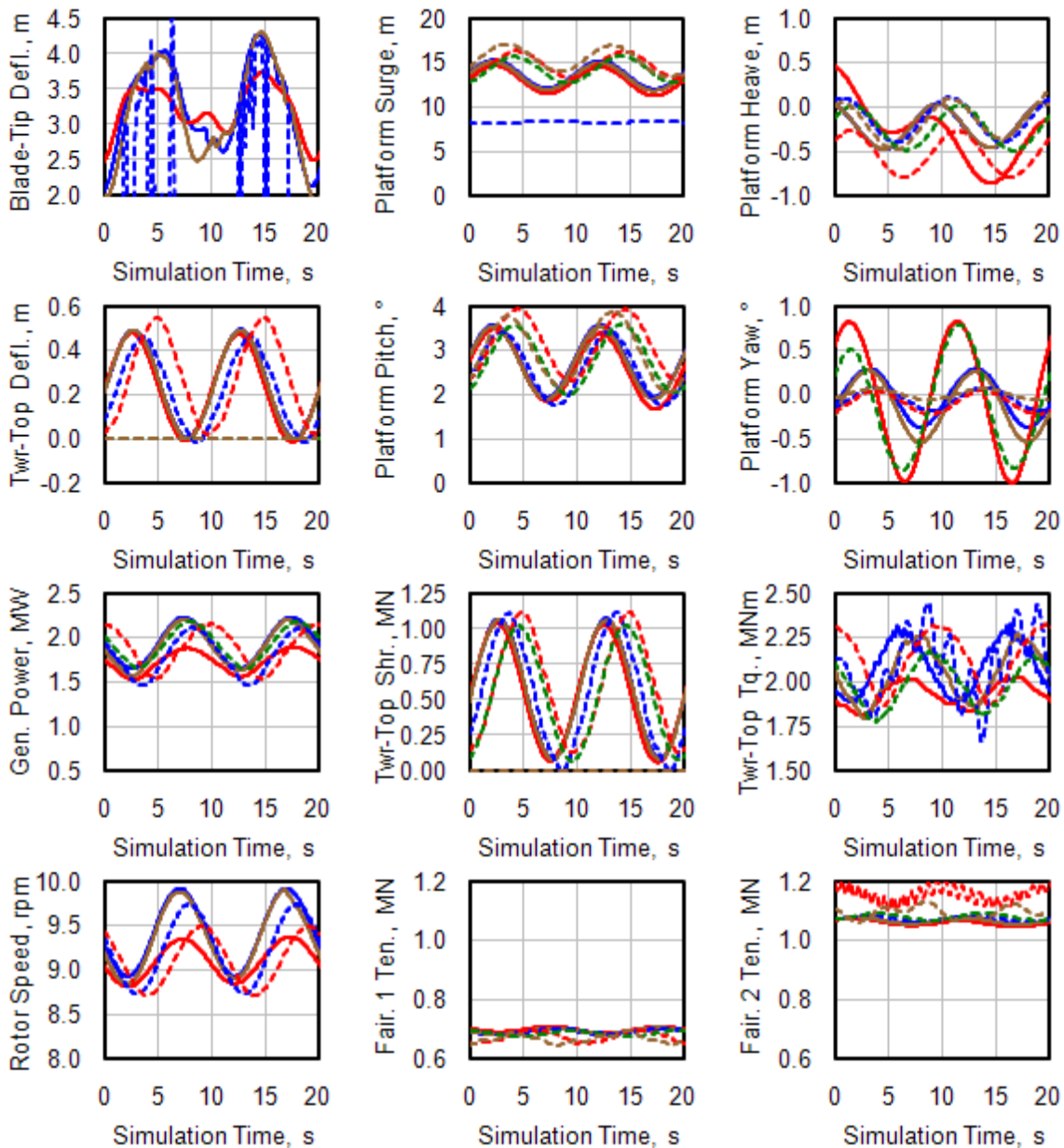
Figure 48. Aero-hydro-servo-elastic time series with regular waves from load case 5.1

platform centerline is highest at 0 and 10 s and lowest at 5 and 15 s, except in 3Dfloat and Simo, which are phase-shifted relative to the other codes.

The generator power agrees quite well between all codes (at least as well as they have in earlier OC3 phases), except FAST by POSTECH, which predicts a lower mean and amplitude. Likewise, all codes agree well in rotor speed, except FAST by POSTECH and 3Dfloat, which predict lower means and amplitudes.

The out-of-plane blade-tip deflection agrees reasonably well between all codes except FAST by POSTECH, which has less overall oscillation, and HAWC2, which may simply have output the wrong parameter. 3Dfloat, Simo, and SESAM predict no deflection because their rotors were modeled rigidly.

Except for FAST by POSTECH, all codes predict a similar mean value of the tower-top rotor torque (i.e., roll moment), but the oscillations about this mean vary. FAST by POSTECH predicts a lower mean and oscillation amplitude. All codes agree on the tower-top fore-aft shear (thrust) force, but 3Dfloat results in a larger tower-top deflection. Simo and SESAM predict no deflection because the tower was modeled rigidly in those codes.

For the platform-surge displacement, all codes but HAWC2 agree on the amplitude of oscillation, but the mean values vary despite the agreement on thrust—Simo, 3Dfloat, and SESAM are a bit higher and HAWC2 is very low (HAWC2 also has less amplitude). The results are similar for platform-pitch displacement, except that HAWC2 matches the majority of codes much better. The nonzero means in these displacements are the result of the nonzero mean rotor thrust. The higher amount of platform-surge and -pitch displacements in 3Dfloat results from the slightly higher mean thrust.

The rotor thrust is counteracted by tensions in the mooring lines, with the downstream mooring line less loaded than the upstream lines. The variations in the fairlead tensions are fairly consistent with the variations in platform displacement. That is, the downstream fairlead has a lower tension and the upstream fairleads have higher tension in 3Dfloat and SESAM than in the other codes.

The differing platform-heave displacements imply that the codes differ in how they couple heave with surge and pitch. The slightly negative mean platform-yaw displacement—predicted similarly by most codes—results from the rotor-shaft tilt, which causes some of the rotor torque to act about the yaw axis. The oscillation about this mean—resulting from a gyroscopic moment produced by platform pitching (at the wave period) in combination with spinning rotor inertia—varies a bit between the codes.

5.4.6 Aero-Hydro-Servo-Elastic Response with Irregular Waves

Figure 49 shows power spectra computed in load case 5.3 for the same parameters shown in Figure 48. Case 5.3 tests the same model used in case 5.1, but with excitation from stochastic wind above rated wind speed and irregular (stochastic) waves. Results were obtained from NREL and POSTECH with FAST, GH with Bladed, NREL with ADAMS, MARINTEK with Simo, and Acciona with SESAM.

The power spectra agree very well in most parameters. As in case 4.2, the wave spectrum has the highest amount of energy at 0.1 Hz—corresponding to the peak-spectral period of 10 s—and all codes agree on the energy content of the system response at this frequency, except SESAM in platform-pitch displacement. Unlike case 4.2, there is a high amount of energy at low frequencies (below 0.1 Hz)—corresponding to the highest energy in the wind—and all codes agree on the energy content of the system response at these frequencies, except SESAM again in platform-pitch displacement and Simo in generator power. Simo also has more energy in the generator power above 0.1 Hz. As in the previous SESAM results, the higher energy content in the fairlead tensions above 0.1 Hz is clearly visible. The second

tower and blade bending natural frequencies are visible in the FAST, Bladed, and ADAMS predictions of the tower-top shear force and rotor torque. However, ADAMS predicts less energy at these frequencies, which may result from the increase in numerical damping with frequency that is typical of ADAMS simulations.
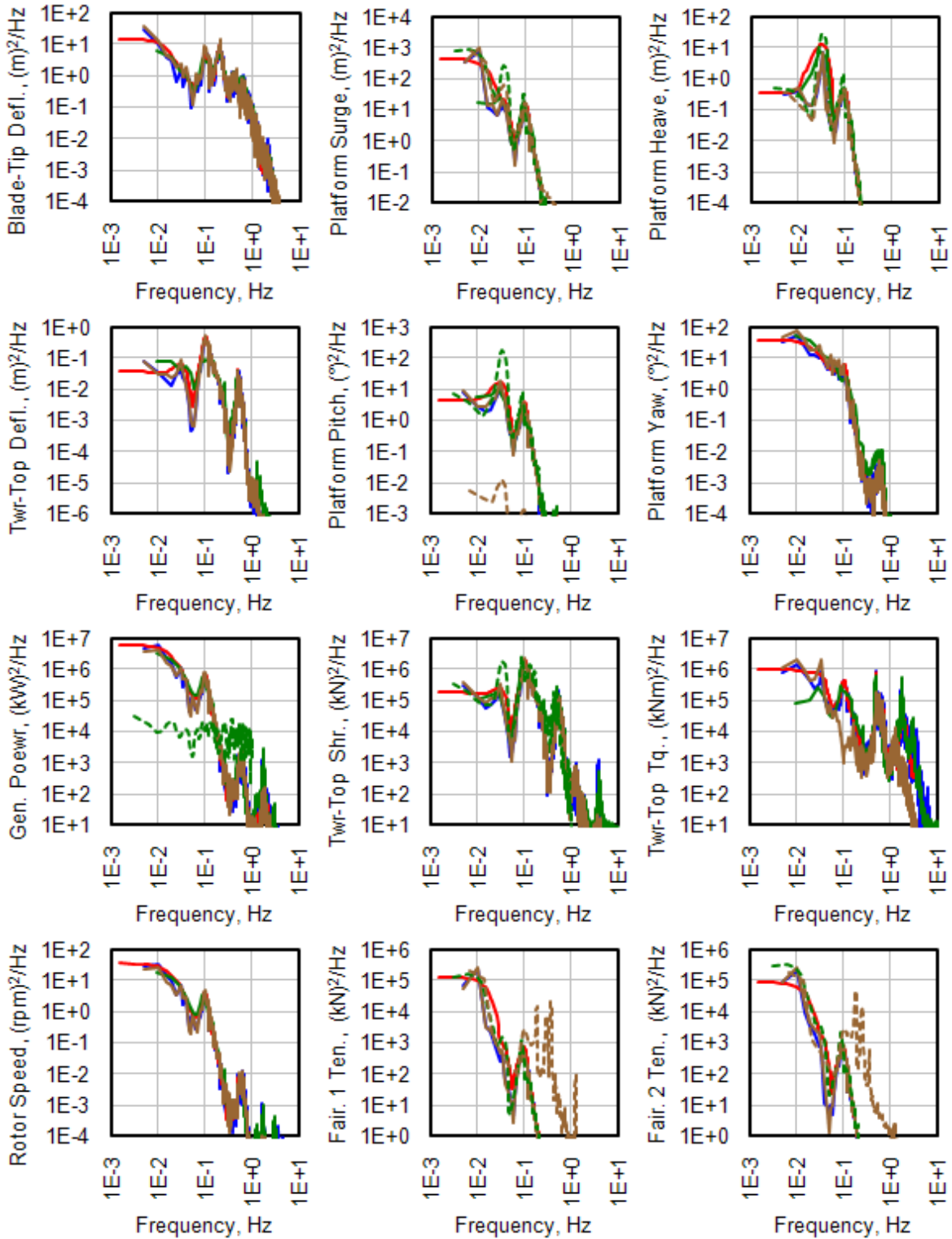
Figure 49. Aero-hydro-servo-elastic power spectra with irregular waves from load case 5.3

5.4.7 "Effective RAOs"

Figure 50 shows "effective RAOs" computed in load case 5.4 for the same parameters shown in Figure 48 and Figure 49. Case 5.4 tests the same model used in case 5.1, but with a set of regular waves at varying frequency. Results were obtained from NREL and POSTECH with FAST, NREL with ADAMS, UMB with 3Dfloat, and Acciona with SESAM.

Typical of conventional RAOs, the "effective RAO" responses are largest at the system's natural frequencies. For platform pitch and heave, the "effective RAOs" show excitation at and around the pitch and heave natural frequencies (both about 0.2 rad/s). For platform surge, the most excitation occurs at the very lowest frequencies and at the platform-pitch natural frequency. The latter indicates coupling between surge and pitch. The behavior of the fairlead tension "effective RAOs" is similar to surge, indicating that the surge is what most influences the tensions. For platform yaw, the "effective RAO" shows excitation at and around the yaw natural frequency (0.75 rad/s), which is caused by gyroscopic loading from the spinning rotor combined with platform pitching. The "effective RAOs" for out-of-plane blade-tip deflection and tower-top fore-aft deflection, shear force, and rotor torque show broadband excitation across all frequencies, with extra excitation at the platform-pitch and first tower-bending (3.0 rad/s) natural frequencies. The generator power and rotor speed "effective RAO" behavior are similar, but contain less energy at the first tower-bending natural frequency.

In the "effective RAO" code-to-code comparisons, ADAMS had trouble converging at 1.5, 2.0, and 2.2 rad/s (hence the "spikes"); otherwise, the ADAMS results agree with the FAST results by NREL.

3Dfloat also agrees well with NREL's FAST results, except that 3Dfloat predicts lower excitation in platform yaw and higher excitation in the fairlead tensions and at and around the first tower-bending natural frequency in all parameters. This latter issue is still under investigation; possible explanations are (1) differences in the aerodynamic damping due to the rigid rotor or differing aerodynamic theories or (2) the modeling of the rigid spar with an artificially high stiffness in 3Dfloat.

SESAM predicts higher excitation in the platform-surge and -pitch displacements and fairlead tensions. The latter are attributed to a lack of convergence in SESAM's FEM-based mooring line solution. SESAM also predicts lower excitation in platform yaw than does FAST and ADAMS.

The "effective RAOs" from FAST by POSTECH differ with those from FAST by NREL over several parameters, including out-of-plane blade-tip deflection; generator power; rotor speed; platform-surge, -heave, and –pitch displacements; and fairlead tensions. The differences in platform displacements and the resulting differences in the fairlead tensions are caused by the lesser amount of hydrodynamic damping in POSTECH's FAST model, as described earlier. Interestingly, this drop in damping leads to surge displacement and resulting fairlead tensions with negative "effective RAOs," which means that there is less system motion with waves than in still water.
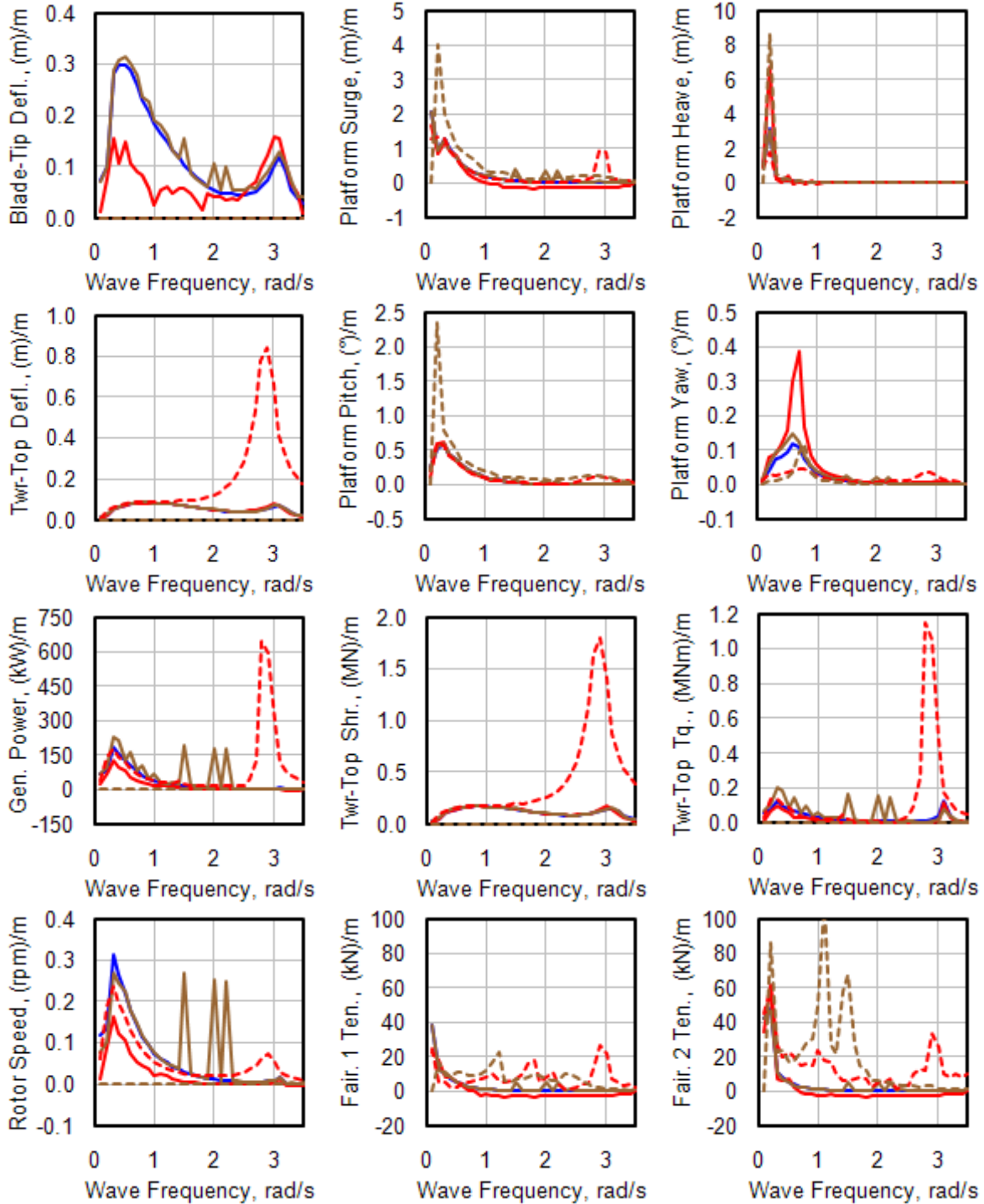
Figure 50. Aero-hydro-servo-elastic "effective RAOs" with regular waves from load case 5.4

The reason for negative "effective RAOs" is as follows. In simulations with wave excitation, the wave-induced motions occur at the wave-excitation frequency, which brings about (potential-flow-based) wave-radiation damping. The wave-radiation damping in surge is not negligible above 0.2 rad/s [5]. In still water, the wave frequency is eliminated from the excitation/response, thereby eliminating the wave-radiation damping, which leads to a minor controller-induced instability of the platform-surge mode. Because of the system's nonlinearities, this instability leads to a limit-cycle oscillation of the platform-

surge mode at the surge natural frequency (where there is negligible hydrodynamic damping) when operating in still water. The wave-radiation damping resulting from wave excitation reduces or eliminates the platform-surge instability (depending on the wave-excitation frequency) and resulting limit-cycle oscillations, thereby reducing the overall motions considerably.

The controller-induced instability and resulting limit-cycle oscillations in still water are largest at rated wind speed and are present in the system even with the proper amount of hydrodynamic damping. Due to the strong influence of the (potential-flow-based) wave-radiation damping in these results, it is noted that neglecting this damping will likely lead to vastly different "effective RAOs" at and around rated wind speed.

5.5 Phase IV Conclusions

In Phase IV of OC3, participants used an assortment of codes to model the coupled dynamic response of the NREL 5-MW wind turbine installed on a deeply drafted, slender spar buoy with catenary mooring lines in 320 m of water. Code predictions were compared from load-case simulations selected to test different model features. The comparisons have resulted in a greater understanding of offshore floating wind turbine dynamics and modeling techniques, and better knowledge of the validity of various approximations. The results from Phase IV can be summarized as follows:

- All of the results of Phase I also apply to the results of Phase IV.

- The natural frequencies of the six (primarily) rigid-body modes of the OC3-Hywind system (with only minor couplings to the turbine flexibilities) are strongly influenced by hydrodynamic added mass. Some codes (such as MSC.ADAMS) can model acceleration-dependent loads within time-domain simulations but neglect acceleration-dependent loads during a linearization solution. To calculate natural frequencies through a linear eigensolution, the models implemented in such codes must have their platform physical mass and inertia augmented with the additional mass and inertia associated with hydrodynamic added mass; otherwise, such codes will predict unreasonably high natural frequencies.

- Gravity has multiple influences on the dynamics of offshore systems (e.g. buoyancy, surface waves, component weight, platform-pitch and -roll natural frequencies). Consequently—while gravity is often neglected in land-based wind turbine codes during model linearization—gravity must be included in the model linearization process by codes that calculate natural frequencies through a linear eigensolution.

- Codes developed to model offshore wind turbines on floating spar buoys incorporate one of two hydrodynamics models: (1) Morison's equation augmented with hydrostatics and wave-excitation heave forces or (2) potential-flow theory augmented with the nonlinear viscous-drag term from Morison's equation. Either hydrodynamic model can be used to predict equivalent hydrodynamic loading of the OC3-Hywind spar in (most) conditions where radiation damping is negligible. For codes that employ Morison's equation, the augmented heave force can be approximated as the change in buoyancy brought about by direct integration of the hydrostatic pressure dependent on the time-varying wave elevation.

- Codes that neglect the additional linear hydrodynamic damping clearly show less overall damping in their responses than codes that include it.

- Codes developed to model offshore floating wind turbines incorporate either quasi-static or dynamic formulations for the mooring system. The quasi-static mooring models can be further divided into (1) a linearized representation of the complete mooring system, (2) a nonlinear load-displacement relationship of the complete mooring system, (3) a nonlinear load-displacement relationship for each individual mooring line, or (4) direct solution of the implicit nonlinear catenary equations. Due to the nonlinear behavior of the catenary mooring system, the quasi-

static model (1) is valid only for small displacements about the linearization point. Quasi-static models (2) through (4) and the dynamic models can be derived and implemented so as to predict equivalent mooring reactions of the OC3-Hywind spar in most conditions. Models (1) and (2), however, cannot be used to calculate the reactions of the individual mooring lines.

- Unlike codes with a quasi-static mooring model, codes (such as SESAM and DeepC) that model the dynamics of the mooring system predict higher energy in the spectra of fairlead tension above the peak wave period. These higher excitations—indicating larger elastic strain and higher dynamic tension—are caused mainly by drag forces normal to the line delaying the static catenary deflection, but are also caused by (nonphysical) problems in the codes' numerical solutions.

- There is considerable statistical uncertainty of the response spectra in the low frequency range of the platform natural frequencies and wave excitation frequencies because of the relatively short duration of the prescribed time series compared to the wave and platform periods. Spectral shape estimates in this frequency range are sensitive to time-series sampling.

- Many offshore floating wind turbine codes cannot model turbine flexibilities such as blade and tower deflection. While neglecting these flexibilities influences the resulting motions and loading of the blades and tower, it does not have a strong influence on the platform motions in the OC3-Hywind system.

- The coupled dynamics of the turbine and platform varied a bit between the codes. The nonzero mean rotor thrust results in nonzero means in the tower-top fore-aft deflection and platform-surge, -pitch, and -heave displacements. The rotor thrust is counteracted by tensions in the mooring lines, with the downstream mooring line less loaded than the upstream lines. The rotor-shaft tilt causes some of the rotor torque to act about the yaw axis that leads to a nonzero mean platform-yaw displacement. Oscillations about these means result from turbulent-wind and regular- or irregular-wave excitation. Oscillations in platform yaw result from a gyroscopic moment produced by platform pitching in combination with spinning rotor inertia.

- While it is desirable to determine the influence of the wave-excitation frequency on the response of a floating wind turbine system, the operation of the turbine makes it impossible to calculate the Response Amplitude Operator (RAO) in a conventional manner, due to (1) nonlinear dynamics, (2) active rotor control, and (3) the rotor rotation introducing additional periodicities. The floating wind turbine system's response to periodic waves will be a superposition of multiple frequencies: (1) the wave excitation frequency, (2) the rotor-rotational frequency, and (3) any system mode's natural frequency (such as for platform surge) from which the response is a limit-cycle oscillation due to a controller-induced instability with a reaction limited by nonlinear behavior. To resolve this problem, an "effective RAO" was defined to mean the difference in response amplitudes between nonlinear time-domain simulations run with and without wave excitation. Using this definition, turbine operation at and around rated wind speed—when compared to a parked turbine—was found to have a dramatic effect on the frequency response of the OC3-Hywind system. Moreover, the (potential-flow-based) wave-radiation damping was found to have strong influence on this response. Thus, codes that neglect wave-radiation damping will likely predict vastly different "effective RAOs" for the OC3-Hywind system at and around rated wind speed.

5.6 Phase IV References

[1] Jonkman J, Butterfield S, Musial W, and Scott G. *Definition of a 5-MW Reference Wind Turbine for Offshore System Development*. NREL/TP-500-38060. NREL: Golden, CO, 2009.

[2] Nielsen FG, Hanson TD, and Skaare B. "Integrated Dynamic Analysis of Floating Offshore Wind Turbines." *25th International Conference on Offshore Mechanics and Arctic Engineering*, 4–9 June, Hamburg, 2006. (CD-ROM)

[3] Skaare B, Hanson TD, and Nielsen FG. "Importance of Control Strategies on Fatigue Life of Floating Wind Turbines." *26th International Conference on Offshore Mechanics and Arctic Engineering*, 10–15 June, San Diego, CA, 2007. (CD-ROM)

[4] Larsen TJ, and Hanson TD. "A Method to Avoid Negative Damped Low Frequent Tower Vibrations for a Floating, Pitch Controlled Wind Turbine." *The Second Conference on The Science of Making Torque From Wind*, 28–31 August, Copenhagen, 2007. [Online]. Available: http://iopscience.iop.org/1742-6596/75/1/012073/pdf?ejredirect=.iopscience.

[5] Jonkman J. *Definition of the Floating System for Phase IV of OC3*. NREL: Golden, CO, 2009 (to be published).

REPORT DOCUMENTATION PAGE

Form Approved
OMB No. 0704-0188

1. REPORT DATE *(DD-MM-YYYY)* December 2010	2. REPORT TYPE Technical Report	3. DATES COVERED *(From - To)*

4. TITLE AND SUBTITLE Offshore Code Comparison Collaboration (OC3) for IEA Task 23 Offshore Wind Technology and Deployment	5a. CONTRACT NUMBER DE-AC36-08-GO28308
	5b. GRANT NUMBER
	5c. PROGRAM ELEMENT NUMBER
6. AUTHOR(S) J. Jonkman and W. Musial	5d. PROJECT NUMBER NREL/TP-5000-48191
	5e. TASK NUMBER WE10.1211
	5f. WORK UNIT NUMBER

7. PERFORMING ORGANIZATION NAME(S) AND ADDRESS(ES) National Renewable Energy Laboratory 1617 Cole Blvd. Golden, CO 80401-3393	8. PERFORMING ORGANIZATION REPORT NUMBER NREL/TP-5000-48191
9. SPONSORING/MONITORING AGENCY NAME(S) AND ADDRESS(ES)	10. SPONSOR/MONITOR'S ACRONYM(S) NREL
	11. SPONSORING/MONITORING AGENCY REPORT NUMBER

12. DISTRIBUTION AVAILABILITY STATEMENT
National Technical Information Service
U.S. Department of Commerce
5285 Port Royal Road
Springfield, VA 22161

13. SUPPLEMENTARY NOTES

14. ABSTRACT *(Maximum 200 Words)*
Wind turbines are designed and analyzed using simulation tools (i.e., design codes) capable of predicting the coupled dynamic loads and responses of the system.Land-based wind turbine analysis relies on the use of aero-servo-elastic codes, which incorporate wind-inflow, aerodynamic (aero), control system (servo), and structural-dynamic (elastic) models in the time domain in a coupled simulation environment. In recent years, some of these codes have been expanded to include the additional dynamics pertinent to offshore installations, including the incident waves, sea current, hydrodynamics, and foundation dynamics of the support structure. The sophistication of these aero-hydro-servo-elastic codes, and the limited data available with which to validate them, underscore the need to verify their accuracy and correctness. The Offshore Code Comparison Collaboration (OC3), which operates under Subtask 2 of the International Energy Agency (IEA) Wind Task 23, was established to meet this need. The OC3 project was performed through technical exchange among a group of international participants from universities, research institutions, and industry across the United States of America, Germany, Denmark, the United Kingdom, Spain, the Netherlands, Norway, Sweden, and Korea. Moreover, most of the aero-hydro-servo-elastic codes developed for modeling the dynamic response of offshore wind turbines were tested within OC3.

15. SUBJECT TERMS
offshore wind turbines; design codes; aero-servo-elastic codes; aero-hydro-servo-elastic codes; Offshore Code Comparison Collaboration

16. SECURITY CLASSIFICATION OF:			17. LIMITATION OF ABSTRACT	18. NUMBER OF PAGES	19a. NAME OF RESPONSIBLE PERSON
a. REPORT Unclassified	b. ABSTRACT Unclassified	c. THIS PAGE Unclassified	UL		
					19b. TELEPHONE NUMBER *(Include area code)*

Standard Form 298 (Rev. 8/98)
Prescribed by ANSI Std. Z39.18